Functional Thin Films Fabricated by Plasma Polymerization and Their Biological Applications

Dissertation

zur Erlangung des Grades

„Doktor der Naturwissenschaften“

am Fachbereich Chemie, Pharmazie und Geowissenschaften

der Johannes Gutenberg-Universität Mainz

Li-Qiang Chu

geb. in Liaoning, V. R. China

Mainz, 2007

Tag der mündlichen Prüfung: 09 May, 2007

……To my wife and my parents

CONTENTS

Abbreviations

AAc	Acrylic acid
AFM	Atom force microscopy
BSA	Bovine serum albumin
CA	Contact angle measurement
DEA	N,N-diethylacrylamide
DNA	Deoxyribonucleic acid
EO2	Di(ethylene glycol) monovinyl ether
FT-IR	Fourier transform infrared spectroscopy
GMA	Glycidyl methacrylate
LCST	Lower critical solution temperature
LOD	Limit of detection
OWS	Optical waveguide spectroscopy
PAAc	Poly(acrylic acid)
PBS	Phosphate buffered saline
PEG	Polyethylene glycol
PET	Poly(ethylene terephthalate)
PNA	Peptide nucleic acids
ppAA	Plasma polymerized allylamine
ppDEA	Plasma polymerized N,N-diethylacrylamide
ppEO2	Plasma polymerized di(ethylene glycol) monovinyl ether
ppGMA	Plasma polymerized glycidyl methacrylate
PSP	Plasmon surface polaritons
PTPP	Poly(terephthalate-co-phosphate)
SAM	Self-assembled monolayer
SDS	Sodium dodecyl sulfate
SPFS	Surface plasmon enhanced fluorescence spectroscopy
SPR	Surface plasmon resonance spectroscopy
UV	Ultra-violet light
XPS	X-ray photoelectron spectroscopy

Chapter 1

General Introduction

1.1 Background

Over the past two decades plasma polymerization techniques have been proved to be a simple and effective method for both the preparation of a large variety of functional thin films and the surface modification of different materials.[1-5] By careful choice of precursors and deposition parameters, the physical and chemical properties of plasma polymers, as well as, their surface properties, can be well tailored, which make them very attractive for biological or biomedical applications. Indeed, the use of plasma polymers as biomaterials has been successfully demonstrated and some excellent reviews have been published recently.[6-9]

Rapid and sensitive detection of a specific biomolecule is essential in modern clinical diagnosis. Therefore, the development of various biosensors has attracted considerable interest worldwide during the past several decades.[10-13] A biosensor generally consists of a biological recognition element, a physicochemical transducer and a signal output system, as depicted in Scheme 1-1. The biological recognition elements, which are usually attached on the surface of transducers, can recognize the presence or the concentration of a specific analyte in solution, resulting in a physical/chemical change. This change is then converted by the transducer into a quantifiable signal for electrochemical, optical, piezoelectric, magnetic or other measurements.

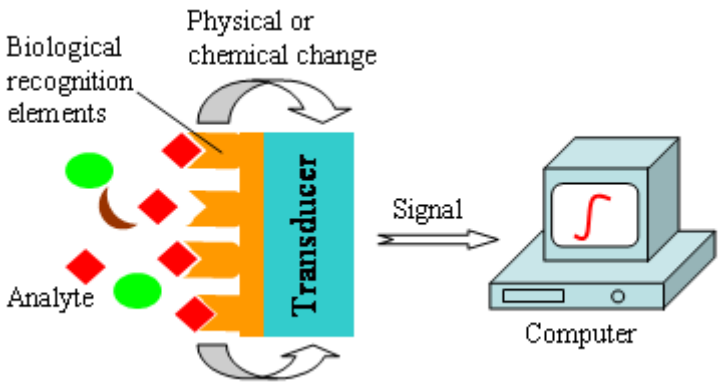

Scheme 1-1: Schematic representation of the components in a biosensor.

Detection of a specific DNA sequence has become increasingly important in the diagnosis of genetic and infectious diseases, particularly after the entire sequence of human genomes was uncovered from the human genome project in 2001.[14-16] Moreover, identification of a gene sequence in bacterial, viral or food is also crucial with respect to the environmental monitoring, as well as, for food control. In this regard, a variety of DNA sensors have thus been proposed based on different transduction principles, including those which detect mass or changes in optical or electrochemical properties, while others depend on a labeling step for the detection of the hybridized stands.[17-20] Most available methods rely on the immobilization of single-stranded oligonucleodides (i.e., so called DNA probes or catchers) onto sensor surfaces as the recognition elements, and the subsequent hybridization of the surface attached probes with the complementary DNA target from solution. On the other hand, homogeneous DNA detection methods, which avoid the difficulties associated with probe immobilization, were also demonstrated by some researchers.[21-24]

Nonspecific protein adsorption is a common phenomenon occurring when a biomedical device is brought in contact with a biological solution, e.g., a body fluid. In biosensor applications, it is apparent that nonspecific protein adsorption would interfere with the sensing species attached on the sensor, and increase the background signal, thus reduce a biosensor's selectivity and sensitivity. Therefore, it is highly desirable to make a biosensor resistant to the nonspecific adsorption of proteins. Polyethylent glycol (PEG) is a well-known polymer because of its good resistance to protein adsorption and cell adhesion. Most recently, plasma polymerization has proved to provide a new possibility to prepare protein-resistant surfaces.[25-27]

Surface plasmon resonance spectroscopy (SPR) is widely accepted as a sensitive tool for the investigation of biomolecular interacton analysis (BIA). The fundamentals of SPR and its use for BIA study can be found in a number of excellent reviews and monograph.[28-30] One special advantage of this highly surface sensitive technique is its ability to measure the change at surfaces in a liquid environment in real time, thus allowing for the monitoring of some dynamic processes. Recently, a new highly sensitive optical technique, surface plasmon enhanced fluorescence spectroscopy (SPFS), was developed based on the combination of surface plasmon resonance and fluorescence spectroscopy.[31, 32] The excitation of a surface plasmon mode results in an enhanced optical field, which can excite fluorophores located within the evanescent tail of the surface plasmon mode, resulting in a very strong fluorescence signal. SPFS was successfully employed for DNA sequence

mismatch detection, as well as for the investigation of hybridization kinetics between the surface-attached oligonucleotide and a target DNA from the solution.[33-35]

1.2 Aims of the present study

One of the key factors in biosensor development is the immobilization of biological recognition elements on biosensor surfaces (see Scheme 1-1). It is still a challenge to generate a multifunctional surface, which could provide functionalities for the immobilization of a specific biomolecule (e.g., DNA probes), while at the same time could resist nonspecific adsorption of other biomolecules, such as protein, cell, etc. The first aim of my study is to develop a protein-resistant DNA sensor, which could be used for DNA detection from a complex sample. Pulsed plasma polymerization of di(ethylene glycol) monovinyl ether (EO2) at a low duty cycle resulted in a non-fouling coating, as seen by SPR measurements (Chapter 4). The non-fouling ppEO2 was then used as a covering layer to immobilize streptavidin molecule (Chapter 5). Upon optimizing the thickness of ppEO2 cover layer, the embedded streptavidin still allowed for the binding of biotinylated DNA strands, while at the same time the resulted DNA sensor surfaces exhibited an excellent resistance to nonspecific adsorption of proteins, such as BSA and fibrinogen. This sensor was successfully employed to discriminate different DNA sequences from protein-containing solution (see SPFS data in Chapter 5). Our results clearly demonstrated a new possibility to form multifunctional surfaces.

Besides streptavidin-biotin coupling, the covalent binding is the most widely used strategy for DNA probe immobilization, particularly in most commercial DNA microarrays. In Chapter 6, I explored the DNA probe immobilization on the plasma polymerized epoxide surfaces. Glycidyl methacrylate (GMA) was used as monomer in this work. FT-IR results clearly indicated the presence of epoxide groups in the ppGMA deposited at low duty cycle. DNA sensors were thus made using ppGMA as substrates.

Recently, plasma polymerized functional thin films, particularly those deposited at low input power, have been found to contain some soluble materials, which would dissociate from the plasma deposit when in contact with liquid environments. In Chapter 7, the soluble part in the plasma polymerized allylamine (ppAA) films was measured using surface plasmon resonance spectroscopy (SPR) and optical waveguide spectroscopy (OWS). It was found that ethanol extraction treatment was a simple way to remove the soluble materials from the plasma deposited films. The extracted ppAA films shown better stability in PBS buffer.

In Chapter 8, I demonstrated a new homogeneous DNA detection method, which avoids the step for DNA probe immobilization, thus reducing the complexity and the cost for DNA sensor fabrication. This method takes advantages of the surface sensitivity of SPFS, as well as, the different electrostatic properties of PNA and DNA. The fluorescently labelled peptide nucleic acids (PNA) were used as probes and the ppAA films were used in this work to provide a positively charged surface. A DNA target of 200 pM could be detected using this method.

Besides the use of plasma polymerized films for the development of various DNA sensors, I also explore the preparation of temperature sensitive coatings by plasma polymerization of N,N-diethylacrylamide (DEA) monomer (Chapter 9). Compared to NiPAAm monomer used in the literatures[36-39], one particular advantage of DEA monomer is its higher vapor pressure. Therefore, it does not require heating of either the monomer container or the plasma chamber, which is generally needed in NIPAAm plasma polymerization. Water contact angle measurements showed that the ppDEA coatings deposited at 2 W input power became more hydrophobic when increasing the temperature up to ca. 37 ^{o}C.

References

1. Biederman, H.; Osada, Y., *Plasma Polymerization Processes*. Elsevier: New York, 1992.
2. Yasuda, H., *Plasma Polymerization*. Academic: Orlando, 1985.
3. Ratner, B. D.; Castner, D. G., *Surface Modification of Polymeric Biomaterials*. Plenum: New York, 1997.
4. Inagaki, N., *Plasma Surface Modification and Plasma Polymerization*. Technomic: Lancaster, PA, 1996.
5. d'Agostino, R.; Favia, P.; Wertheimer, M. R., *Plasma Processes and Polymers*. Wiley-VCH Weinheim, 2005.
6. Siow, K. S.; Britcher, L.; Kumar, S.; Griesser, H. J. *Plasma Process. Polym.* **2006,** 3, (6-7), 392-418.
7. Bretagnol, F.; Valsesia, A.; Ceccone, G.; Colpo, P.; Gilliland, D.; Ceriotti, L.; Hasiwa, M.; Rossi, F. *Plasma Process. Polym.* **2006,** 3, (6-7), 443-455.

8. Sardella, E.; Favia, P.; Gristina, R.; Nardulli, M.; d'Agostino, R. *Plasma Process. Polym.* **2006,** 3, (6-7), 456-469.
9. Ratner, B. D. *Biosens. Bioelectron.* **1995,** 10, 797-804.
10. Castillo, J.; Gaspar, S.; Leth, S.; Niculescu, M.; Mortari, A.; Bontidean, I.; Soukharev, V.; Dorneanu, S. A.; Ryabov, A. D.; Csoregi, E. *Sens. Actuators B: Chem.* **2004,** 102, (2), 179-194.
11. Mehrvar, M.; Abdi, M. *Anal. Sci.* **2004,** 20, (8), 1113-1126.
12. Cooper, M. A. *Anal. Bioanal. Chem.* **2003,** 377, (5), 834-842.
13. Rosi, N. L.; Mirkin, C. A. *Chem. Rev.* **2005,** 105, (4), 1547-1562.
14. Lander, E. S.; et.al. *Nature* **2001,** 409, (6822), 860-921.
15. Sachidanandam, R.; et.al. *Nature* **2001,** 409, (6822), 928-933.
16. Venter, J. C.; et.al. *Science* **2001,** 291, (5507), 1304-1351.
17. Kostrikis, L. G.; Tyagi, S.; Mhlanga, M. M.; Ho, D. D.; Kramer, F. R. *Science* **1998,** 279, (5354), 1228-1229.
18. Taton, T. A.; Mirkin, C. A.; Letsinger, R. L. *Science* **2000,** 289, (5485), 1757-1760.
19. Gerion, D.; Chen, F. Q.; Kannan, B.; Fu, A. H.; Parak, W. J.; Chen, D. J.; Majumdar, A.; Alivisatos, A. P. *Anal. Chem.* **2003,** 75, (18), 4766-4772.
20. Hansen, J. A.; Mukhopadhyay, R.; Hansen, J. O.; Gothelf, K. V. *J. Am. Chem. Soc.* **2006,** 128, (12), 3860-3861.
21. Ho, H. A.; Boissinot, M.; Bergeron, M. G.; Corbeil, G.; Dore, K.; Boudreau, D.; Leclerc, M. *Angew. Chem. Int. Ed.* **2002,** 41, (9), 1548-1551.
22. Gaylord, B. S.; Heeger, A. J.; Bazan, G. C. *Proc. Natl. Acad. Sci. USA* **2002,** 99, (17), 10954-10957.
23. Storhoff, J. J.; Lucas, A. D.; Garimella, V.; Bao, Y. P.; Muller, U. R. *Nat. Biotechnol.* **2004,** 22, (7), 883-887.
24. Stoeva, S. I.; Lee, J. S.; Thaxton, C. S.; Mirkin, C. A. *Angew. Chem. Int. Ed.* **2006,** 45, (20), 3303-3306.
25. Beyer, D.; Knoll, W.; Ringsdorf, H.; Wang, J. H.; Timmons, R. B.; Sluka, P. *J. Biomed. Mater. Res.* **1997,** 36, 181-189.
26. Wu, Y. L. J.; Timmons, R. B.; Jen, J. S.; Molock, F. E. *Colloids Surf. B* **2000,** 18, (3-4), 235-248.
27. Bremmell, K. E.; Kingshott, P.; Ademovic, Z.; Winther-Jensen, B.; Griesser, H. J. *Langmuir* **2006,** 22, (1), 313-318.

28. Raether, H., *Surface Plasmons on Smooth and Rough Surfaces and on Gratings*. Springer-Verlag: Berlin, 1988.
29. Knoll, W. *Annu. Rev. Phys. Chem.* **1998,** 49, 569-638.
30. Knoll, W. *MRS Bull.* **1991,** 16, 29-39.
31. Liebermann, T.; Knoll, W. *Colloid. Surface. A* **2000,** 171, (1-3), 115-130.
32. Neumann, T.; Johansson, M. L.; Kambhampati, D.; Knoll, W. *Adv. Func. Mater.* **2002,** 12, (9), 575-586.
33. Kambhampati, D.; Nielsen, P. E.; Knoll, W. *Biosens. Bioelectron.* **2001,** 16, (9-12), 1109-1118.
34. Yao, D. F.; Yu, F.; Kim, J. Y.; Scholz, J.; Nielsen, P. E.; Sinner, E. K.; Knoll, W. *Nucleic Acids Res.* **2004,** 32, (22), 177-192.
35. Robelek, R.; Niu, L. F.; Schmid, E. L.; Knoll, W. *Anal. Chem.* **2004,** 76, (20), 6160-6165.
36. Pan, Y. V.; Wesley, R. A.; Luginbuhl, R.; Denton, D. D.; Ratner, B. D. *Biomacromolecules* **2001,** 2, (1), 32-36.
37. Cheng, X. H.; Canavan, H. E.; Stein, M. J.; Hull, J. R.; Kweskin, S. J.; Wagner, M. S.; Somorjai, G. A.; Castner, D. G.; Ratner, B. D. *Langmuir* **2005,** 21, (17), 7833-7841.
38. Teare, D. O. H.; Barwick, D. C.; Schofield, W. C. E.; Garrod, R. P.; Beeby, A.; Badyal, J. P. S. *J. Phys. Chem. B* **2005,** 109, (47), 22407-22412.
39. Tamirisa, P. A.; Hess, D. W. *Macromolecules* **2006,** 39, (20), 7092-7097.

Chapter 2

Theory

2.1 Plasma polymerization

2.1.1 Plasma and plasma reactors

Plasmas exist widely in nature and are regarded as the fourth state of matter with respect to solids, liquids and gases. A plasma can be defined as a partially ionized gas that contains positively and negatively charged particles, while the plasma as a whole is neutral.[1] Plasmas are highly activated and have an extremely high energy level. In order to achieve the plasma state in man-made plasma systems, two conditions generally have to be fulfilled: 1). Sufficient energy supply for the ionization of atoms and molecules; and 2). A vacuum for maintaining the plasma state. Energy for the ionization of atoms and molecules is required. Electric energy either at direct current (DC) or alternating current (AC) is the common energy employed in various plasma reactors. Either capacitively coupling or inductively coupling is used in different designs of plasma reactors. External electrodes are often employed rather than internal electrodes because this can reduce contaminations from the electrode material. The pressure during the plasma process ranges from 0.01 to 1000 Pa. A low pressure plasma is also known as a glow discharge in the literatures. A radio frequency (13.56 MHz) glow discharge is widely used in plasma polymerization, because it is able to produce a large volume of stable plasma. Two types of reactors are often constructed for plasma polymerization: 1). A bell-jar type reactor with internal parallel-plate electrodes; and 2). A tubular type reactor with an external coil or ring electrode.

2.1.2 Plasma polymerization

Plasma polymerization can be defined as “formation of polymeric materials under the influence of plasma”.[2] Since the first report in the 1950’s,[3, 4] it has received much attention and become an important process for the generation of entirely new materials, as well as, a simple approach for surface modification of various materials. The plasma polymerization process offers some unique advantages compared to other surface modification techniques: 1). Only surface properties will be altered by the plasma polymerized films while the bulk

properties of the substrate materials remain unchanged; 2). It is possible to produce thin film with a great diversity in chemical structures and properties by careful selection of the monomer and the process parameters; 3). Plasma deposition is conformal, and hence can be applied to complex substrates with very good adhesion. The resulting film is pin-hole free; 4). The deposition process is rapid, adjustable, and sterile. An exact control over the film thickness can be achieved easily by adjusting the deposition time.

During the plasma polymerization process, monomers undergo ionization, excitation, fragmentation, bombardment, and combination. As a consequence, plasma polymers are highly cross-linked and do not contain regular repeating units, which makes them chemically different from conventional polymers. However, recently, many research groups become more interested in obtaining functional surfaces using plasma polymerization technique. Two strategies can improve the retention of monomer structure in the deposited films: 1). Deposition at a very low input power under continuous wave (CW) plasma polymerization; or 2). Pulsing the plasma during plasma polymerization, so called "pulsed plasma polymerization". The CW plasma polymerization has intrinsic limitation in that the lowest power that is able to maintain the plasma in a stable state is ca. 0.5 W. For this reason, the concept of pulsed plasma polymerization was developed by Yasuda in 1977.[5] By using this technique the input power can easily reach a level as low as 0.1 W, or even lower. Consequently, the resulting polymer films are relatively similar to conventional polymers with functional groups. A large variety of chemical functionalities, such as fluorocarbon, hydroxyl, carboxyl, amine, epoxide, had been generated using pulsed plasma polymerization technique.

Currently, it is well accepted that two mechanisms, i.e., atomic polymerization and free radical polymerization, respectively, are responsible for the reactions during the plasma on time and off time, respectively.[6-8] As shown in Scheme 2-1, during the plasma on time, monomer molecules gain high energy from electrons, ions, and radicals inside the plasma, and hence are activated and fragmented to small active units. These activated fragments may rearrange to new structures, activate other monomer molecules, or adsorb on the surface of the substrate. Moreover, some free radicals form at the surface of the growing film due to electron impact, ion bombardment, and VUV irradiation in the plasma. All of the free radicals will play a crucial part in the reaction during the plasma off time because they are the species with the longest lifetime. The remaining free radicals in the film will act as the initiation sites for the conventional free-radical polymerization. Although the plasma is switched off, the monomer molecules keep adsorbing onto the film. They are activated by

the free radicals and grow to the polymer chain. In this way, more functional groups of the monomers remain in the pulsed plasma polymerized films.

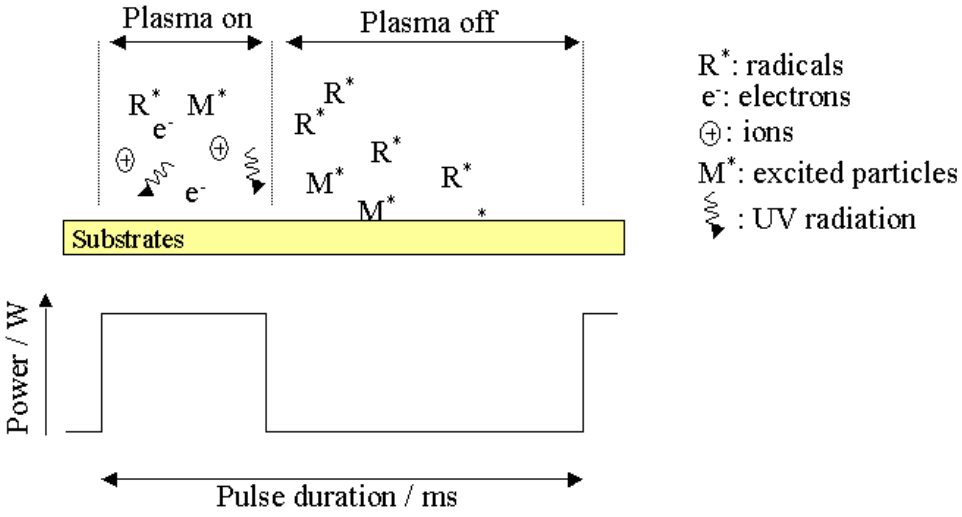

Scheme 2-1: Schematic representation of the plasma processes during a typical pulse. During the plasma on time, the reactions are dominated by electrons, ions, radicals and UV irradiation, while during the plasma off time the reactions are controlled by the longer lived free radicals.

2.2 Surface plasmon optics

2.2.1 Surface plasmon resonance

Surface plasmon resonance spectroscopy (SPR) has become a widely accepted optical technique to investigate surface/interfacial phenomenon with high sensitivity. A surface plasmon, also called plasmon surface polaritons (PSP), is based on the collective oscillation of the (nearly) free electron gas at a metal/dielectric interface,[9, 10] as depicted in Scheme 2-2. It propagates along the x-direction of this interface as a damped oscillatory wave. Surface plasmons decay rapidly and exponentially on both sides, i.e., within the metal and the dielectric, with a finite decay length, L_x. A surface plasmon can be quantitatively described on the basis of dielectric functions of materials involved. The dispersion relationships (i.e., the energy-momentum relation) for a surface plasmon is given by:

$$k_{sp} = \frac{\omega}{c}\sqrt{\frac{\varepsilon_m \cdot \varepsilon_d}{(\varepsilon_m + \varepsilon_d)}} \qquad (2.1)$$

Here k_{sp} is the wavevector of the surface plasmon; ω is the frequency of light; c is the speed of light; and ε_m, ε_d are the dielectric constants of the metal and the dielectric, respectively.

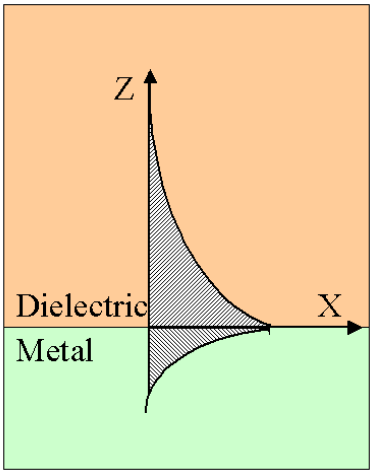

Scheme 2-2: Schematic of a surface plasmon at a metal/dielectric interface.

Surface plasmons can be excited by either electrons passing through a thin metal film or by photons incident on a metal surface. However, surface plasmons can not be excited by externally incident light because the wavevector of surface plasmons do not match with that of the incident light regardless of the wavelength. The wavevector of a free photon propagating in a dielectric medium is:

$$k_{ph} = \frac{\omega}{c}\sqrt{\varepsilon_d} \qquad (2.2)$$

Here k_{ph} is the wavevector of the incoming photon parallel to the surface.

In the frequency (spectral) range of interest:

$$\sqrt{\frac{\varepsilon_m \cdot \varepsilon_d}{\varepsilon_m + \varepsilon_d}} \geq \sqrt{\varepsilon}_d \qquad (2.3)$$

Therefore, the wavevector of a free photon, k_{ph},, is always smaller than that of a surface plasmon mode, k_{sp}. Therefore, surface plasmons can not be excited by externally incident light.

However, the excitation of surface plasmons is possible by a proper coupling of the light. Experimentally, the evanescent wave, characterized by a large momentum, is widely employed to excite surface plasmon resonances. The evanescent wave, associated with total internal reflection, is an optical phenomenon at the interface of two media with different dielectric properties. Total internal reflection occurs above a certain incidence angle (i.e., the critical angle θ_C) if the light wave propagates from the dielectric with high refractive index to the dielectric with low refractive index. The critical angle, θ_c, can be calculated by Snell's law:

$$Sin\theta_c = n_d / n_p \qquad (2.4)$$

Here n_d and n_p are the refractive index of the dielectric and the prism, respectively. For incident angles smaller than θ_c, most of the incoming light is transmitted, and the reflected light is low. Above θ_c, an evanescent wave generates and decays exponentially into the dielectric in z-direction, i.e., normal to the interface. The evanescent wave has a larger momentum, and can exceed the momentum of the surface plasmon mode.

Since surface plasmon propagates in the x-direction, only the x-component of the evanescent wave is relevant to the excitation of a surface plasmon. By changing the incident angle, one can adjust $k_{ph}^{x} = k_{ph} \times \sin\theta$ from zero at normal incidence to the full wavevector k_{ph} at grazing incidence. At a certain angle of incidence, resonant coupling between the evanescent photons and the surface plasmons can be obtained because the energy and the momentum matching conditions are fulfilled.

2.2.2 SPR with prism coupling

Excitation of surface plasmon resonance can be achieved using the evanescent wave in a prism coupling arrangement. In this regards, two kinds of prism arrangements, i.e., the Otto configuration and the Kretschmann configuration, had been developed. In the Otto configuration (Scheme 2-3a),[11] a prism is brought close to a metal, and the evanescent field couples across the small air gap onto the metal surface. The Otto configuration is based on the total internal reflection of a plane wave incident at an angle θ at the base of a prism. The evanescent tail of this inhomogeneous wave can excite surface plasmons at the Ag/dielectric interface provided that the coupling gap is sufficiently narrow. The major technical drawback of the Otto configuration is that it is difficult to get the metal surface close enough

to the prism base, typically within 200 nm. Furthermore, a few dust particles may prevent efficient coupling.

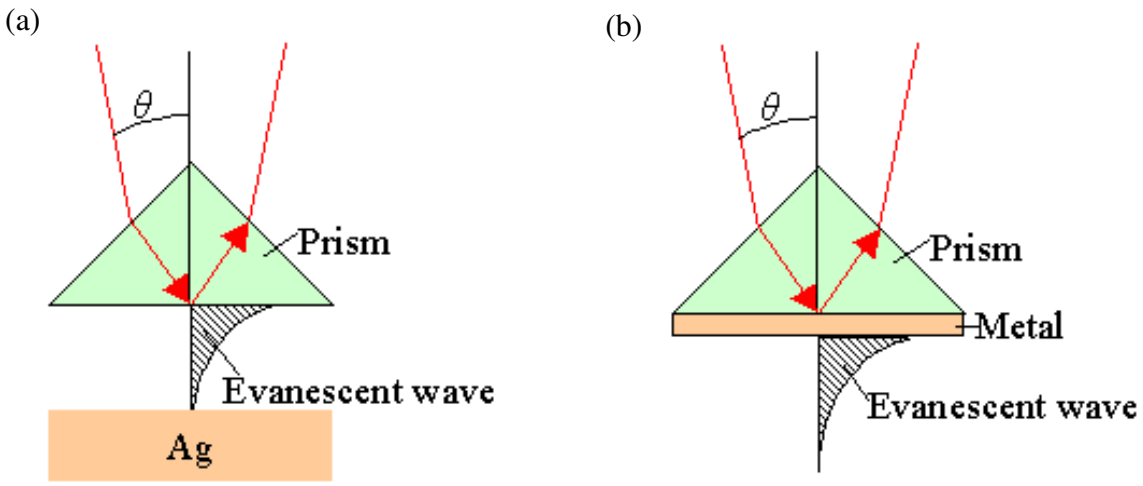

Scheme 2-3: Schematic of SPR excitation by prism coupling: (a) The Otto configuration; and (b) The Kretschmann configuration.

The Kretschmann configuration[12] (Scheme 2-3b) is the most widespread version for practical surface plasmon resonance spectroscopy. In this configuration, a thin metal layer is evaporated directly onto the base of the prism or a glass slide, which is then index-matched to the base of the prism. In this case, photons in the prism couple through the thin layer metal to the surface plasmons on the other side which is in contact with the dielectric medium. The thickness of the metal film should be sufficiently thin for the evanescent wave to penetrate into the opposite surface, but still thick enough to avoid undue reradiation back into the prism. Compared to the Otto configuration, the Kretschmann configuration is much easier to be achieved because the thickness of the metal film can be well controlled.

In both configurations, resonance coupling is observed by monitoring the reflected light intensity as a function of the incident angle (Figure 2-1). If the incident angle is varied, the reflectivity curve shows a relatively narrow dip, which indicates the surface plasmon resonance. The light energy is coupled to the SPR and hence the reflected light intensity reaches a minimum.

Surface plasmon modes can only be excited at the interface of two media with dielectric constants of opposite sign. Therefore, metals with negative dielectric constant, such as silver and gold, are used to generate surface plasmons. Ag can provide a good

resonance enhancement, but is not stable against oxidation. Au is stable and hence is widely used.

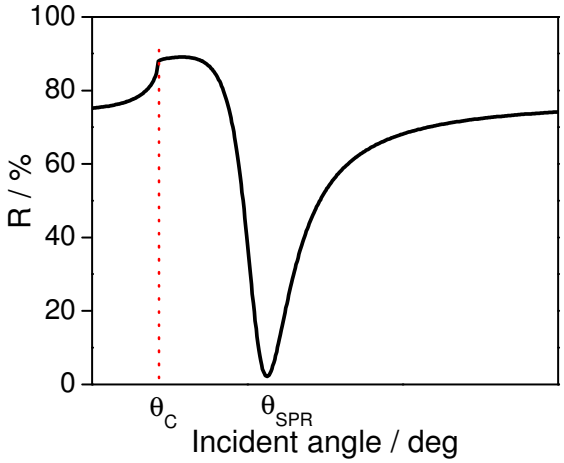

Figure 2-1: A typical SPR curve, i.e., reflectivity as a function of incident angle. The minimum above θ_c indicates SPR occurring.

The surface charge density associated with a surface plasmon can be induced only by an electromagnetic mode which has a component normal to the surface (//Z). Consequently, it should be noted that surface plasmons can only be excited by transverse magnetic (TM) mode, i.e., p-polarized light. Transverse electric (TE) mode, i.e., s-polarized light, can not excite surface plasmons because it propagates along x-direction and has an E-field component parallel to the surface.

Quantitative treatment of SPR curve is based on the Fresnel theory for calculating the overall transmission and reflection of a multilayer system. Different algorithms for calculating the Fresnel equations, based on either a matrix formalism or a recursion formula procedure, have been developed. The angular dependence of the overall reflectivity can be calculated and compared with the measured curve. The best fit then results in a set of parameters, which describe the Au layer and dielectric materials.

If a thin layer ($n_{\text{layer}} > n_{\text{air}}$) is deposited onto the metal, it is equivalent to an increase of the overall effective refractive index integrated over the evanescent field of a surface plasmon mode. The net effect is a slight shift of the dispersion curve corresponding to the increase of k_{sp} for any given energy. As a consequence, the incident angle that determines the photon wavevector along the surface plasmon propagation direction has to be slightly

increased in order to couple resonantly to the surface plasmon mode again (Figure 2-2). The critical angle is unaffected by the presence of a thin dielectric layer.

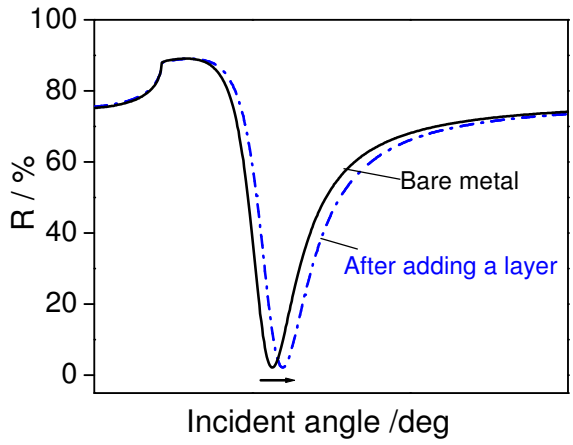

Figure 2-2: Schematic of SPR curves before and after adding a thin dielectric layer to the metal.

Upon increasing the refractive index *n* or the thickness d of the dielectric layer, the resonance angle shifts toward higher angles. The angular shift $\Delta\theta$ is a function of d and the optical contrast to the surrounding medium, which is given by:

$$\Delta\theta = f\,(d_{layer}, (\varepsilon_{layer} - \varepsilon_d)) \qquad (2.5)$$

This indicates that d and *n* cannot be determined independently by SPR with one angle shift only. However, if the refractive index of the material is known, the geometrical thickness can be obtained, and vice versa.

2.2.3 Optical waveguide spectroscopy

If the thickness of a dielectric coating increases further to above 200 nm (depending on the refractive index), guided optical wave can be observed.[13] This waveguide format is a special version of the general principle of guiding light in a transparent medium with confined (optical) dimensions (Scheme 2-4a). The excitation of these modes (of different order m) can be seen if the reflected intensity is monitored as a function of the incident angle, as shown in Scheme 2-4b.

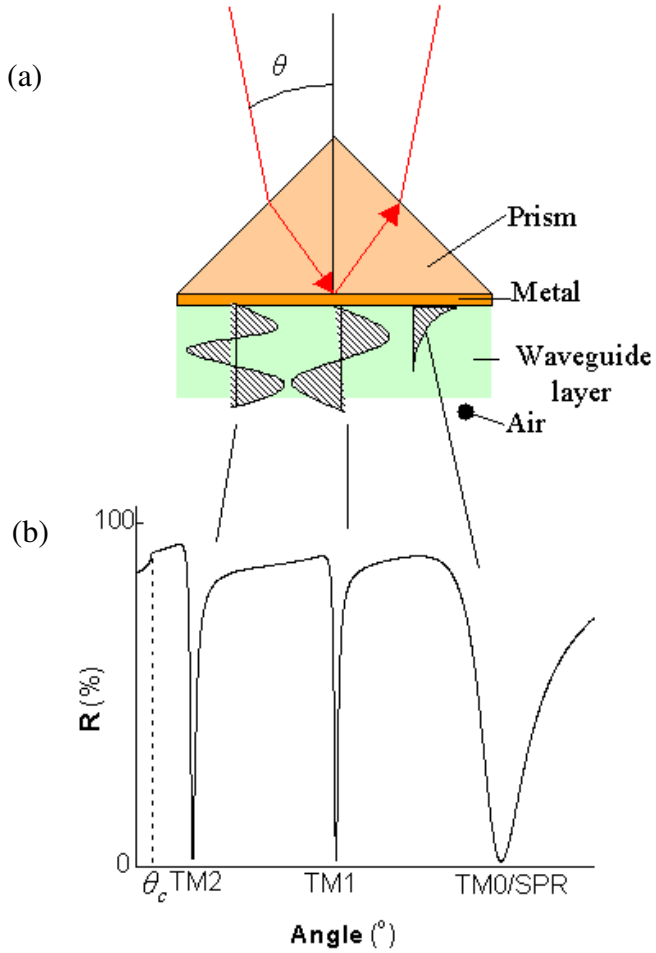

Scheme 2-4: (a) Schematic of waveguide mode excitation; (b) Waveguide modes can be seen in the reflectivity curve if one measures the reflectivity as a function of incident angle.

In order to better understand the phenomenon of guiding light in confined geometries, a basic theoretical approach (within Maxwell's theory) is given. For simplicity, a planar waveguide structure, the so called asymmetric slab configuration, is considered here, in which there is a solid high index substrate and a low index material as the superstrate, e.g., air or water. The thin waveguide layer (the film with refractive index n_2 and thickness d) is bound by the substrate (n_3) and the superstrate (e.g., air $n_1 = 1$). In order to obtain the total internal reflection at each interface, the waveguide material must fulfill two requirements: $n_1 < n_2$ and $n_3 < n_2$.

The waveguide modes are described by the eigenvalue equation with Maxwell's theory[14]:

$$k_{2z}d = \tan^{-1}\beta_{21} + \tan^{-1}\beta_{23} + m\pi \qquad (2.6)$$

Here m is the order of the guided mode. For a given set of materials and hence refractive index combinations (which determine $\tan^{-1}\beta_{21}$ and $\tan^{-1}\beta_{23}$ for a fixed optical frequency), the number of eigenmodes depends only on the thickness of the waveguide layer. For a given waveguide in a planar structure with a fixed thickness, if excited by a prism, the number of waveguide modes and their angular positions depends on the wavelength employed and the refractive index of the various layers. For an unknown waveguide film, this allows for the determination of the corresponding film parameters, i.e., the refractive index and the thickness. The optical field distribution for each eigenmode can be obtained according to Maxwell's equations. It should be noted that the optical field extends as an evanescent wave into both the substrate and the superstrate. It decays exponentially as a function of distance from the interface. For this asymmetric slab, it decays in asymmetric way.

Like SPR, the excitation of waveguide modes by light can be achieved only via a coupling device because the momentum (in the x-direction) of the waveguide modes is larger than that of the photons in free space. In the case of prism coupling, the projection of the photon wavevector at the base of the prism must be equal to the wavevector of the guided mode:

$$k_{x,m} = k_{ph} \cdot n_p \cdot \sin\theta \qquad (2.7)$$

with n_p being the refractive index of the prism. This requires a prism with an index higher than that of the waveguide material. The prism coupling conditions for the guided wave excitation are completely equivalent to the corresponding schemes for the SPR excitation.

Our configuration is somewhat special because the coupling of the laser light is obtained though the thin metal layer. In this geometry, the m = 0 mode is just the surface plasmon mode, as shown in Scheme 2-4. Its optical intensity reaches a maximum at the metal/waveguide interface and decays completely within the waveguide film. Therefore, SPR here is sensitive only to the refractive index of the waveguide film but not to its thickness. Other waveguide modes can be excited with either s-polarized or p-polarized light. For optically anisotropic media, they depend on all three indices, n_x, n_y, n_z, as well as the film thickness. This makes optical waveguide spectroscopy a sensitive probe for characterizing anisotropic films. Another important feature of our configuration is the fact that this geometry ensures that the guided light is constantly coupled out again through the prism so that the propagation length L_x is also reduced to a few μm. This is an important feature in waveguide microscopy.

The measured OWS curves are evaluated with the same fitting program as for SPR data. If more than one waveguide mode is detected in OWS, the refractive index and the thickness of the layer can be determined. It is an important advantage of OWS compared with SPR that both p-polarized and s-polarized light can be used in OWS, thus allowing for the characterization of anisotropic thin films.

2.2.4 Surface plasmon enhanced fluorescence spectroscopy

The excitation of a surface plasmon mode results in an enhanced optical field, which could be used to excite fluorophores located within the evanescent tail of the surface plasmon mode, resulting in a very strong fluorescence signal. The concept leads to surface plasmon enhanced fluorescence spectroscopy (SPFS).[15-17] The SPR evanescent field decays exponentially into the dielectric medium with a penetration depth of approximately L_x = 150 nm, which provides the surface sensitivity of SPFS. That is, only fluorophores adsorbed, adhered, or bound to the surface will be excited, while the fluorophores in the bulk solution will not be excited.

One important feature that needs to be taken into account when using SPFS is the fact that the metal is a very efficient quencher for chromophores in the immediate proximity of the metal surface. As schematically depicted in Scheme 2-5a, if the chromophore/metal separation distance is in the range of 5-10 nm, i.e., a typical distance for Förster energy transfer processes, all excitation energy is dissipated into the metal such that the dye molecules do not emit fluorescence photons. When the separation distance is increased to 10-20 nm (see Scheme 2-5b), complex interaction channels can be observed: the SPR excited chromophores can vibronically relax some of the electronic excitation, resulting in a red-shifted surface plasmon in the metal, upon the de-excitation of the dye. The red-shifted SPR mode can then reradiate, according to the dispersion curve of surface plasmons (at an emission angle slightly different from the resonant excitation angle) via the prism. Scheme 2-5c shows the ideal situation that the chromophores are separated from the metal at a certain distance. As a consequence, there is no loss in fluorescence intensity due to the quenching process in the metal, while at the same time the dyes are located close enough to the metal to be excited by the enhanced PSP field.

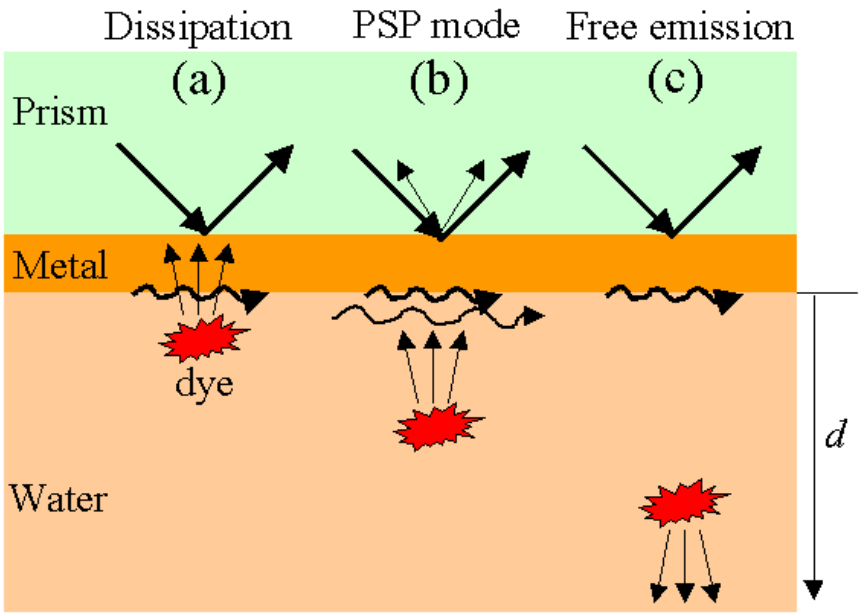

Scheme 2-5: Major decay channels for excited chromophores near metallic surfaces at different distances *d* to a metal surface. a).The chromophore is within a Förster radius (5-7 nm) and hence most of the fluorescence is dissipated in the metal. b). For a larger separation distances, the PSP mode excites the chromophore, but some of the red-shifted fluorescence light is coupled back to the metal, exciting an energetically lower-lying surface plasmon state. c). If the chromophore is placed further away, but still within the evanescent tail of the PSP mode, the normal de-excitation via emission of a fluorescence photon dominates.

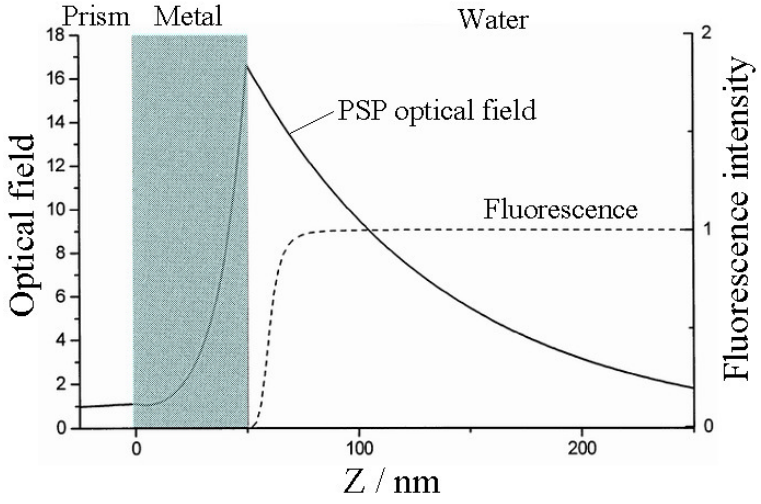

Figure 2-3: Intensity profile of a surface plasmon resonance mode with the evanescent field extending into the dielectric medium (water) in contact with (Au) metal layer and the relative fluorescence intensity of a chromophore placed at a certain distance above the metal/water interface.

The desired separation distance can be theoretically estimated as depicted in Figure 2-3. Noted that in this simulation a gold substrate is used, which results in an enhancement factor of about 16. The fluorescence is scaled to the intensity far away from the metal and plotted as a function of the separation distance. Within about two Forster radii, a significant quenching of the chromophores can be observed, resulting in a significant loss in fluorescence sensitivity. Above this separation distance, the enhanced optical field is only slightly lower than the maximum value, which is reached at the metal/dielectric interface. It has been shown experimentally that the fluorescence intensity reached the maximum value if the separation distance is about 30-50 nm.[18]

References

1. Boenig, H. V., *Fundamentals of Plasma Chemistry and Technology*. Technomic: Lancaster, PA, 1988.
2. Yasuda, H., *Plasma Polymerization*. Academic: Orlando, 1985.
3. König, H.; Helwig, G. *Z. Physik* **1951,** 129, 491-503.
4. Goodman, J. *J. Polym. Sci.* **1960,** 44, (144), 551-552.
5. Yasuda, H.; Hsu, T. *J. Polym. Sci., Polym. Chem.* **1977,** 15, 81-97.
6. Ryan, M. E.; Hynes, A. M.; Badyal, J. P. S. *Chem. Mater.* **1996,** 8, 37-42.
7. Förch, R.; Zhang, Z. H.; Knoll, W. *Plasma Process. Polym.* **2005,** 2, (5), 351-372.
8. Roucoules, V.; Fail, C. A.; Schofield, W. C. E.; Teare, D. O. H.; Badyal, J. P. S. *Langmuir* **2005,** 21, (4), 1412-1415.
9. Raether, H., *Surface Plasmons on Smooth and Rough Surfaces and on Gratings*. Springer-Verlag: Berlin, 1988.
10. Knoll, W. *Annu. Rev. Phys. Chem.* **1998,** 49, 569-638.
11. Otto, A. *Z. Phys.* **1968,** 216, 398-409.
12. Kretschmann, C.; Raether, H. *Z. Naturforsch.* **1968**, 2135-2136.
13. Asanuma, H.; Kashida, H.; Liang, X. G.; Komiyama, M. *Chem. Commun.* **2003**, (13), 1536-1537.
14. Tien, P. K. *Rev. Mod. Phys.* **1977,** 49, 361-407.
15. Liebermann, T.; Knoll, W. *Colloid. Surface. A* **2000,** 171, (1-3), 115-130.
16. Liebermann, T.; Knoll, W.; Sluka, P.; Herrmann, R. *Colloid. Surface. A* **2000,** 169, (1-3), 337-350.

17. Neumann, T.; Johansson, M. L.; Kambhampati, D.; Knoll, W. *Adv. Func. Mater.* **2002,** 12, (9), 575-586.

18. Vasilev, K.; Knoll, W.; Kreiter, M. *J. Chem. Phys.* **2004,** 120, (7), 3439-3445.

Chapter 3

Experimental Section

3.1 Materials and substrates

Most monomers used in plasma polymerization, such as di(ethylene glycol) monovinyl ether (98%), glycidyl methacrylate monomer (97%), and allylamine (99%), were purchased from Sigma-Aldrich, Germany. N,N-diethylacrylamide monomer (95%) was purchased from ABCR, Karlsruhe, Germany. Their chemical structures are given in Figure 3-1. The monomers were out gassed three times before use, but were not purified further.

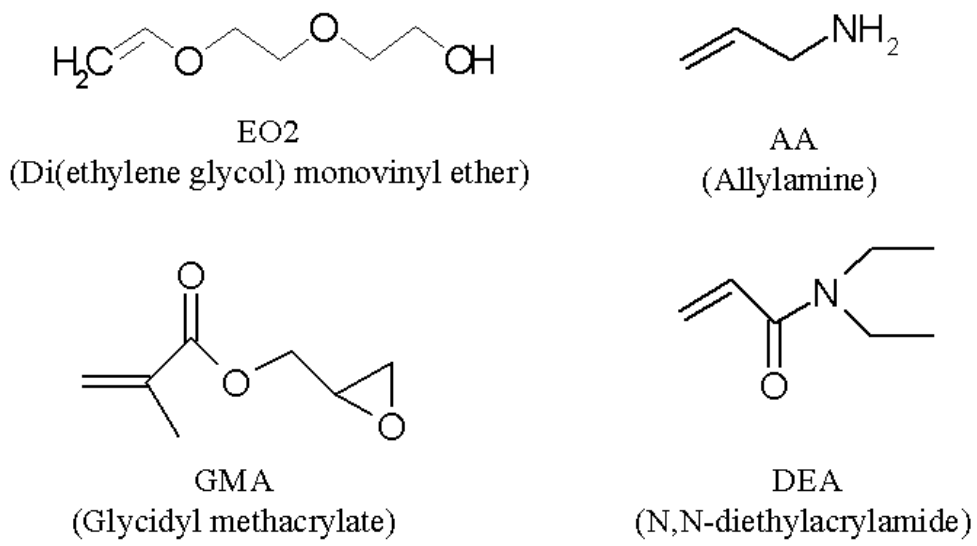

Figure 3-1: Chemical structure of the monomers used in the present work.

Bovine serum albumin (BSA) and Fibrinogen were also purchased from Sigma-Aldrich (Germany). Streptavidin was kindly provided by Roche Diagnostics GmbH. All protein and DNA solutions were prepared in phosphate buffered saline buffer (0.01 M with 0.0027M KCl and 0.137M NaCl at pH=7.4, Sigma-Aldrich). Milli-Q water was used throughout the experiments. All ssDNA used in this study were purchased from MWG Biotech, Ebersberg, Germany. The sequences chosen in this work were:

Probes: Biotin-DNA: 5'-Biotin-TTT TTT TTT TTT TTT TGT ACA TCA CAA CTA-3'

Biotin-DNA-Cy5: 3'-Biotin-TTT TTT TTT TTT TTT TGT ACA TCA CAA CTA-cy5-5'

NH_2-DNA: 5'-NH_2-C_6H_{12}-TTT TTT TTT TTT TTT TGT ACA TCA CAA CTA-3'

Targets: MM0 (complementary target): 3'-ACA TGT AGT GTT GAT-Cy5-5'

MM1 (single base pair mismatch): 3'-ACA TGC AGT GTT GAT-Cy5-5'

MM2 (two base pair mismatch): 3'-ACA TGC ACT GTT GAT-Cy5-5'

The substrates used for SPR, OWS and SPFS were LaSFN9 glass slides (n = 1.844 at λ = 633 nm, Hellma Optik, Jena, Germany). The LaSFN9 slides were cleaned with 2% Hellmanex detergent, rinsed extensively with water, then with ethanol, and finally dried thoroughly with pure nitrogen gas. A 2-nm chromium layer and a 50-nm gold layer were thermally evaporated onto the glass slides (Edwards FL400 evaporator). Here the chromium layer is used to enhance the adhesion of gold on the LaSFN9 glass. To ensure optimum adhesion of plasma polymers to the gold, a monolayer of 1-octadecanethiol (5 mM in ethanol, 10 min immersion) was self-assembled on the gold. Si wafers were used as the substrates for XPS measurements and water contact angle measurements. The plasma polymerized films for FT-IR measurements were deposited onto 30 x 25 mm glass slides coated with 80 nm gold. Both Si wafers and mica were used as the substrate for atom force microscopy (AFM) measurements.

3.2 Plasma polymerization

Plasma polymerization was carried out in a home-built capacitively coupled cylindrical radio frequency (13.56 MHz) plasma reactor, as depicted in Scheme 3-1. The reaction chamber, enclosed in a Faraday cage, consists of a cylindrical Pyrex tube, 30 cm in length and 10 cm in diameter. The plasma power is generated by a RF generator (Coaxial, RFG150), which passes through a matching network and is delivered to the reactor via a coil placed around the exterior of the reactor tube. The plasma can be run either in the continuous wave (CW) mode or in the pulsed mode. A home-built pulse generator is connected to the RF generator to allow pulsing of the radio frequency signal. The reaction chamber is

evacuated using a rotary pump (Leybold Trivac, D16B) and a liquid nitrogen cold trap is used to collect excess organic vapor. A baratron module (MKS, Type 627B) is connected near the inlet to monitor the pressure inside the chamber. Side arms at the reactor inlet allow for the introduction of gases such as oxygen, argon, and monomer vapors. A flask containing 10 ml of monomer liquid is attached to the plasma chamber via a valve. The flow rate of monomer vapor is controlled by a Kobold floating ball flowmeter.

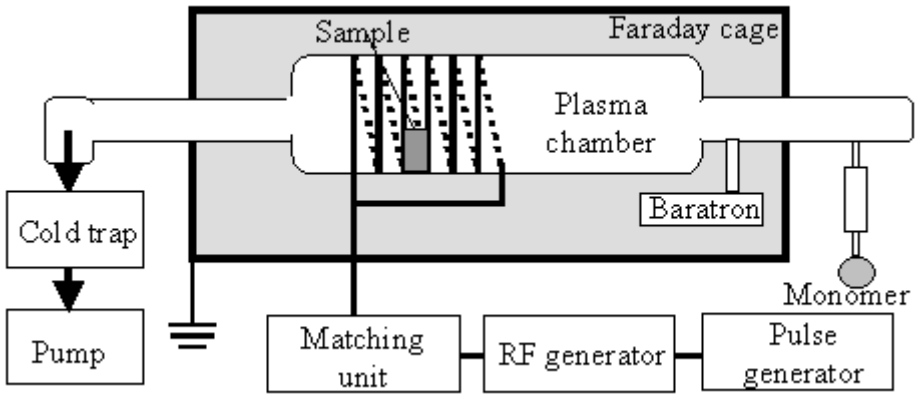

Scheme 3-1: Schematic representation of plasma polymerization system.

Substrates were placed on a glass holder and were put at a (approximately) fixed location inside the chamber, thus allowing for an identical plasma region for all depositions. Subsequently, the chamber was evacuated to a background pressure of 1×10^{-3} mbar. Then monomer vapor was introduced into the chamber at a certain pressure. After that, plasma was switched on and allowed to run for a certain time to provide sufficiently thick films for subsequent measurements. After completing the deposition, the plasma was switched off, and the chamber was flushed with monomer vapor for 5 min prior to venting up to atmosphere. The plasma chamber was cleaned via an air plasma for about 30 min at a power of 120 W. The power can be adjusted in a range from 0 to 150 W for the present system. In the pulsed plasma polymerization, the plasma-on time varies from 1-10 ms, while the plasma-off time ranging from 10 to 100 ms. The ratio of plasma-on time (t_{on}) to the sum of plasma-on time and -off time (t_{off}) is defined as duty cycle, i.e., $DC=t_{on}/(t_{on}+t_{off})$, which is an important parameter in pulsed plasma polymerization.

3.3 SPR and OWS measurements

SPR and OWS measurements were carried out with a home-built setup based on a Kretschmann configuration (see Chapter 2.2.2). The schematic description of the setup is depicted in Scheme 3-2. In brief, a HeNe laser beam (λ = 633 nm, JDS Uniphase, Model 1125p) is mechanically chopped at a frequency of 1150 Hz (PerkinElmer, Model 197) and then passes though two polarizers (Owis). The second polarizer generates a plane wave with the desired polarization, whereas, the first one is used for the attenuation of the laser. The reflected beam is collected and focused onto a photodiode (Spindler). The incident angle (θ) is varied by rotating the prism sample on a fine goniometer (Humber, 414a-10162) with an angle resolution of 0.001 degree. The collection lens and the detector are rotated by an angle of 2θ in order to catch the reflected light. The output of the photodiode circuit is sent to a lock-in amplifier (PerkinElmer, Model 7265) to demodulate the signal voltage. In this manner, reflectivity versus incident angle curve is obtained.

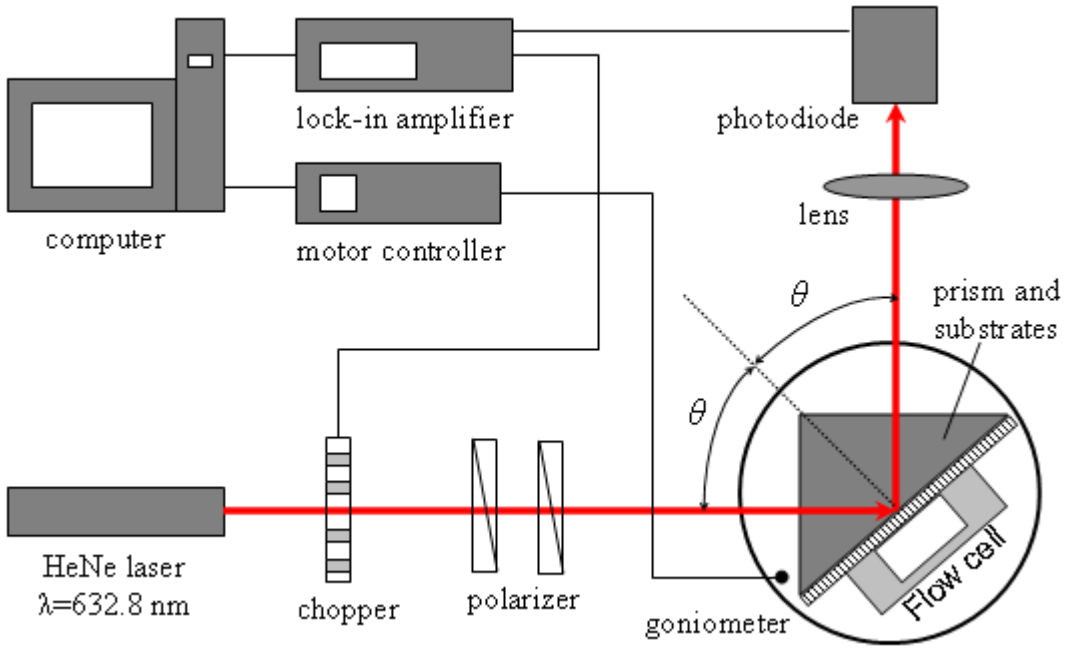

Scheme 3-2: Schematic representation of SPR and OWS setup.

As mentioned before, LaSFN9 glass slides (n = 1.844) were used as substrates for OWS and SPR measurements. On one side a 50 nm thick Au film was evaporated. The other

side of the glass slide was optically matched to the base of a 90° LaSFN9 glass prism by using a refractive index oil (n = 1.700, L-RIB-1162, Cargille lab, NJ). This allowed for the excitation of evanescent waves at the metal/dielectric interface, upon the total internal reflection of a laser beam at the prism base. The sample instalment was schematically depicted in Scheme 3-3. A peristatic pump (ISMATEC, Type: ISM596B) was employed to introduce the sample solution at a flow rate of 2 ml/min.

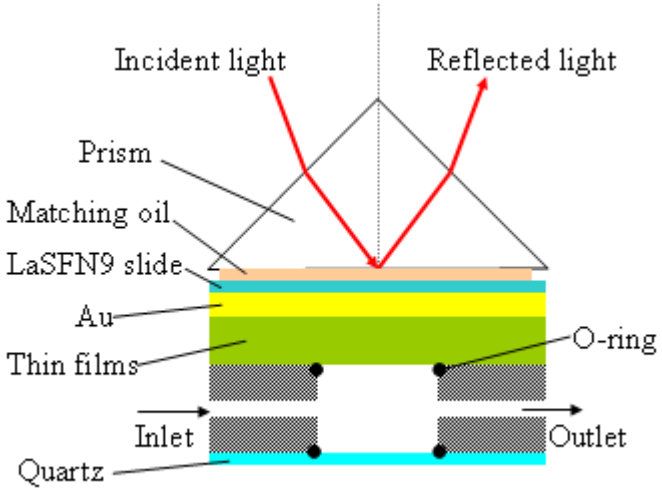

Scheme 3-3: Sample arrangement in SPR/OWS/SPFS measurements.

The usual reflectivity scan, i.e., reflectivity vs incident angle θ, was achieved by monitoring the reflected light intensity as a function of the incident angle. By comparing the calculated reflectivity curve (Fresnel calculation, using a simple box model) with the experimental data, the thicknesses and the refractive index of the sample can be determined. If the reflected intensity (at a fixed angle near the SPR angle) was recorded as a function of time, kinetic information about interfacial changes would be monitored. Another approach to obtain kinetic information was to follow the angle shift by tracking the minimum of a reflectivity dip, which is suitable for large angle shifts.

3.4 SPFS measurements

SPFS measurements were carried out with a home-built setup as depicted in Scheme 3-4. Briefly, a fluorescence detection system was added to a conventional SPR setup (Scheme 3-3). A computer-controlled shutter was mounted in the optical path in order to

minimize the photobleaching of the fluorophores. The emitted fluorescence light from the sample surface was collected by a photomultiplier tube (PMT, Hamamatsu), coupled to a photon counter (Hewlett-Packard). A lens (f = 40 mm, Owis) focused the light through an interference filter (λ=670 nm, Δλ=10 nm), which blocks the scattered and out-coupled excitation light. In the case where the fluorescence intensity is beyond the PMT's linear input-vs-output range (2.5 x 10^6 cps), an appropriate attenuator was added to adjust the light intensity. The whole fluorescence detection unit was mounted on a goniometer such that its position was fixed relative to the sample. In the present SPFS system, both SPR reflectivity and the fluorescence intensity could be recorded simultaneously. Instrument control and data acquisition were handled by a computer. The kinetic measurements were done by recording the fluorescence intensity as a function of time at a fixed incident angle. For DNA hybridization measurements, the DNA sensor was attached to a flow cell for liquid exchange, which was covered by a quartz glass window with a low intrinsic fluorescence background.

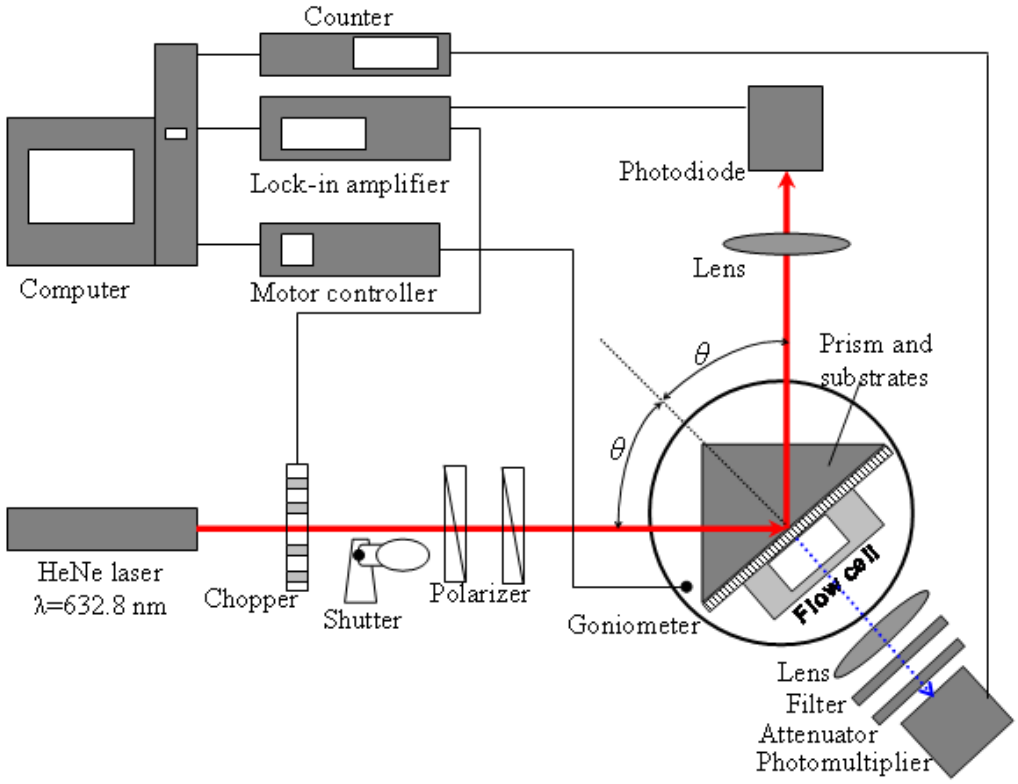

Scheme 3-4: Schematic of SPFS setup.

3.5 Other characterization techniques

3.5.1 Fourier transform infrared spectroscopy

FT-IR measurements were carried out using a Nicolet 850 spectrometer operated in the reflection mode. An Au-coated glass slide, as a referee, was also putted on the sample stage. The chamber was flushed with Nitrogen gas for ca. 15 min in order to eliminate the CO_2 adsorption. FT-IR spectra were recorded at a resolution of 4 cm^{-1}.

3.5.2 X-ray Photoelectron Spectroscopy

XPS measurements were carried out using a Physical Electronics 5600 A instrument. The Mg K_α (1253.6 eV) X-ray source was operated at 300 W. A pass energy of 117.40 eV was used for the survey spectrum. The spectra were recorded using a 45° take off angle relative to the surface normal. The XPS detailed scan was analysised using MultiPak 5.0 and XPSPeak 4.1.

3.5.3 Atomic force microscopy

AFM measurements were carried out using Veeco Dimension 3100 instrument in the tapping mode in ambient air. The surface roughness for a certain area was obtained using standard AFM software (Nanoscope 6.11r1). In order to measure the film thickness, the sample was scratched with a needle in order to obtain a step. AFM measurements at different temperatures were carried out using a EnviroScope atomic force microscopy (Veeco). The sample can be heated in situ on the stage of EnviroScope AFM, allowing for measurements at different temperature but at the identical position.

3.5.4 Contact angle measurements

The static water contact angle measurements were carried out on a DSA 10-MK2 (Krüss), equipped with a thermostat chamber (TC3010, Krüss). A vessel containing pure water was put into the chamber in order to obtain higher humidity.[1,2] Measurements were taken every 2-5°C from 20 to 60°C. The sample was equilibrated at each temperature for 20 minutes. Five sample positions were measured at each temperature.

References

1. Rao, G. V. R.; Krug, M. E.; Balamurugan, S.; Xu, H. F.; Xu, Q.; Lopez, G. P. *Chem. Mater.* **2002,** 14, (12), 5075-5080.
2. Zhang, J.; Pelton, R.; Deng, Y. L. *Langmuir* **1995,** 11, (6), 2301-2302.

Chapter 4

Non-Fouling Coatings by Plasma Polymerization*

4.1 Introduction

Prevention of nonspecific protein adsorption continues to be a challenge in the application of polymeric materials in a variety of fields, such as in biomedical device, for membrane separation, biosensors, etc. Many efforts have thus been put into the modification of polymer surfaces in order to render them resistant against protein adsorption. Surface modification with polyethylene glycol (PEG) (or polylethylene oxide (PEO)) is well known as an effective method to reduce protein adsorption and cellular adhesion.[1-3] The protein resistant properties of PEG coating are generally ascribed to steric repulsion effects,[4,5] which originate from the hydrophilicity and flexibility of the PEG chains. This explanation is particularly suitable for those systems with long PEG chains. Previous theoretical and experimental work has shown that the non-fouling performance of PEG coatings is proportional to the length and the density of PEG chains.[4,6,7] On the other hand, the hydration of PEG leads to a layer of tightly bound water molecules around the PEG chain, a so-called shielding layer.[8-11] This water layer is also believed to play an important role in preventing protein adsorption and may explain why densely packed, shorter OEG-SAMs (oligo(ethylene glycol) self-assembled monolayers) also show non-fouling properties.[12-14]

Various strategies for PEG attachment onto surfaces have been investigated, including graft polymerization,[6,15] self-assembly of monolayers (SAM),[14,16,17] as well as simple adsorption. Physical adsorption has a problem in long-term stability due to detachment, delamination and desorption. SAM of thiols are limited to only a few substrates, e.g. noble metals such as Au and Ag. Other strategies involve several steps of wet chemical reactions. Recently, several groups[18-26] have demonstrated that plasma polymerization provides a new possibility for achieving non-fouling surfaces. Plasma polymerization of PEO containing molecules resulted in coatings with abundant PEO, which gave them excellent non-fouling properties.

While previously only thicker (d > 30 nm) films were studied,[21] the objective of the present study was to investigate the protein adsorption behavior on a series of plasma

* Part of the work in this chapter has been published in *Chem. Mater*. **2006**, 18, 4840-4844.

polymerized non-fouling films with thicknesses ranging from 1-10 nm. Di(ethylene glycol) monovinyl ether (EO2) was used as the monomer in the pulsed plasma polymerization process. BSA and fibrinogen were employed in this work to test non-fouling properties of the deposited pp-EO2 films. SPR is a very sensitive and label-free technique for detection of protein adsorption[21,27,28] and thus was employed in this work. SPR can quantify the protein adsorption in real time with high sensitivity and can be used to estimate the thickness of protein layers adsorbed on the surface by fitting the SPR curve based on Fresnel's equation.

4.2 Experimental section

4.2.1 Preparation of pp-EO2 films

Plasma polymerization was carried out using a home-built setup, as described in Chapter 3. The pp-EO2 films were deposited at 20 W with various duty cycles (DCs), i.e. 5/100 and 1/100 ms, respectively. The monomer pressure varied from 0.01 to 0.05 mbar. The deposition time was adjusted to obtain the desired thickness. Mica here was used as substrate for AFM measurements since mica provides an atomically flat surface.

4.2.2 Protein adsorption measured by SPR

The protein solutions were prepared immediately before use by dissolving BSA and Fibrinogen into phosphate buffered saline (PBS) solutions at a concentration of 10 wt %. SPR measurements were carried out with a home-built setup (see Chapter 3), which was based on the Kretschmann configuration. In order to measure protein adsorption in real time, the pp-EO2 sample was attached to a SPR flow cell immediately after plasma polymerization. PBS buffer was introduced into the flow cell in order to stabilize the film. Then protein solution was injected into the cell. The kinetics of protein adsorption can be obtained by monitoring the reflectivity at a fixed angle. After the protein adsorption reached equilibrium, PBS buffer was injected again to rinse the surface. SPR spectra were recorded before and after protein adsorption in order to determine the thickness of adsorbed layer. The SPR spectrum, i.e. the reflectivity vs. angle curve, can be fitted using Fresnel's equation to obtain the optical thickness ($n*d$) of the dielectric medium. If the refractive index of the thin film is available, one can determine the geometrical thickness of the film. The refractive index for BSA and fibrinogen used here are 1.45 and 1.39, respectively.[21, 29] The

experimental results for protein adsorption were presented in terms of surface density, which can be calculated using de Feijter's equation:[30]

$$M = d_A \frac{n_A - n_{sol}}{dn/dc} \qquad (4.1)$$

Here d_A is the thickness of the adsorbed layer and dn/dc is the refractive index increment of the molecules. n_A and n_{sol} are refractive index of adsorbed layer and cover media, respectively. For proteins, the dn/dc is equal to approximately 0.182 g/cm^3. [29, 30]

4.3 Results and discussion

4.3.1 Film analysis

Based on the experience in previous work in this group, 20 W input power and low duty cycles (from 5/100 to 1/100) were employed to ensure that the resulting pp-EO2 films exhibit good protein resistance for thicknesses larger than 30 nm. The non-fouling properties of these pp-EO2 films were confirmed by SPR experiments (data not shown here). While many reports generally investigate antifouling properties with respect to the density of the ether functional group, there are no reports relating this issue to the thickness of the film studied.

In order to investigate protein binding as a function of film thickness low DC antifouling EO2-films were deposited onto a gold coated glass substrates for SPR measurements. By adjusting the deposition time, the thickness of pp-EO2 coating can be well controlled. Figure 4-1 gives the SPR results for the determination of d in air. The deposition rate for the low DC pp-EO2 was calculated to be 0.024 nm/sec.

The chemistry of pp-EO2 films could be tailored by varying the plasma power and the duty cycle employed. Figure 4-2 shows the FT-IR spectra of the pp-EO2 films deposited at different plasma conditions. It is apparent that the IR bands for the ether group (C-O-C) at 1138 cm^{-1} and the –OH group at 3453 cm^{-1} can be observed for the pulsed plasma polymerized films, indicating a good retention of monomer structures. In contrast, the two bands are relatively weak for the pp-EO2 films deposited at a CW plasma mode. This can be ascribed to the higher fragmentation occurring during CW plasma processes. Upon reducing

the DC from 5/100 to 1/100, the IR absorption at 1138 cm^{-1} shows a small increase, suggesting that a higher structural retention occur under a lower DC condition. These results are in good agreement with previous work done in this group.

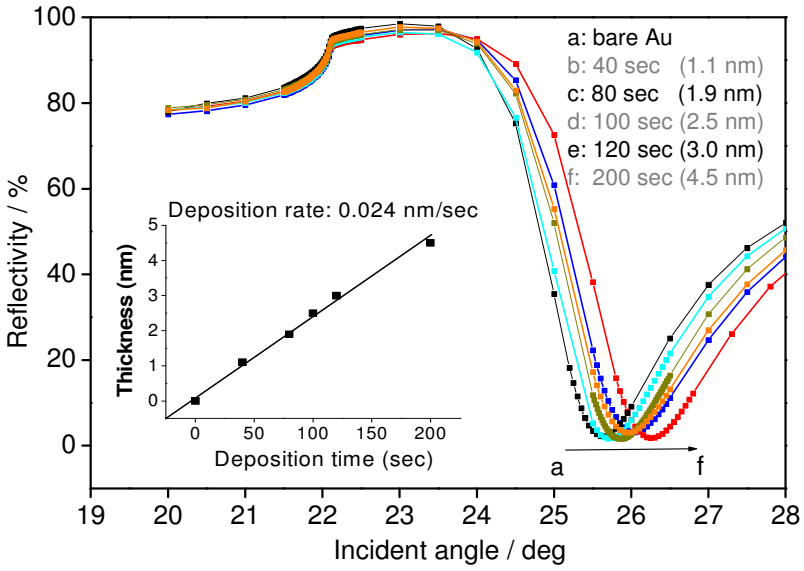

Figure 4-1: SPR data showing the thickness evolution over exposure time to the plasma, giving a deposition rate of 0.024 nm s^{-1}. The refractive index of the polymer layer was taken to be 1.451.

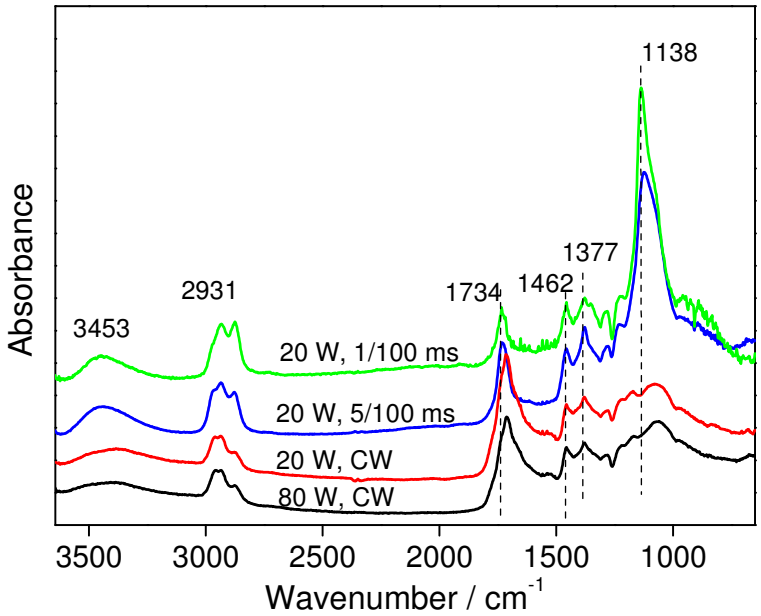

Figure 4-2: FT-IR spectra of the pp-EO2 films deposited at different conditions.

Furthermore, the surface composition of pp-EO2 films was characterized using XPS. Figure 4-3 gives the XPS C1s spectra of the pp-EO2 films deposited at different duty cycles, i.e. 5/100 and 1/100 ms, respectively. The C1s spectra clearly show two peaks at 285 eV and 286.5 eV, which can be attributed to C-C and C-O-C functional groups, respectively. It is evident that a high retention of ether groups was achieved at these plasma conditions. As the DC was decreased, the relative C-O-C peak intensity (at 286.5 eV) increased, indicating more ether groups in the deposited films. The retention of ether group can also be confirmed from the O/C as determined from XPS wide scan (Table 4-1). The O/C ratio of pp-EO2 deposited at a duty cycle of 5/100 ms is 0.44. If duty cycle is decreased to 1/100 ms, the O/C ratio increased to 0.5, which is the theoretical value for the monomer molecule.

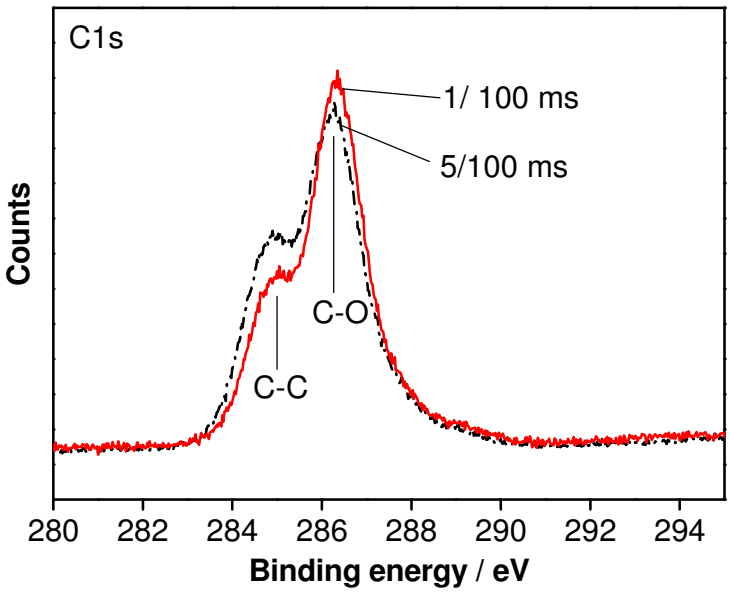

Figure 4-3: XPS C1s spectra of pp-EO2 films deposited at different duty cycles (as indicated).

Table 4-1: Surface composition from XPS measurements for a series of pp-EO2 films deposited at various duty cycles. Plasma power is 20 W.

Sample	%C	%O	O/C
5/100 ms	69.3	30.7	0.44
1/100 ms	66.5	33.5	0.50
Theoretical	66.7	33.3	0.50

AFM was utilized to study the surface morphology of pp-EO2 films with thicknesses ranging from 2 to 20 nm. The AFM images of the pp-EO2 films with different thicknesses are shown in Figure 4-4, with mica being also shown as a control. The surface roughness can easily be obtained using standard AFM software. It is found that there is no significant change in surface roughness with increasing film thickness. The roughness of pp-EO2 with less than 3 Å is comparable to that of the bare substrate regardless of the film thickness, indicating that the plasma polymerized films were very flat. It was previously suggested that plasma films only cover the substrate surface completely when thickness d > 5 nm, while for very thin films, island formation dominates the process.[31, 32] The island formation would however lead to some increase in roughness, which is not observed. Hence, AFM results seems to suggest that already a 2 nm thick pp-EO2 film covers the substrate completely. Additionally, it should be noted that the roughness of a 2 nm thick pp-EO2 is 1.9 Å, which is much lower than the film thickness. This also supports the hypothesis that 2 nm thick pp-EO2 already covers the substrate completely. One likely explanation for the present results is that the pp-EO2 films was deposited onto the substrate very slowly and, hence, the plasma film was deposited evenly onto the substrate.

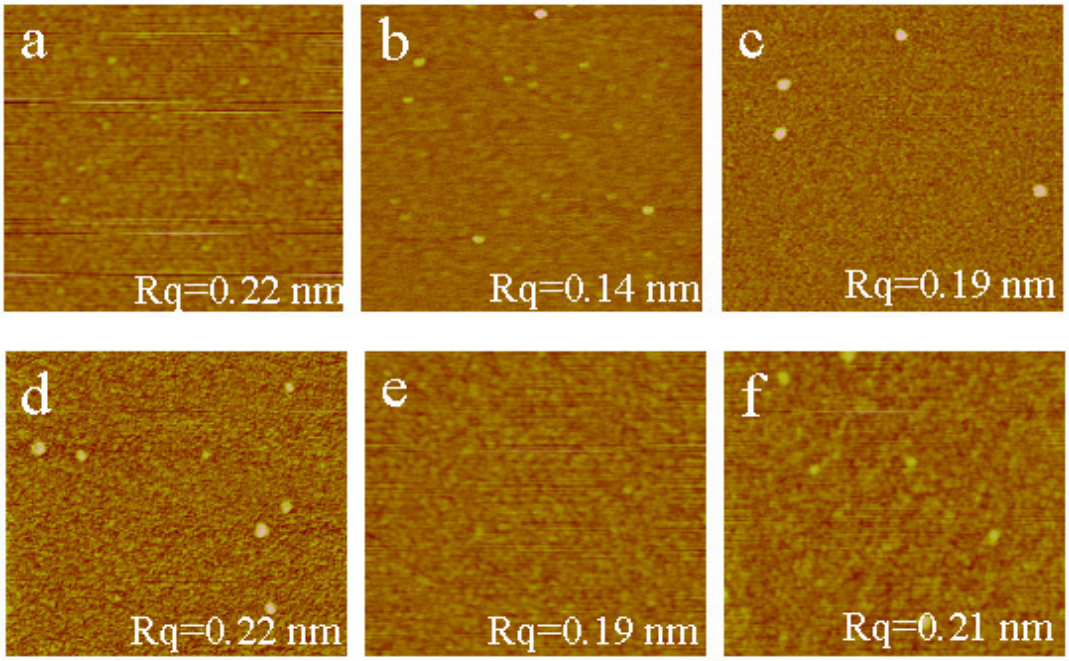

Figure 4-4: Tapping mode AFM images of pp-EO2 films with increaseing thickness taken in ambient air. (a): bare mica as control; (b): 1.7 nm; (c): 3.4 nm; (d): 7.9 nm; (e): 17.1 nm; (f): 32.9 nm. The scan area is 1 x 1 μm^2 in each case. The thickness of the pp-EO2 films was measured by SPR. Plasma conditions: 20 W, 5/100 ms.

The pp-EO2 films with thicknesses ranging from 1 to 30 nm were also deposited onto silicon wafer for the static water contact angle measurements. While the water drop can easily spread on the surface of the present silicon wafer, the pp-EO2 coating shows a contact angle of 50-60 deg (Figure 4-5). The hydrophilic nature of the pp-EO2 coatings may be explained by the presence of hydroxyl groups in the deposited films, as indicated in FT-IR results. Note it is surprising that the contact angle of 1 nm thick pp-EO2 coatings was almost at same level as that for the film of 22 nm thick. It appears that such thin coating is already able to cover the substrate completely.

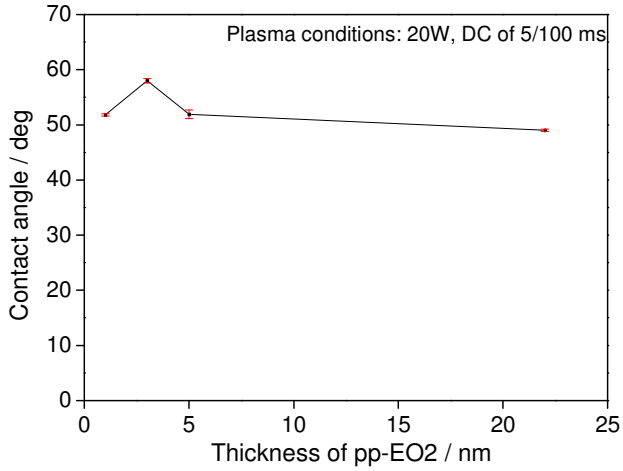

Figure 4-5: Water contact angle of pp-EO2 coatings with different thicknesses.

4.3.2 Protein adsorption measured by SPR

Protein adsorption on the pp-EO2 films was measured in real time using the SPR kinetic mode. The kinetics of BSA and fibrinogen adsorption onto pp-EO2 films of different thickness are given in Figure 4-6. There is a clear correlation between protein adsorption and the thickness of the pp-EO2 film. With increasing film thickness, the adsorption of both proteins onto the surface decreases, and drops to almost zero after rinsing for pp-EO2 film thicknesses exceeding a threshold value. Figure 4-7 shows the surface density of BSA adsorbed onto pp-EO2 as a function of the film thickness. For BSA and pp-EO2 deposited at DC of 1/100 ms, the threshold value is about 2-3 nm.

A

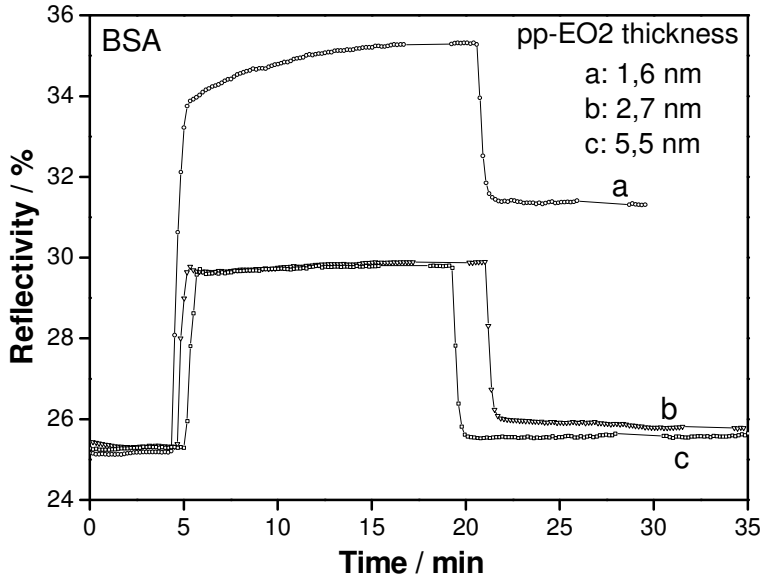

B

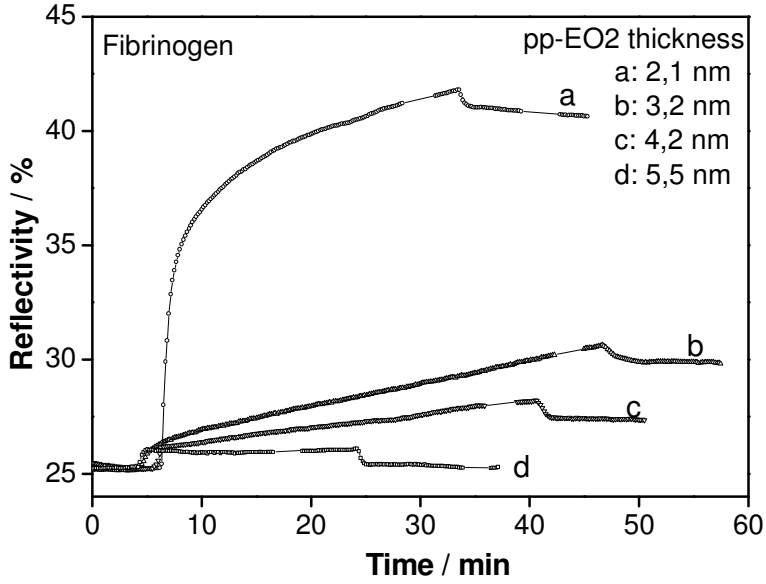

Figure 4-6: Kinetics of protein adsorption on pp-EO2 films with different thicknesses. (A) BSA; (B) Fibrinogen. Plasma conditions: 20 W, 1/100 ms.

In order to test the effect of the pp-EO2 surface chemistry on the BSA adsorption, pp-EO2 deposited at DCs of 5/100 ms and 1/100 ms, respectively, were compared in Figure 4-7. Clearly, with decreasing DC, less BSA adsorption was observed for pp-EO2 film with identical thickness.

The adsorption of a larger protein, i.e. fibrinogen, onto the pp-EO2 films of different thickness is given in Figure 4-8. As the pp-EO2 thickness increased, less fibrinogen adsorbed to the surface. It can be noticed that pp-EO2 prepared at DC of 5/100ms cannot resist fibrinogen adsorption completely in the present thickness range. For the surface prepared at 1/100 ms, 5-6 nm would be required to resist fibrinogen adsorption. Consequently, it appears that the duty cycle employed has a strong influence on the fibrinogen adsorption behavior.

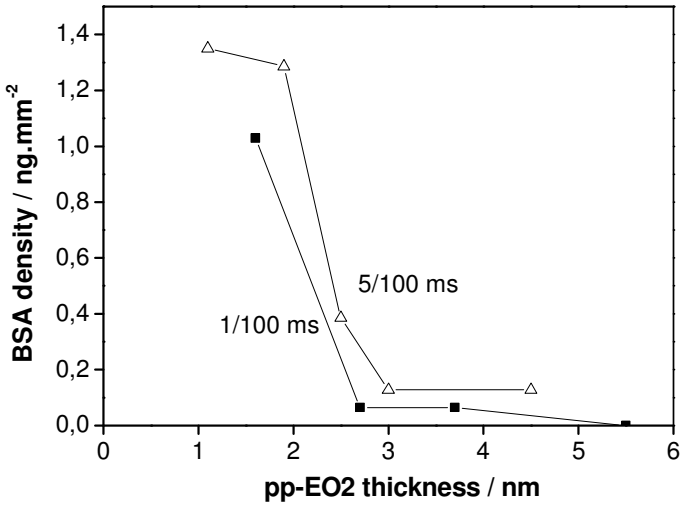

Figure 4-7: BSA adsorption on pp-EO2 films deposited at different duty cycles.

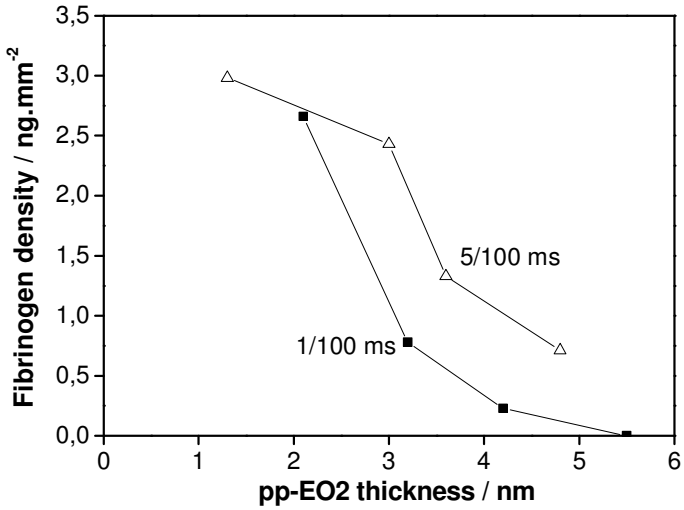

Figure 4-8: Fibrinogen adsorption on pp-EO2 films deposited at different duty cycles.

Figure 4-9 shows a comparison of BSA and fibrinogen adsorption onto pp-EO2 films deposited at a DC of 1/100 ms. The adsorption of both proteins on bare Au is also given as a reference. The amount of BSA adsorbed on bare Au is calculated to correspond to a surface density of 225 ng/cm^2, which is in agreement with previous reports.[19] From Figure 4-9, it can be found that thicker pp-EO2 (i.e. ca 5.5 nm thick) is required to resist fibrinogen adsorption compared to only ca. 2.5 nm for BSA. Additionally, the number of BSA molecules adsorbed on Au is higher than fibrinogen. This result may be related to the size of the proteins: BSA molecules are 68 500 Daltons, which is much lower than fibrinogen molecules with their 340 000 Daltons. It has been documented that protein adsorbed on Au would form a monolayer.[27] On the other hand, after coating Au with a 3 nm thick pp-EO2 film, fibrinogen still adsorbs readily, whereas BSA does not. This indicates that the size of the protein is not the reason for the different behavior of BSA and fibrinogen on a 3 nm thick pp-EO2. Vert et al.[33] reported that albumin and PEG are compatible in PBS buffer at room temperature, whereas fibrinogen and PEG are incompatible and show phase-separation in solution. They proposed that the compatibility of PEG segments to albumin account for the stealth behavior of PEG bearing molecules or surfaces.

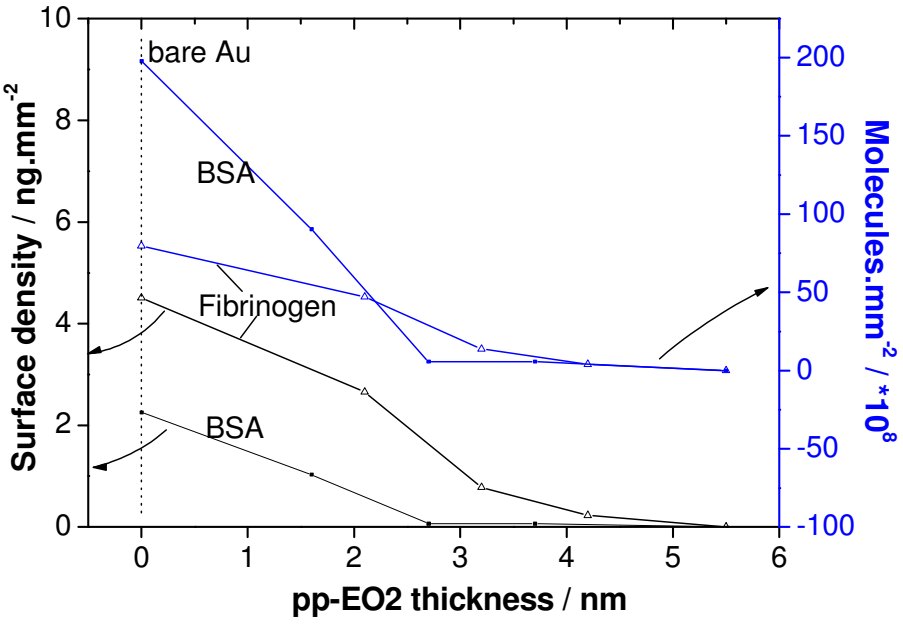

Figure 4-9: Comparison of BSA and Fibrinogen adsorption on pp-EO2 films with increasing thickness. Plasma conditions: 20 W, 1/100 ms.

4.3.3 Discussion

Based on the experimental results, it appears that there is a correlation between the pp-EO2 film thickness and its protein resistant properties. A threshold value for pp-EO2 thickness seems to exist, which is approximately 3 nm for BSA and 6 nm for fibrinogen, respectively. Several possibilities may account for this phenomenon.

1). Defects in the pp-EO2 coatings. If the substrate is not covered completely by thin pp-EO2 coating, proteins may adsorb onto the substrate (Au in the present case) at defect sites.

2). Diffusion of proteins into the swollen pp-EO2 film. Proteins would diffuse into the pp-EO2 films and approach the underlying substrate, which is active for protein adsorption.

3). A certain thickness is required because more EO units exist in the thicker pp-EO2 coating. It is possible that only for films with an mount of EO units higher than a threshold value, a water barrier layer, which was regarded as the "functional layer" to resist protein adsorption, can form on the pp-EO2 deposit.

The protein adsorption due to defects should be related to the size of the protein molecules. However, as mentioned in Figure 4-9, the ability of pp-EO2 films to resist protein adsorption is not size selective. Moreover, AFM data in Figure 4-4 suggest a complete coverage of the substrate by a pp-EO2 film of 2 nm thickness. Consequently, it is believed that the defect in the thin pp-EO2 film is not the cause for protein adsorption, provided the pp-EO2 coating is thicker than 2 nm.

Protein diffusion through the thin PEG layer has been proposed as an explanation for the protein adsorption on the PEG coating with long PEG graft chains.[15] The swelling of pp-EO2 film may lead to some diffusive pathways for proteins. The results in the next chapter also shown that biotin molecules can pass through a 5.5 nm thick pp-EO2 coating. Therefore, diffusion of protein or parts of a protein may account for some adsorption. However, this cannot explain why the bigger protein (i.e., fibrinogen) rather than the smaller BSA would adsorb onto 4 nm thick pp-EO2 films as shown in Figure 4-9.

As indicated before, the higher amount of EO units in the low DC pp-EO2 is the reason why BSA and fibrinogen show a reduced protein adsorption deposited at lower duty cycles. The thicker the pp-EO2 coating, the larger the number of EO units. Since the EO units provide a molecular basis for a water barrier layer, the thin pp-EO2 cannot generate a sufficient barrier, in contrast to thicker pp-EO2 films. The density of EO units in the film may also explain why BSA and fibrinogen behave differently with respect to the pp-EO2

surface chemistry and film thickness. Considering the incompatibility of fibrinogen with the PEG segments, more EO units are required to resist fibrinogen adsorption. In contrast, BSA is compatible with PEG and thus requires less EO units.

4.4 Conclusions

The aim of this work was to investigate the non-fouling properties of ultra-thin pp-EO2 films with thickness lower than 10 nm, providing more insights onto the relationship between the structure of pp-EO2 coatings and their ability to resist protein adsorption. XPS results showed that the pp-EO2 deposited at duty cycles of 1/100 ms consisted of a high amount of ether groups. These pp-EO2 coatings show excellent resistance to BSA and fibrinogen provided that their thicknesses are higher than a threshold value. A thicker film of pp-EO2 was required to resist absorption of fibrinogen than of BSA suggesting that the threshold is not size selective, and the mount of EO units in the pp-EO2 film is of great importance for the protein resistance of surfaces.

References

1. Harris, J. M., *Poly(ethylene glycol) Chemistry: Biotechnical and Biomedical Applications*. Plenum Press: New York, 1992.
2. Kingshott, P.; Griesser, H. J. *Curr. Opin. Solid State Mat. Sci.* **1999,** 4, (4), 403-412.
3. Castner, D. G.; Ratner, B. D. *Surf. Sci.* **2002,** 500, (1-3), 28-60.
4. Jeon, S. I.; Lee, J. H.; Andrade, J. D.; Degennes, P. G. *J. Colloid Interface Sci.* **1991,** 142, (1), 149-158.
5. Jeon, S. I.; Andrade, J. D. *J. Colloid Interface Sci.* **1991,** 142, (1), 159-166.
6. Kingshott, P.; Thissen, H.; Griesser, H. J. *Biomaterials* **2002,** 23, (9), 2043-2056.
7. McPherson, T.; Kidane, A.; Szleifer, I.; Park, K. *Langmuir* **1998,** 14, (1), 176-186.
8. Wang, R. L. C.; Kreuzer, H. J.; Grunze, M. *J. Phys. Chem. B* **1997,** 101, (47), 9767-9773.
9. Feldman, K.; Hahner, G.; Spencer, N. D.; Harder, P.; Grunze, M. *J. Am. Chem. Soc.* **1999,** 121, (43), 10134-10141.
10. Pertsin, A. J.; Grunze, M. *Langmuir* **2000,** 16, (23), 8829-8841.
11. Heuberger, M.; Drobek, T.; Voros, J. *Langmuir* **2004,** 20, (22), 9445-9448.

12. Harder, P.; Grunze, M.; Dahint, R.; Whitesides, G. M.; Laibinis, P. E. *J. Phys. Chem. B* **1998,** 102, (2), 426-436.
13. Li, L. Y.; Chen, S. F.; Jiang, S. Y. *Langmuir* **2003,** 19, (7), 2974-2982.
14. Li, L. Y.; Chen, S. F.; Zheng, J.; Ratner, B. D.; Jiang, S. Y. *J. Phys. Chem. B* **2005,** 109, (7), 2934-2941.
15. Wang, P.; Tan, K. L.; Kang, E. T. *J. Biomater. Sci. Polym. Ed.* **2000,** 11, (2), 169-186.
16. Palegrosdemange, C.; Simon, E. S.; Prime, K. L.; Whitesides, G. M. *J. Am. Chem. Soc.* **1991,** 113, (1), 12-20.
17. Prime, K. L.; Whitesides, G. M. *J. Am. Chem. Soc.* **1993,** 115, (23), 10714-10721.
18. Beyer, D.; Knoll, W.; Ringsdorf, H.; Wang, J. H.; Timmons, R. B.; Sluka, P. *J. Biomed. Mater. Res.* **1997,** 36, 181-189.
19. Mar, M. N.; Ratner, B. D.; Yee, S. S. *Sens. Actuators B: Chem.* **1999,** 54, (1-2), 125-131.
20. Wu, Y. L. J.; Timmons, R. B.; Jen, J. S.; Molock, F. E. *Colloids Surf. B* **2000,** 18, (3-4), 235-248.
21. Zhang, Z.; Menges, B.; Timmons, R. B.; Knoll, W.; Forch, R. *Langmuir* **2003,** 19, (11), 4765-4770.
22. Johnston, E. E.; Bryers, J. D.; Ratner, B. D. *Langmuir* **2005,** 21, (3), 870-881.
23. Shen, M. C.; Martinson, L.; Wagner, M. S.; Castner, D. G.; Ratner, B. D.; Horbett, T. A. *J. Biomater. Sci. Polym. Ed.* **2002,** 13, (4), 367-390.
24. Sardella, E.; Gristina, R.; Ceccone, G.; Gilliland, D.; Papadopoulou-Bouraoui, A.; Rossi, F.; Senesi, G. S.; Detomaso, L.; Favia, P.; d'Agostino, R. *Surf. Coatings Technol.* **2005,** 200, (1-4), 51-57.
25. Sardella, E.; Gristina, R.; Senesi, G. S.; d'Agostino, R.; Favia, P. *Plasma Process. Polym.* **2004,** 1, (1), 63-72.
26. Bremmell, K. E.; Kingshott, P.; Ademovic, Z.; Winther-Jensen, B.; Griesser, H. J. *Langmuir* **2006,** 22, (1), 313-318.
27. Green, R. J.; Davies, J.; Davies, M. C.; Roberts, C. J.; Tendler, S. J. B. *Biomaterials* **1997,** 18, (5), 405-413.
28. Green, R. J.; Frazier, R. A.; Shakesheff, K. M.; Davies, M. C.; Roberts, C. J.; Tendler, S. J. B. *Biomaterials* **2000,** 21, (18), 1823-1835.
29. Voros, J. *Biophysical J.* **2004,** 87, (1), 553-561.
30. de Feijter, J. A.; Benjamins, J.; Veer, F. A. *Biopolymers* **1978,** 17, 1759-1772.

31. Jacobsen, V.; Menges, B.; Scheller, A.; Förch, R.; Mittler, S.; Knoll, W. *Surf. Coat. Technol* **2001,** 142-144, 1105-1108.

32. Jacobsen, V.; Menges, B.; Förch, R.; Mittler, S.; Knoll, W. *Thin Solid Films* **2002,** 409, 185-193.

33. Vert, M.; Domurado, D. *J. Biomater. Sci. Polym. Ed.* **2000,** 11, (12), 1307-1317.

Chapter 5

Protein-Resistant DNA Sensor*

5.1 Introduction

DNA sensors based on a surface attached single-stranded catcher oligonucleotide continue to attract a lot of attention due to their potential applications, such as medical diagnosis, food control, and environmental monitoring.[1-4] The efficiency and the kinetics of hybridization reactions between DNA catchers (also known as DNA probes) and a complementary target DNA depend on many factors, such as the ionic strength of the buffer, the steric accessibility of the surface attached catchers and the degree of mismatch.[5] Many of these fundamental aspects have been investigated. DNA probe immobilization via a streptavidin-biotin coupling has proved to be very successful in commercial DNA sensors.[6, 7]

For biosensor applications, the non-specific interaction of other body fluid constituents in realistic sample mixtures may interfere at the sensor surface and reduce the performance of the biosensor. Despite many advances in biosensor development, it is still a challenge to create a novel interface, which allows for the detection of some specific molecules by a biosensor, but at the same time prevents the unspecific adsorption of body fluid constituents such as proteins, e.g. antibodies and even cells. Therefore, the present work was to develop an interface, which uses the well-known biotin-streptavidin immobilization procedure and an antifouling layer as the uppermost layer. The resulting interface permits interactions of the embedded streptavidin with biotinylated molecules from solution, but at the same time reduces, or inhibits, non-specific interactions of proteins at the sensor surface. This has previously been studied by Miyachi et al using HMDSO/ O_2 plasma polymer to minimize the nonspecific binding of BSA to the substrate in DNA microarrays.[8, 9]

As discussed in Chapter 4, pp-EO2 coatings show excellent antifouling properties towards proteins. Even small deviations from the low duty cycle conditions and all continuous wave conditions, however, lead to a fouling polymer surface which will readily bind proteins. The minimum thickness of a ppEO2 coating required to resist BSA and fibrinogen adsorption was found to be only 3 and 5.5 nm, respectively, depending on the plasma conditions. It appears possible to use such thin nonfouling coatings to coat a

* Part of the work in this chapter has been published in *Plasma Processes Polym.* **2006**, 3, 498-505.

"reactive" surface (e.g., a surface bound streptavidin monolayer) such that the underlying reactive-, or embedded sites, are still available for the immobilization of other selected molecules. In order to test this, a multilayer system was designed, as shown in Scheme 5-1. In the present work Au-coated LaSFN9 was used as substrates because SPFS was utilized to monitor the binding and hybridization events. A fouling pp-EO2 layer was firstly deposited to Au/LaSFN9 as the separation layer. Streptavidin molecules were then placed on the fouling layer, and were embedded within an extremely thin antifouling layer. By careful control of process conditions, the streptavidin was found to remain active for reaction with biotinylated DNA probes. The resulting DNA sensor was successfully used to distinguish different DNA targets from a protein containing solution.

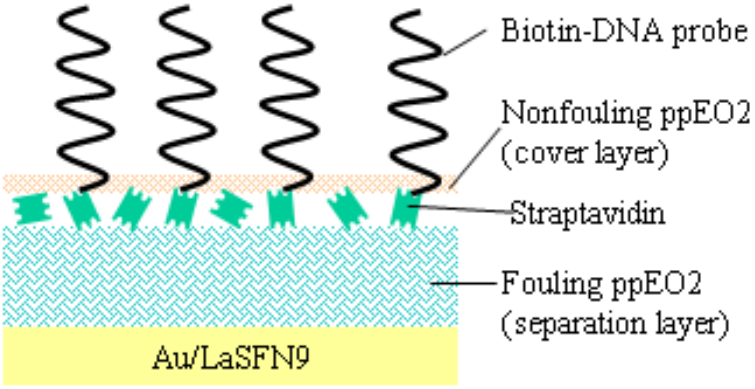

Scheme 5-1: Schematic of the multilayer structure in a protein-resistant DNA sensor.

5.2 Experimental section

5.2.1 Preparation of ppEO2 coatings

Deposition of the fouling ppEO2 was carried out at continuous wave plasma conditions with an input power of 80W. The nonfouling ppEO2 coatings were deposited at pulsed mode plasma conditions. The input power employed was 20 W, and the duty cycles were 5/100 and 1/100 ms, respectively. The monomer pressure varied from 0.01 to 0.05 mbar. The thickness of all ppEO2 coatings was well controlled by adjusting the deposition time.

5.2.2 Preparation of DNA sensor

Scheme 5-2 shows the preparation process for a multilayer protein-resistant DNA sensor. On the Au-coated LaSFN9 slide (i.e., the substrates for SPFS measurements) a

fouling pp-EO2 film was firstly deposited at a power of 80 W under continuous wave conditions. This layer was used here to avoid the quenching of fluorescent dyes on the Au substrates, and is refereed to as the "separation layer". The freshly deposited pp-EO2 separation layers were then immersed into pure water overnight to remove the soluble materials from plasma films. After this washing step, the surfaces were dried with nitrogen gas. Then a drop of 100 µl aqueous solution containing streptavidin was placed on the surface. The water evaporated over a period of 6 h and the streptavidin molecules were thus physically adsorbed on the separation layer. The dried, streptavidin-modified surface was then placed in the plasma reactor and a second, much thinner layer of antifouling pp-EO2 (20 W, DC 5/100 or 1/100, respectively) was deposited. Subsequent experiments showed that the low DC plasma treatment did not damage or remove the surface attached streptavidin. The resulting multilayer substrates were attached to the SPFS flow cell. When biotin-modified DNA probe solution was injected into the flow cell, the biotin would bind to the embedded streptavidin, thus form a DNA sensor.

5.2.3 Activity of the embedded streptavidin

SPFS has been used in the present work to study the activity of the surface embedded streptavidin. A biotinylated oligonucleotide modified with a cy5-fluorescent label (i.e., biotin-DNA-Cy5 in Chapter 3) was used here as the test molecule. The testing principle was based upon the high binding affinity between a streptavidin and a biotin in aqueous solution ($K_A \approx 10^{14}$ M^{-1}). The streptavidin/biotin complexes are also extremely stable over a wide range of temperature and pH.

5.2.4 DNA hybridization monitored by SPFS

SPFS has been described and discussed in a number of articles in the study of hybridization reactions at interfaces. The multilayer DNA sensors were attached to a flow cell for liquid exchange. PBS buffer solution was firstly introduced into the flow cell to stabilize the sensor. Then different DNA targets of 100 nmol were injected into the flow cell. The fluorescent signal was recorded in real time. In order to test the performance of the present DNA sensor in contact with protein containing solution, DNA targets were mixed with proteins, i.e., either BSA or fibrinogen, at a certain concentration. A sodium dodecyl sulfate (SDS) solution of 0.01% was added to regenerate the sensor surface.

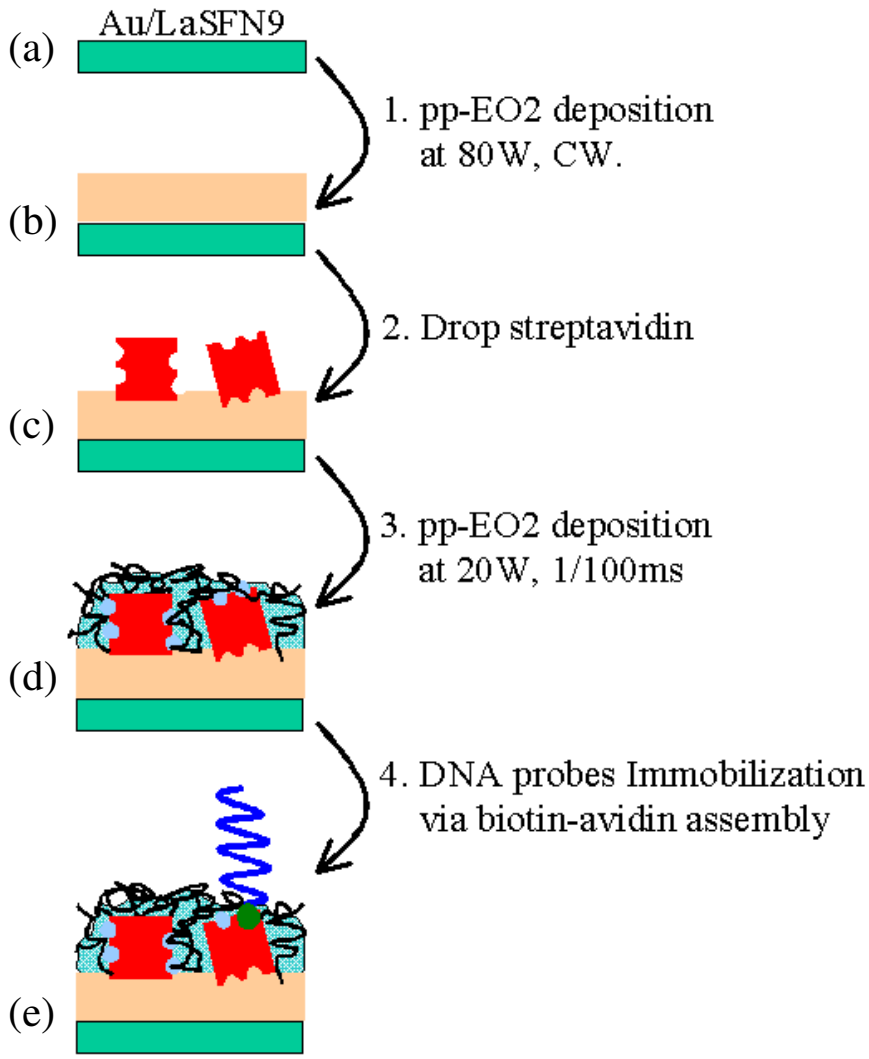

Scheme 5-2: Preparation process for the multilyer, protein-resistant DNA sensor.

5.3 Results and discussion

5.3.1 Optimization of separation layer

As discussed in Chapter 2, the fluorescene signal in SPFS is dependent on the distance between the dye molecules and the metal substrates (i.e., Au in this work). Therefore, one requirement of SPFS is a sufficient separation of the dye molecule from the metal substrate. This was achieved by depositing a fouling ppEO2 thin layer (80W, CW) on the Au/LaSFN9 substrates. When used as separation layer, plasma polymer has two main advantages: 1). Its thickness is easily controlled by tuning the deposition time; 2) Plasma polymer could be highly cross-linked and thus is stable in aqueous media. A series of 80W ppEO2 coatings

were prepared with increasing deposition time, and their thicknesses were measured by SPR (Figure 5-1). The refractive index used in SPR fitting are n=1,538 for fresh films, and n=1,536 for washed films. From Figure 5-1, it is apparent that the thickness of either fresh and washed 80W ppEO2 could be well controlled by adjusting the deposition time, even through water extraction treatment to 80W ppEO2 resulted in a very small decrease in their thickness. The very low loss of unbound materials indicates that 80W ppEO2 coatings might have a very high cross-linking density.

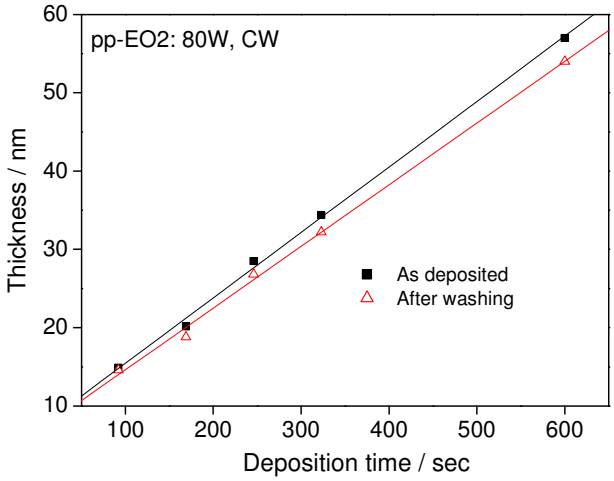

Figure 5-1: Thickness of 80W ppEO2 films with increasing deposition time.

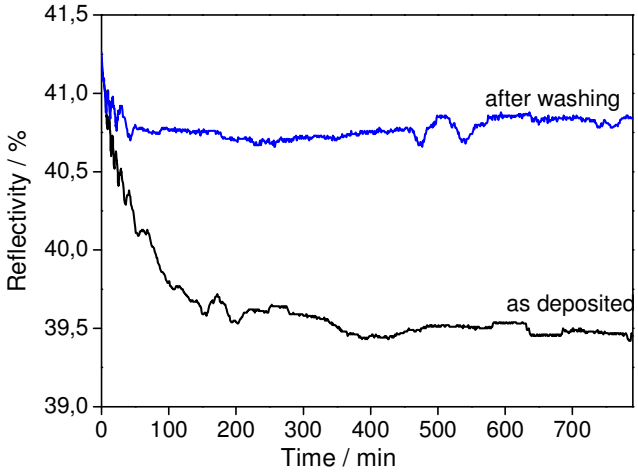

Figure 5-2: Swelling behaviour of the fresh and the washed ppEO2 films in PBS buffer. Deposition condition: 80 W, CW, d = 31.2 nm.

The behaviour of 80W ppEO2 in PBS buffer solution was also monitored by SPR kinetic measurement (Figure 5-2). For the fresh ppEO2, it could reach equilibrium after about 100 min. The rapid decrease in SPR reflectivity at the first 100 min could be explained

by the loss of unbound materials. After removing the unbound materials by H_2O washing, 80W ppEO2 became very stable in PBS buffer.

In subsequent experiments, the effect of separation layer thickness to SPFS signal intensity was tested. 80W ppEO2 of different thicknesses were used as separation layer in the multilayer structure (Scheme 5-1). A fixed amount of streptavidin were placed on each 80W ppEO2 coated substrate and were then covered by a extremely thin ppEO2, which was deposited at identical conditions for all samples. Consequently, the embedded streptavidin are expected to provide similar amount of active sites for the reaction with biotin-DNA-Cy5, and hence the fluorescence intensity in SPFS is influenced only by the thickness of the fouling ppEO2. SPFS were recorded for each sample after injecting the biotin-DNA-Cy5 solution, as well as, after rinsing the surface with PBS buffer. The results are given in Figure 5-3. After PBS rinsing, the fluorescence intensity of SPFS decreased because of the removal of the physically adsorbed biotin-DNA-Cy5. Moreover, the highest fluorescence intensity was observed for the sample with a 40 nm separation layer. This result is in good agreement with the literature.[10] Consequently, the fouling ppEO2 separation layer with a thickness of ca 40 nm was employed for all DNA sensors in the present study.

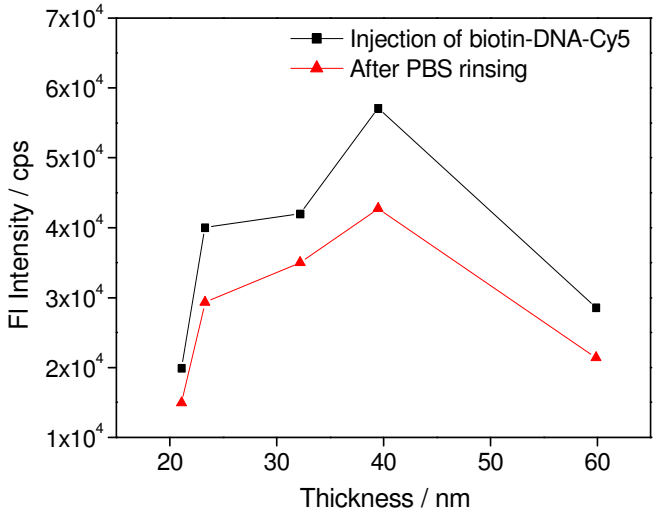

Figure 5-3: Effect of the thickness of ppEO2 separation layer onto SPFS intensity.

5.3.2 Streptavidin immobilization by extremely thin ppEO2

The fouling ppEO2 coating here serves not only as the separation layer, but also as the active layer for streptavidin immobilization. The number of the surface immobilized streptavidin was estimated by measuring the binding of biotin-DNA-Cy5 with SPFS. Figure

5-4 shows the comparison of two streptavidin immobilization methods: 1). Immobilization via non-specific adsorption (Figure 5-4: scheme ii); 2). Immobilization by a 2 nm layer of antifouling pp-EO2 (Figure 5-4: scheme iii). The non-specific adsorption of biotin-DNA-Cy5 on the fouling ppEO2 substrate (Figure 5-4: scheme i) was also measured as a reference. The low fluorescence intensity observed for the immobilization of biotin-DNA-Cy5 on the fouling ppEO2 (Figure 5-4: scheme i) suggests merely some unspecific binding to occur on the surface. The use of physically adsorbed streptavidin to immobilize biotin-DNA-cy5 (Figure 5-4: scheme ii) clearly leads to higher immobilization efficiency. The highest immobilization efficiency in this work, however, was obtained for surface bound streptavidin embedded in a 2nm thick antifouling EO2 layer (Figure 5-4: scheme iii). The most likely reason for this is that in the latter case the streptavidin is trapped by the overlying pp-EO2 layer and is less likely to dissociate from the surface. This data clearly shows that there is still a strong interaction between the biotin-DNA-cy5 and the streptavidin, even though this is embedded in, or covered by a thin layer of pp-EO2 layer.

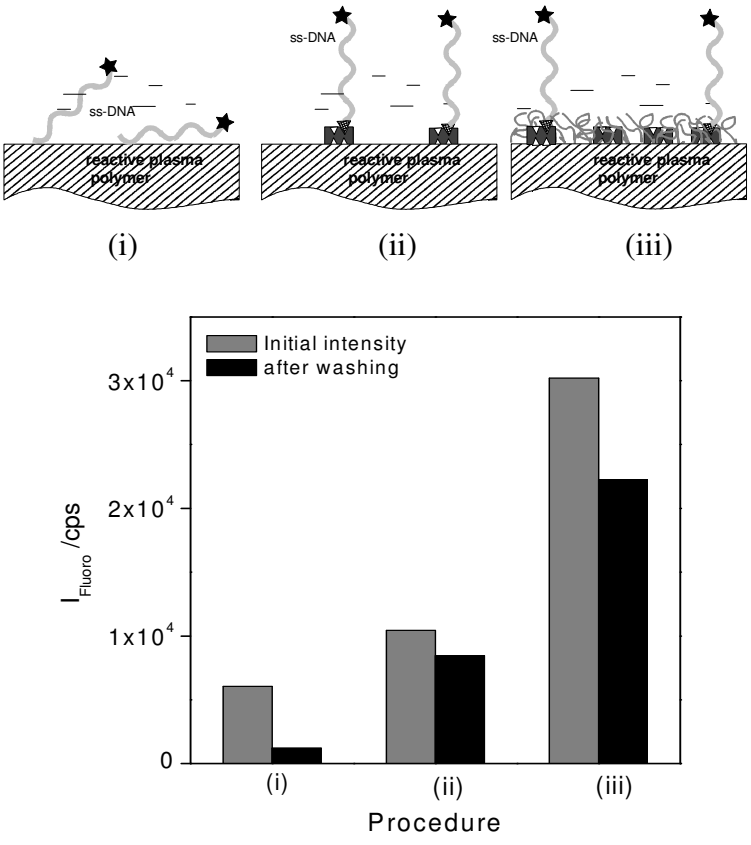

Figure 5-4: Comparison of different immobilization protocols: (i) biotin-DNA-Cy5 on the fouling 80W ppEO2, (ii) biotin-DNA-Cy5 immobilized on surface attached streptavidin and (iii) streptavidin immobilized on reactive pp-EO2, coated with a 2 nm layer of antifouling pp-EO2 and reacted with biotin-DNA-Cy5. For each protocol the fluorescence intensity from the biotin-DNA-Cy5 was measured by SPFS to estimate reactivity.

5.3.3 Effect of streptavidin concentration

In subsequent experiments the concentration of streptavidin was optimised. This was tested by repeating Scheme 5-2d and monitoring the maximum fluorescence intensity for different streptavidin concentrations using SPFS. A streptavidin concentration of 370 nM/L was found to be optimum and further increases in the concentration did not lead to a significant increase in immobilized, fluorescently labelled ss-DNA (Figure 5-5). The stability of the multilayer architecture (Scheme5-2d) in PBS buffer was monitored using SPR (Figure 5-6). Clearly, the multilayer structure became stable after PBS rinsing for ca. 100 mins. The reflectivity decrease at the beginning may be caused either by some loss of the embedded streptavidin, or by the swelling of the whole architecture.

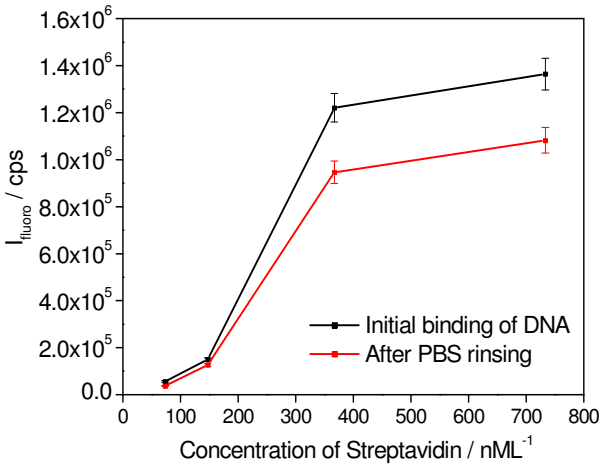

Figure 5-5: SPFS intensity after the binding of biotin-DNA Cy5 to embedded streptavidin as a function of the streptavidin concentration.

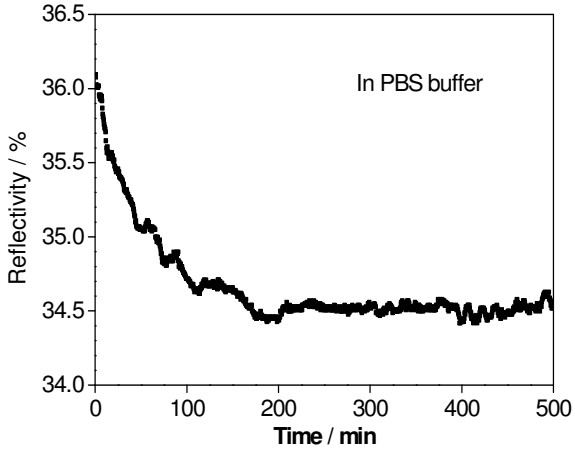

Figure 5-6: SPR kinetic measurement showing the behaviour of embedded straptavidin by a 2 nm layer of antifouling pp-EO2 over time.

AFM microscopy showed that these multilayer DNA sensors were very flat with Rq values of 1.1 nm (Figure 5-7). The roughness measured was approximately the same as the substrate material (i.e., Au coated LaSFN9 glass slide). This seems to suggest that the streptavidin molecules distribute evenly on the substrates. A possible reason for this result is the low streptavidin concentration (i.e., 370 nM/L) used in this work. A such dilute solution lead to a low degree of aggregation either in liquid state or on the surface.

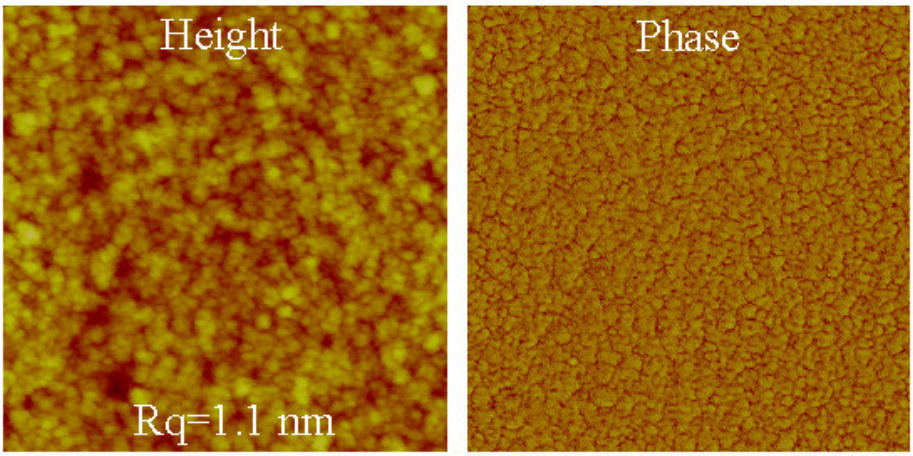

Figure 5-7: Tapping mode AFM images of a typical multilayer DNA sensor (see Scheme 5-2e) in ambient air. The scan area is 1 x 1 μm^2.

5.3.4 Optimization of ppEO2 cover layer

5.3.4.1 ppEO2 at a DC of 5/100 ms

Since the ppEO2 coatings deposited at 20W, DC of 5/100ms showed excellent resistance to BSA (see Chapter 4), those thin films were employed in the primary study. The thickness of nonfouling ppEO2 also plays an important part in the present multilayer sensor because a thick film would cover all the active sites of the embedded streptavidin. The nonfouling ppEO2 deposited at a DC of 5/100 ms is refereed to as high-DC ppEO2.

The high-DC ppEO2 with different thicknesses were deposited on the streptavidin modified substrates. The binding of biotin-DNA-Cy5 was used to test the accessibility of the embedded streptavidin. Figure 5-8 shows the SPFS results. When the nonfouling ppEO2 thickness is d=1.9 nm (this value was estimated according to Chapter 4.3.1), a fluorescence signal could be observed immediately after the injection of the biotin-DNA-Cy5 solution. Rinsing the surface with PBS buffer lead to a big decrease in SPFS intensity, but is still

much higher compared to the background value. This indicates that some embedded streptavidin are able to bind biotinylated molecules. Upon increasing the thickness of the nonfouling pp-EO2 cover layer to d = 3.5 nm, the fluorescence signal in SPFS returned to the background value after PBS rinsing. Clearly, the lock-and-key reaction between embedded streptavidin and biotinylated DNA no longer worked. The fluorescence observed immediately after injecting biotin-DNA-Cy5 may come from the bulk solution, which could be partly excited by the tail of the evanescent field of the SPFS.

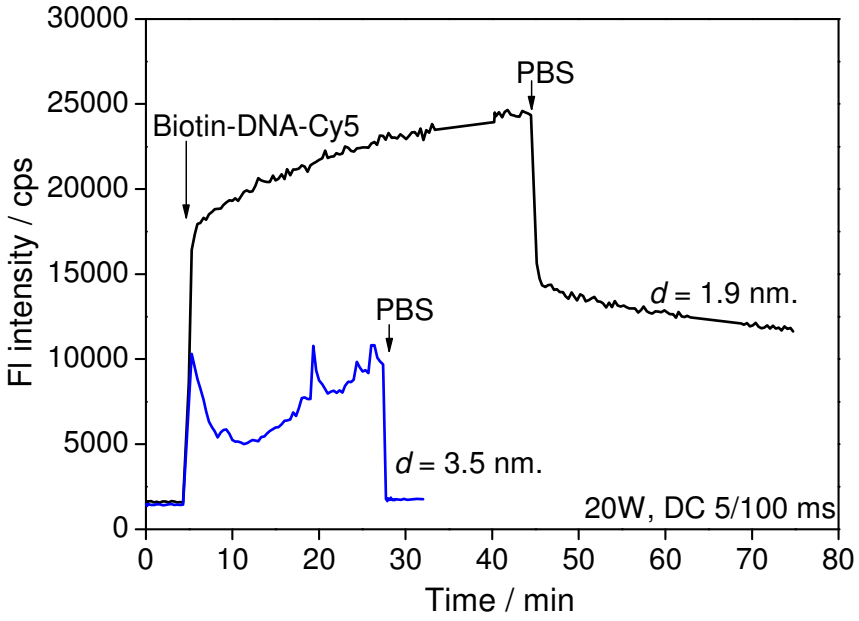

Figure 5-8: The binding of biotion-DNA-Cy5 to the embedded streptavidin using nonfouling ppEO2 (20W, DC of 5/100ms) cover layer with different thicknesses.

The next test is to measure the protein adsorption on the multilayer DNA sensor (Scheme 5-2e). In order to attach DNA probes, the multilayer structure (Scheme 5-2d) was attached to a flow cell for liquid exchange. Firstly PBS buffer solution was introduced into the flow cell to stabilize the sensor. Then 1 ml biotin-DNA of 100 nM was injected into the flow cell, and was circulated using a peristaltic pump for 2 hours. After that, PBS buffer was injected again to the flow cell to remove the unbound DNA probes. Once the biotin-DNA had been immobilized on the multilayer system, this DNA-functionalized-multilayer was again tested for BSA adsorption. Tests with BSA in PBS buffer (10 mg/ml) showed the DNA functionalized multilayer to exhibit excellent antifouling properties towards BSA, Figure 5-9.

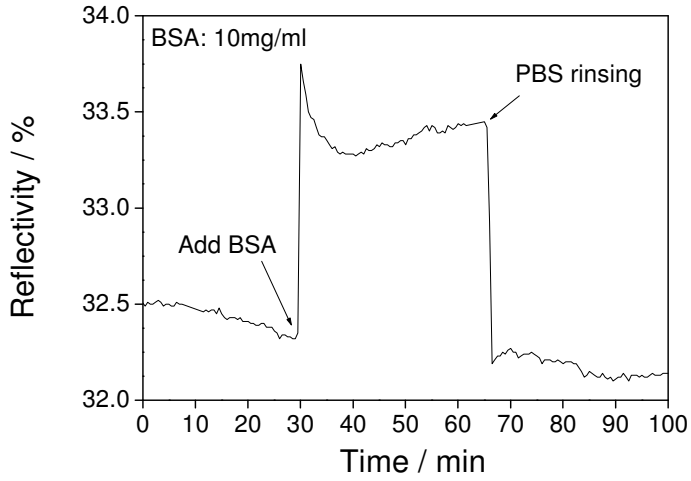

Figure 5-9: SPR kinetic measurement showing the BSA adsorption on the multilayer structure with a 2 nm pp-EO2 and cy5-DNA-biotin immobilized through the antifouling layer. In this case the 2 nm pp-EO2 layer behaved as a true antifouling layer and no BSA binding could be observed. Plasma conditions: 20W, DC of 5/100ms.

5.3.4.2 ppEO2 at a DC of 1/100 ms

From Chapter 4, the ppEO2 coatings deposited at a DC of 1/100 ms exhibited better protein resistant properties, particularly for fibrinogen adsorption. Therefore, these nonfouling coatings were employed to create a DNA sensor resisting not only BSA but also fibrinogen adsorption. The nonfouling ppEO2 deposited at a DC of 1/100 ms is refereed to as low-DC ppEO2.

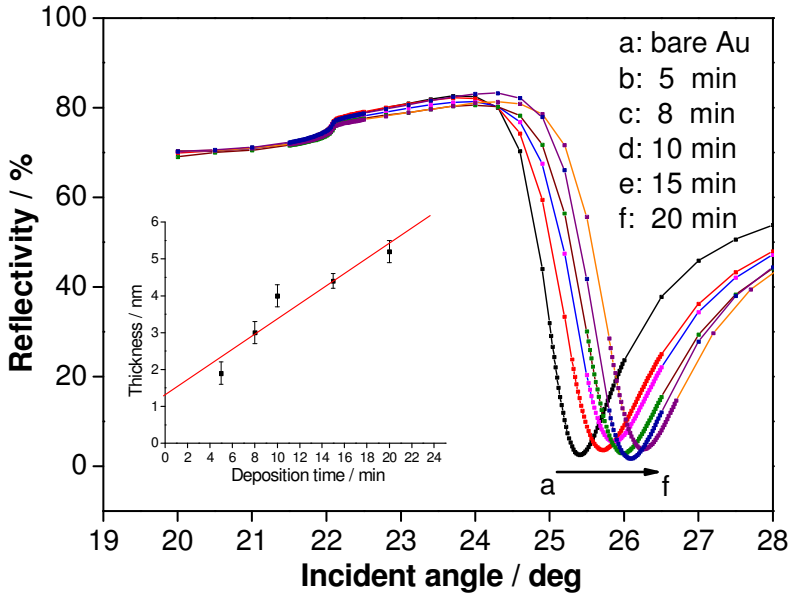

Figure 5-10: SPR measurements showing the thickness evolution of pp-EO2 films (20 W, 1/100 ms) as a function of the deposition time. For SPR fitting, the refractive index of pp-EO2 is n=1.451.

The thickness of the low-DC ppEO2 was also controlled by varying the deposition time (Figure 5-10). The low-DC ppEO2 of different thicknesses were used as the cover layer in the multilayer structure (Scheme 5-2d). The DNA probe immobilization was performed using the same procedure as that in Chapter 5.3.4.1. SPR measurements, as shown in Figure 5-11, indicated that the DNA functionalized multilayer exhibited excellent antifouling properties towards both BSA and fibrinogen (10mg/ml) when increasing the low-DC ppEO2 thickness up to 5.5±0.2 nm (deposition time: 20 min).

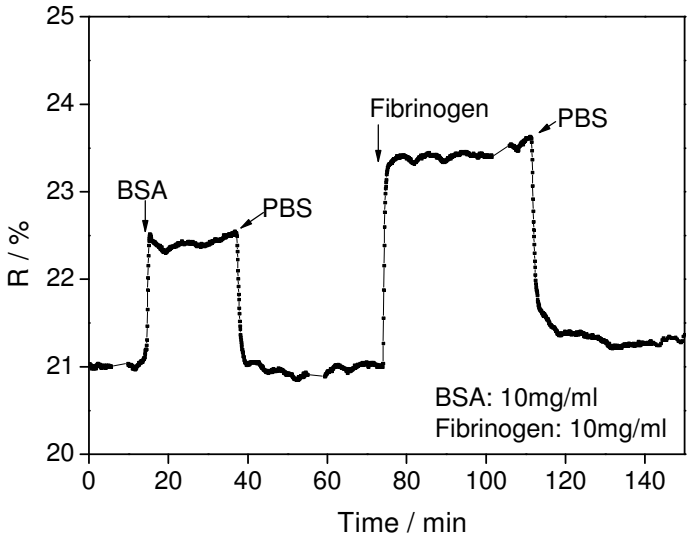

Figure 5-11: SPR kinetic measurement of BSA and fibrinogen adsorption on the multilayer DNA sensor with a 5.5±0.2 nm pp-EO2 cover layer. Plasma conditions: 20W, DC of 1/100ms.

The presence of DNA probes in the DNA sensor with a 5.5 nm low-DC ppEO2 was confirmed indirectly by the hybridization of labeled target DNA (see the following section 5.3.5). While a 3 nm high-DC ppEO2 was able to block the binding sites of the embedded streptavidin (see Figure 5-8), it is really surprising to find that a 5.5 nm low-DC ppEO2 cover layer here still allowed for the binding of bintin-DNA probes to the embedded species. This seems to suggest that the structure of the low-DC ppEO2 is different from that for a high-DC coating. A recent study indicated that the ppEO2 surface prepared under a lower power might consist of longer PEO-like chains, thus forming linear polymers rather than the highly cross-linked structure in a traditional plasma polymer.[11] The low-DC ppEO2 in this work was also prepared at a very low power (P_{eq}=0.2 W), thus containing some longer PEO-like chains. Compared to the low-DC ppeO2, the high-DC ppEO2 (P_{eq}=1 W) are more cross-linked. As a result, it is likely that the swelling of the low-DC ppEO2 lead to a polymeric

hydrogel, thus providing some diffusive pathways for small molecules, like biotin. On the other hand, the cross-linked structure in the high-DC ppEO2 would not allow for the diffusion of biotin molecules at greater thickness.

5.3.5 DNA detection from DNA/protein mixture solution

5.3.5.1 DNA hybridization without proteins

SPFS was employed in this study to monitor the hybridization events between the surface bound biotin-DNA probes and the cy5-labelled DNA targets, including mismatch 2 (MM2), mismatch 1 (MM1) and complementary (MM0) targets (Figure 5-12). After introduction of MM2, a small jump in SPFS fluorescence could be observed, which originated from the labeled DNA in bulk solution being excited by the tail of SPR mode. This jump could also be seen when changing the MM2 with PBS buffer. During the circulation of the MM2 for 30 mins, the SPFS intensity showed a small decrease for the first several minutes and then remained almost constant. The fluorescence decrease in the beginning could be ascribed to the bleaching effect of dye molecules upon laser irradiation. The fluorescence intensity could return to the original background after injecting PBS buffer. The results suggest that there is very few MM2 bound to the surface attached probes, which could be easily washed away. Clearly, the reason for this is the presence of two base pair mismatch between MM2 and the DNA probes.

For MM1, a slow increase in SPFS fluorescence could be observed, which reached the equilibrium after about 30 min. When rinsing the surface with PBS, a step-wise decrease in SPFS fluorescence was observed firstly, which further decreased over time. For the complementary DNA target, i.e., MM0, one could observe a very rapid increase of fluorescence intensity immediately after the injection of sample solution. The SPFS signal reached the equilibrium after only about 5 min. Rinsing the surface with PBS buffer did not remove all the hybrided MM0. A significant fluorescence could be seen even after PBS rinsing overnight. Clearly, different DNA targets, i.e., MM0, MM1 and MM2, respectively, showed great difference in their hybridization behavior to the surface attached probes. The present DNA sensor can successfully discriminate the DNA targets with one base pair mismatch.

On the other hand, SPR results showed no response upon injections of either DNA solutions or PBS buffer. The small decrease in SPR reflectivity over the hours could be regarded at the baseline drift. Therefore, in the subsequent experiments, SPR was used to

monitor protein binding on the sensor surface, while SPFS was used to monitor DNA hybridizations in real time.

From SPFS kinetic measurements, the association/dissociation rate constants (K_{on} and K_{off}) of DNA hybridization could be determined by fitting the working curve based on a simple Langmuir model, assuming pseudo-first order association/dissociation kinetics.[12] The association process can be described by:

$$I_{Fl}(t) = I_{\max}(1 - \exp((k_{on}c_0 + k_{off})t)) \qquad (5.1)$$

and the dissociation process can be calculated by the following equation:

$$I_{Fl}(t) = I_{\max} \times \exp(-k_{off}t) \qquad (5.2)$$

The red curves in Figure 5-12 shows the fitting curve based on the above equations, giving the rate constants summarized in Table 5-1. Within the Langmuir model, the affinity constant K_A is given by:

$$K_A = k_{on} / k_{off} \qquad (5.3)$$

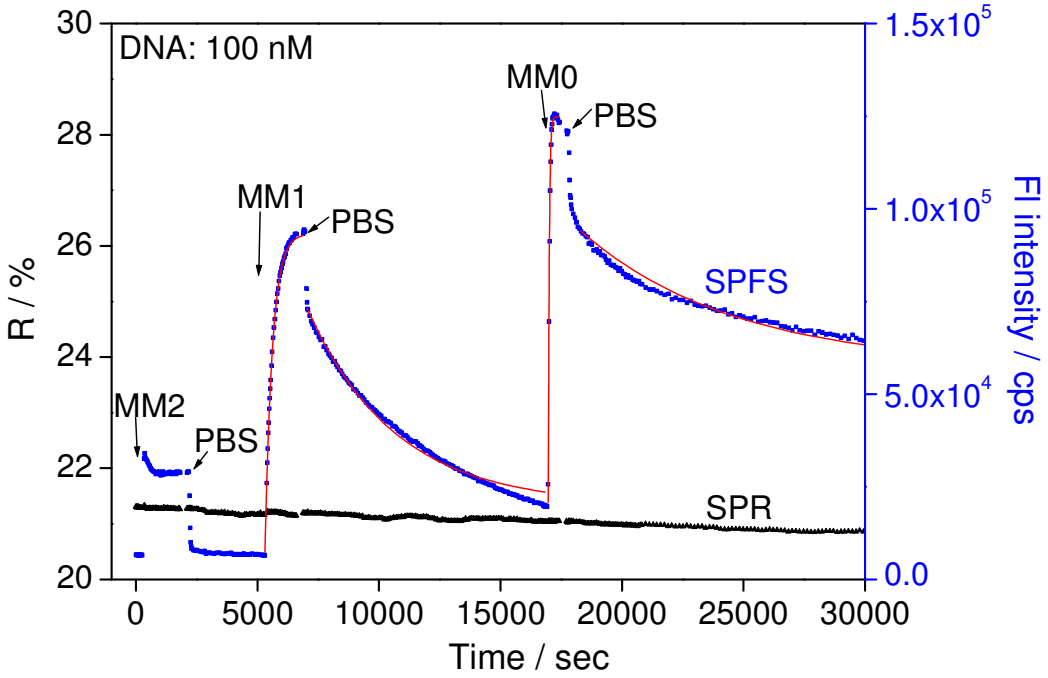

Figure 5-12: SPFS kinetic measurements for hybridization (association) and dissociation processes between the probe DNA and three different target DNA: MM0; MM1; MM2, respectively. The red curves are theoretical calculations based on a simple Langmuir model. The rate constants are given in Table 5-1.

Table 5-1: Comparison of the kinetic constants for the hybridization process between the probe DNA and MM0 or MM1.

	K_{on} / $M^{-1}s^{-1}$	K_{off} / s^{-1}	K_A /M^{-1}
MM0	2.5×10^{5}	1.6×10^{-4}	1.6×10^{9}
MM0+BSA	2.2×10^{5}	1.4×10^{-4}	1.6×10^{9}
MM0+Fibrinogen	1.5×10^{5}	1.5×10^{-4}	1.0×10^{9}
MM1	3.0×10^{4}	2.8×10^{-4}	1.1×10^{8}
MM1+BSA	4.1×10^{4}	3.0×10^{-4}	1.3×10^{8}
MM1+Fibrinogen	3.6×10^{4}	3.6×10^{-4}	1.0×10^{8}

5.3.5.2 DNA hybridization in presence of BSA protein

In order to test the protein resistance of the present DNA sensor, a mixture of DNA targets (100nM) and BSA (10μM (1mg/ml)) was made in this study. The mixtures for different DNA targets were injected into the flow cell of SPFS. The reactions at the surface were monitored in real time using SPR to monitor BSA binding and SPFS to monitor hybridization events (Figure 5-13). Clearly, different DNA targets, i.e., MM0, MM1 and MM2, respectively, could be successfully discriminated using the present DNA sensor. The hybridization kinetic constants for MM1 and MM0 were also fitted based on the Langmuir model (Table 5-1).

Moreover, SPR measurements showed there is no BSA bound to the sensor surface. The small jump in SPR reflectivity observed when change PBS buffer to DNA/BSA mixture, or vice versa, is caused by a change in the refractive index of the liquid media.

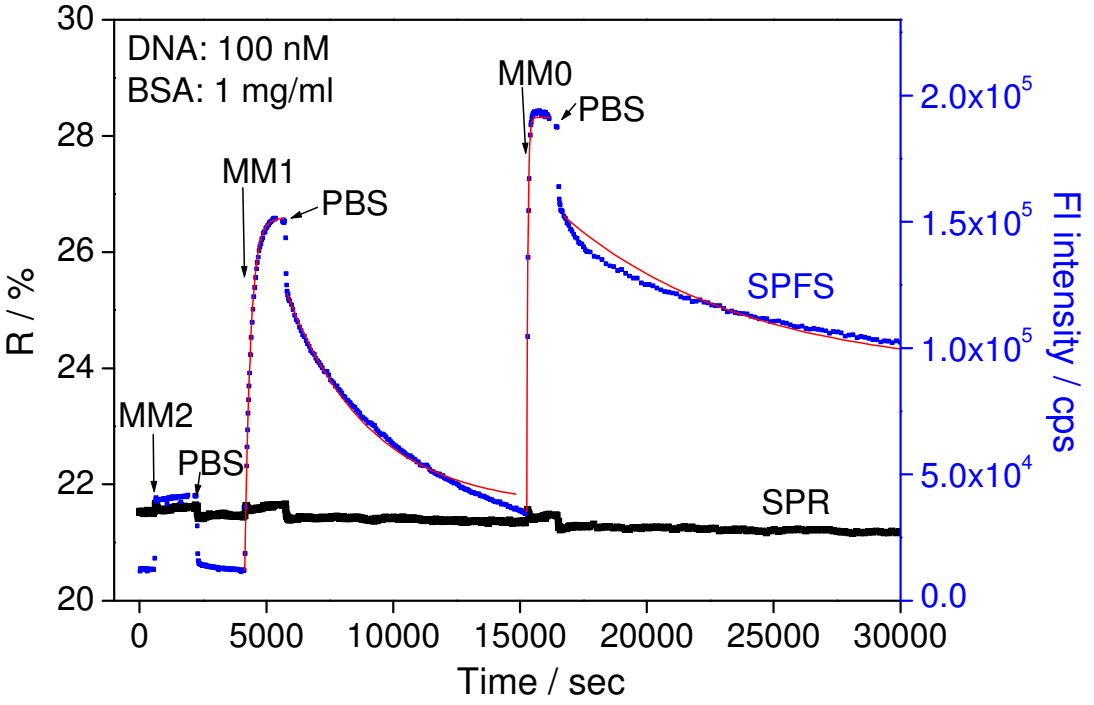

Figure 5-13: SPR and SPFS kinetic measurements for hybridization processes between the probe DNA and three different target DNA: MM0; MM1; MM2, respectively, in presence of BSA (1mg/ml). The red curves are theoretical calculations based on a simple Langmuir model.

5.3.5.3 DNA hybridization in presence of fibrinogen

A final test to verify the protein resistance of this multilayer DNA sensor was the hybridization of different DNA targets in the presence of 1mg/ml fibrinogen (Figure 5-14). Clearly, different DNA targets, i.e., MM0, MM1 and MM2, respectively, exhibited different hybridization behaviour as seen by SPFS with the present DNA sensor. SPR measurements indicated that the sensor surface could resist fibrinogen adsorption.

The hybridization kinetic constants for MM1 and MM0 were also fitted based on the Langmuir model (Table 5-1). The affinity (K_A) of MM0 to the surface attached probes is one order higher than those for MM1 because MM0 is complementary to the probes used here. For the same DNA target (e.g., MM0), the hybridization kinetics with or without proteins are in the same order. This suggests that the proteins in the DNA solution have no influence to DNA hybridization behaviour. Therefore, the present DNA sensor might be very promising for the DNA detection from a complex DNA sample.

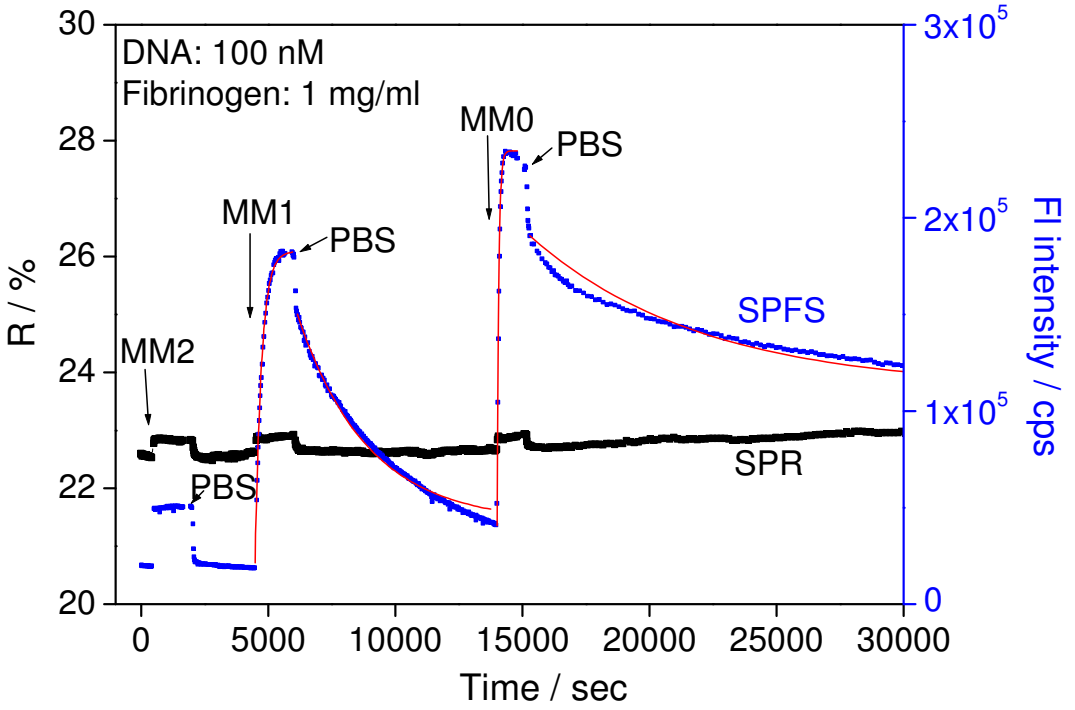

Figure 5-14: SPR and SPFS kinetic measurements for hybridization processes between the probe DNA (P2) and three different target DNA: MM0; MM1; MM2, respectively, in presence of fibrinogen (1mg/ml). The red curves are theoretical calculations based on a simple Langmuir association /dissociation model.

5.3.6 Regeneration of DNA sensors

An important aspect in the development of sensor surfaces is the possibility of surface regeneration allowing for multiple use and thus a reduction in cost and waste. This has generally been done by treatment of the surfaces using sodium dodecyl sulfate (SDS). In this work, as well as on the previous work using plasma polymerised allylamine it was found that SDS generally damages the polymer films. However, reducing the concentration of the SDS to 0.01% does not seem to cause any significant damage as seen by the overall relatively high fluorescence intensity after consecutive treatment in Figure 5-15. SDS treatment of the surface carrying the hybrid led to a fluorescence intensity decrease to 0%, indicating the dissociation of the DNA hybrid, a loss by wash-out of the cy5-labelled target and thus a regeneration of the surfaces. Subsequent hybridization and regeneration steps show that this can be done for several cycles.

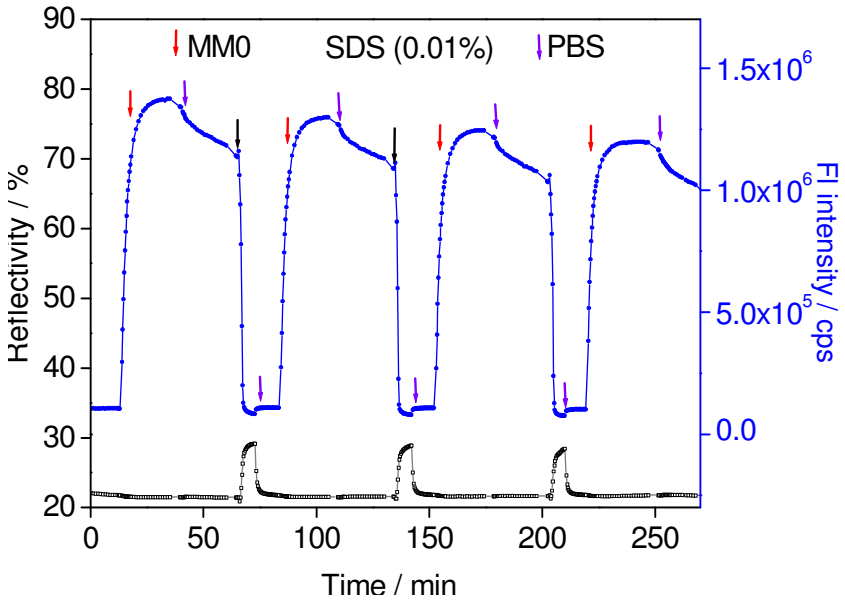

Figure 5-15: SPR and SPFS kinetics showing 4 subsequent regeneration/ hybridisation reactions of the surface using SDS to dissociate the double helix.

5.3.7 Limit of detection

In order to identify the limit of detection (LOD) of the present sensor, a series of MM0 DNA solution ranging from 10 pM to 500 pM were tested sequentially, as shown in Figure 5-16A. After a certain period for hybridization, a SDS solution of 0.01% was injected for 3 mins in order to regenerate the surface. At such low concentrations, the initial hybridization process is controlled by the diffusion of DNA target from the bulk to the surface, showing a linear signal increase over time. The slope of the fluorescence intensity (Fl) increase is proportional to the DNA concentration c_0, which can be described by the following equation:

$$\frac{d_{Fl}}{dt} = k_m \times c_0 \qquad (5.4)$$

Here k_m is the mass-transport rate constant. A calibration curve is thus obtained by plotting the slopes versus the DNA concentration. The LOD is reached if the calibration curve intersects with the baseline. The baseline is defined as three times the standard deviation of measurements of the time-dependent fluorescence intensity at c_0 =0, which is about 4.8 cps·min^{-1} in the present experiments. From Figure 5-16B, it can be seen that the LOD of the sensor is 0.73 pM.

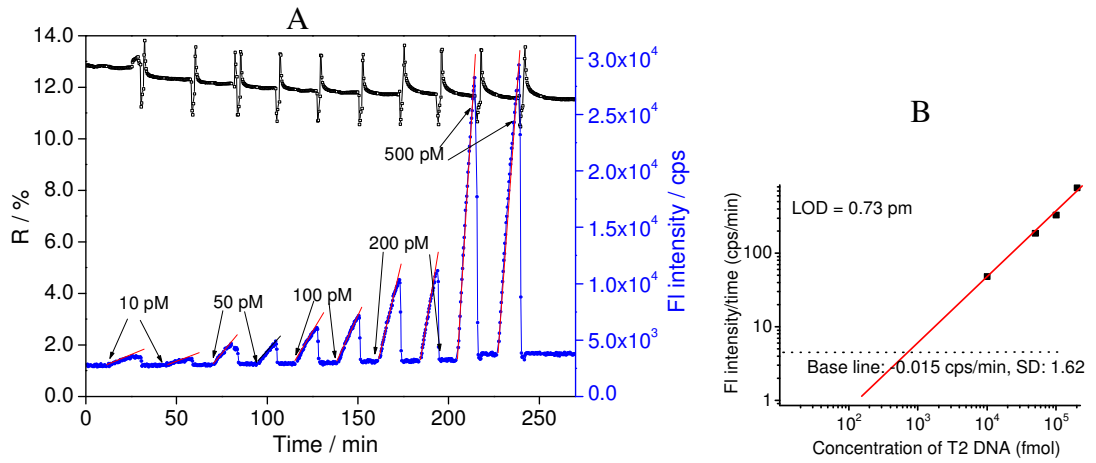

Figure 5-16: (A) SPFS kinetic measurements of the hybridization of MM0 target with concentration ranging from 10 to 500 pmol. The red lines represent the slope. (B) Calibration curve from (A).

5.4 Conclusions

The present work further aimed at investigating a novel strategy for the detection of DNA from a protein-DNA mixture. By careful control over the process conditions it was possible to synthesize an extremely thin layer of low DC pp-EO2, which on the one hand can act as an antifouling layer towards proteins (such as BSA and fibrinogen) while on the other hand is thin enough to permit lock-and-key-type reactions to occur between surface embedded streptavidin and biotin from solution. The bi-functional nature of the multilayers designed has been used for biotinlylated DNA immobilization and MM1 and MM2 hybridization reactions to occur in the presence of either BSA or fibrinogen. The results presented here are based on simple, synthetic DNA/BSA (or fibrinogen) mixtures in PBS and represent a basis for further work to investigate strategies for more complex mixtures and for realistic samples of body fluids.

References

1. Piunno, P. A. E.; Krull, U. J. *Anal. Bioanal. Chem.* **2005,** 381, (5), 1004-1011.
2. Rosi, N. L.; Mirkin, C. A. *Chem. Rev.* **2005,** 105, (4), 1547-1562.
3. Pirrung, M. C. *Angew. Chem. Int. Ed.* **2002,** 41, (8), 1277-1289.
4. Homs, W. C. I. *Anal. Let.* **2002,** 35, (12), 1875-1894.

5. Levicky, R.; Horgan, A. *Trends Biotechnol.* **2005,** 23, (3), 143-149.
6. Knoll, W.; Park, H.; Sinner, E. K.; Yao, D. F.; Yu, F. *Surf. Sci.* **2004,** 570, (1-2), 30-42.
7. Knoll, W.; Zizlsperger, M.; Liebermann, T.; Arnold, S.; Badia, A.; Liley, M.; Piscevic, D.; Schmitt, F. J.; Spinke, J. *Colloids Surf. A* **2000,** 161, (1), 115-137.
8. Miyachi, H.; Hiratsuka, A.; Ikebukuro, K.; Yano, K.; Muguruma, H.; Karube, I. *Biotechnol. Bioeng.* **2000,** 69, (3), 323-329.
9. Miyachi, H.; Ikebukuro, K.; Yano, K.; Aburatani, H.; Karube, I. *Biosens. Bioelectron.* **2004,** 20, (2), 184-189.
10. Vasilev, K.; Knoll, W.; Kreiter, M. *J. Chem. Phys.* **2004,** 120, (7), 3439-3445.
11. Bremmell, K. E.; Kingshott, P.; Ademovic, Z.; Winther-Jensen, B.; Griesser, H. J. *Langmuir* **2006,** 22, (1), 313-318.
12. Neumann, T.; Johansson, M. L.; Kambhampati, D.; Knoll, W. *Adv. Func. Mater.* **2002,** 12, (9), 575-586.

Chapter 6

Plasma Polymerized Epoxide Coating for DNA Sensor

6.1 Introduction

One of the key issues in the development of DNA sensors is the immobilization of single-stranded oligonucleotides, so called DNA probes, onto the sensor surfaces. In this regards, a variety of approaches [1, 2] have been developed, including covalent attachment, Avidin-Biotin assembly or simple adsorption. Covalent coupling of chemically modified ssDNA on the functionalised surfaces, including aldehyde,[3, 4] maleimide,[5-7] or epoxide,[8-10] is the most widely used strategy for the preparation of commercial DNA sensors because of its good stability and specificity. Compared to other functionalities, the epoxide functional surface is relatively hydrophobic and thus reduces the spreading of solution, which makes it ideal for DNA microarray preparation.

Plasma polymerization techniques have proved to be an effective and economical method for functionalising solid surface with various functionalities by a careful choice of monomers. Recently, two research groups[11, 12] have demonstrated that plasma polymerization of glycidyl methacrylate (GMA) lead to a epoxide-functionalized surface. High retention of monomer structure could be achieved either at low plasma input power or at low duty cycle. Therefore, the resulting ppGMA films contained high amount of epoxide groups, which could undergo coupling interaction with various amine-containing compounds. Plasma polymerization has some advantages for the modification of surfaces. The plasma polymerized films are highly conformable and thus can be deposited readily onto many types of substrates in different shapes with good adhesion. Moreover, plasma polymerization technique is a one-step, all dry process, and is well-established in industry, thus allowing for a large-scale production. Additionally, the commonly employed silanization process tends to form irreproducibility in the microscopic wettability property, while the plasma polymerised films have no problem in this regard because it is very homogeneous.

In this work, epoxide functional surfaces were achieved simply by pulsed plasma polymerization of glycidyl methacrylate at a low duty cycle. The presence of epoxide groups in the resulting ppGMA was confirmed by FT-IR measurements. The resulting ppGMA films were found to be resistant to the non-specific adsorption of DNA strands, while the

epoxide groups obtained could react with amine-modified DNA probes via amine-epoxide coupling reaction in a mild basic environment. DNA sensing is achieved using SPFS.

6.2 Experimental section

6.2.1 Preparation of ppGMA films

Plasma polymerization of glycidyl methacrylate was carried out using a home-built plasma reactor (see Chapter 3). The plasma power employed in this work ranged from 20 and 100 W. The ppGMA films were deposited at various duty cycles (DCs) from 1/10 to 1/80 ms with the monomer vapor pressure of about 0.03 mbar. The deposition time was adjusted to obtain the desired thickness. In the present study the typical film thickness ranged from 30 to 50 nm. In order to remove the soluble part from the deposited ppGMA, the samples were submersed into H_2O and shaken for overnight. After extraction, the films were washed with excess H_2O to remove small molecules adsorbed on the surface, and then dried at T = 50°C for 2 h. The ppGMA film (20W, DC of 1/40) exhibits very low UV adsorption.

6.2.2 Immobilization of NH_2-DNA

DNA probe immobilization was carried out according to the procedure in the literature,[10] as depicted in Scheme 6-1. DNA solution of 10uM in 0.1M $NaHCO_3$ and 0.3M NaCl was placed on the ppGMA surface, and was incubated overnight at 45 °C in a humid chamber. After the reaction, the samples were rinsed with water and dried with nitrogen gas.

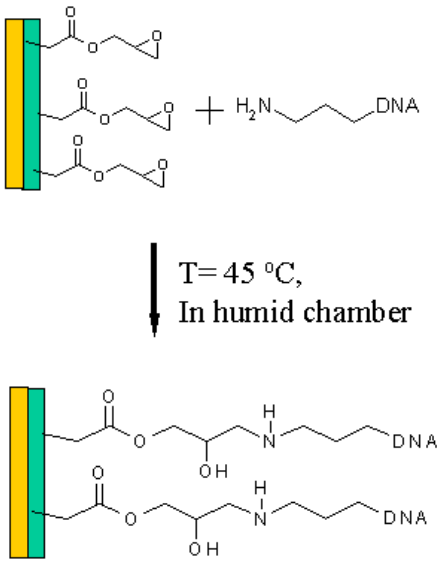

Scheme 6-1: Immobilization of NH_2-DNA on ppGMA films via aminolysis reaction.

6.2.3 DNA hybridization measured by SPFS

The SPFS measurements were carried out with a home-built setup as described in Chapter 3. The resulting DNA sensor was attached to a flow cell for liquid exchange. A sodium dodecyl sulfate (SDS) solution of 0.01% was added to regenerate the sensor surface.

6.3 Results and discussion

6.3.1 Film analysis

FT-IR was employed to monitor the chemical structure of the ppGMA films deposited at various duty cycles (Figure 6-1). The FT-IR spectrum of the ppGMA deposited in continuous wave mode is also given as a reference in Figure 6-2. According to the literature,[11] epoxide groups would be associated with four characteristic bands, i.e. epoxide ring C-H stretching at 3063 cm^{-1}, epoxide ring breathing at 1258 cm^{-1}, antisymmetric epoxide ring deformation at 910 cm^{-1}, and symmetric epoxide ring deformation at 852 cm^{-1}. For the ppGMA deposited at 40 W in the continuous mode, all of these four bands could not be observed, indicating that the epoxide groups of GMA monomer was damaged at high power CW plasma polymerization. In contrast, the FT-IR of the ppGMA deposited in the pulsed mode clearly shows the four characteristic bands associated with epoxide ring. With decreasing the duty cycle from 1/10ms to 1/80 ms, the corresponding bands become more intense, suggesting that more epoxide group exist in the deposited films.

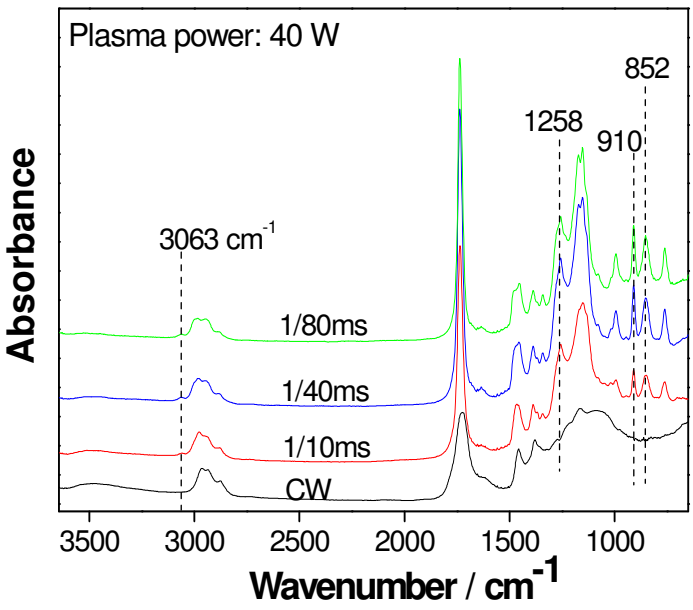

Figure 6-1: FT-IR spectra of the ppGMA films deposited at various duty cycles.

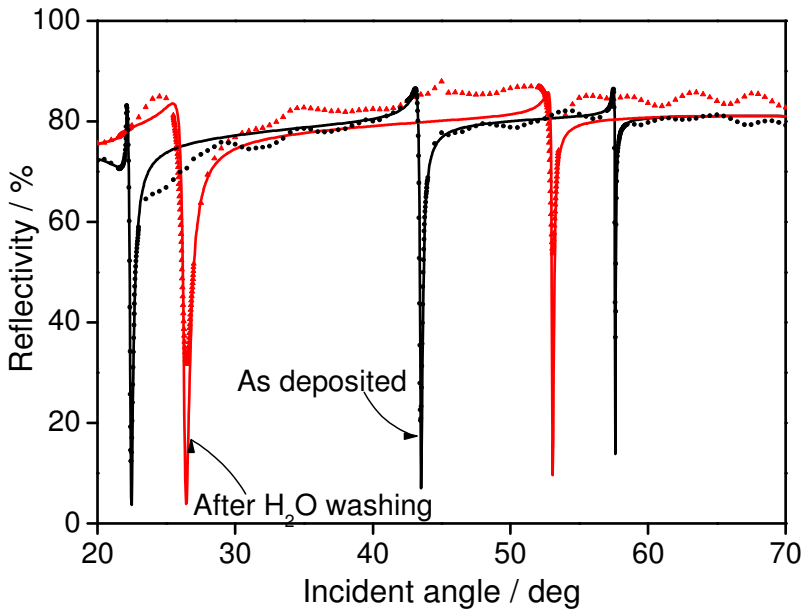

Figure 6-2: s-polarized OWS spectra of a ppGMA film before and after H_2O washing. Plasma conditions: 20W, 1/40ms.

The plasma polymerized films, particularly those deposited at low duty cycle, generally contains some unstable part, which would be washed away by extraction treatment. In this work, OWS was employed to measure the change of ppGMA thickness upon the H_2O extraction. The ppGMA was measured against ambient air immediately after the deposition. Then the ppGMA was immersed into H_2O and shaken for 20 h at room temperature. The extracted film was dried with nitrogen gas, and its thickness was determined using OWS. Figure 6-2 compares the OWS spectra of a freshly deposited ppGMA film with a extracted film. The thickness of a freshly deposited ppGMA was determined to be 689.4 nm (at n=1.502). After extraction, it reduced to 444.8 nm (at n=1.508).

Non-specific adsorption of ssDNA on the sensor surface will increase the background and reduce the selectivity of the DNA sensor. Therefore, the ideal DNA sensor should avoid the non-specific adsorption of DNA strands. The adsorption of ssDNA strands on ppGMA films was firstly investigated using SPFS. Figure 6-3 shows the kinetic measurement of SPFS upon adding the fluorescently labelled ssDNA. It can be found that no fluorescent signal could be observed after rinsing the surface with PBS buffer solution, indicating that no DNA strands adsorbed on the ppGMA surface. The fluorescent signal observed upon injecting the DNA sample is due to the DNA strands in solution (which is also partly excited by surface plasmon mode) rather than the DNA strands adsorbing on the surface.

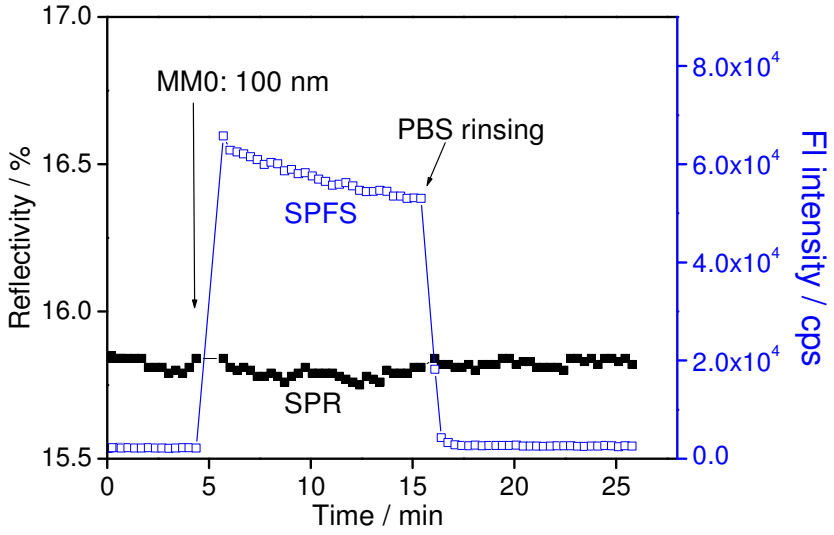

Figure 6-3: SPFS kinetic measurements of the adsorption of fluorescently labelled ssDNA (i.e., MM0) on a ppGMA film. Plasma conditions: 40 W, 1/40 ms.

6.3.2 DNA probe immobilization

DNA probe immobilization was achieved simply by placing an aminated-DNA solution on the ppGMA surfaces without any activation step, as depicted in Scheme 6-1. The resulting DNA-modified ppGMA films are referred to as ppGMA/DNA. The water contact angle of a ppGMA films after H_2O washing is about 64.7 ± 2.1 deg (Table 6-1). After immobilization of DNA probes, its contact angle decreased to 59.7 ± 1.3 deg. The small decrease in water contact angle after DNA probe immobilization could be explained by the ionic nature of ssDNA.

Table 6-1: Static water contact angles of the ppGMA surfaces (20W, 1/40ms) after H_2O washing and after DNA immobilization. A polished si-wafer was used as substrate. Its contact angle is difficult to be measured because water drop can easily spread on si-wafer.

Surfaces	**Contact angle / deg**
pp-GMA after washing	64.7±2.1
ppGMA/DNA	59.7±1.3
Si-wafer	<10

The presence of DNA probes on the ppGMA surface was also confirmed indirectly by detecting the hybridization of complementary target DNA (i.e., MM0), which was labelled with a Cy5 fluorophore (see the following section). In the literatures, DNA immobilization via amine-epoxide reaction was carried out successfully either in 0.1M KOH [8] or in 0.1M $NaHCO_3$ [10]. However, my results indicated that no DNA probes were immobilized in a 0.1M KOH solution, perhaps because of the dissociation of carboxylate groups (See GMA structure in Chapter 3) in a strong basic environment, which lead to the loss of the immobilized probes. Therefore, DNA probe immobilization in this study was carried out in a mild basic environment, i.e., 0.1M $NaHCO_3$.

6.3.3 DNA hybridization

The hybridization of DNA targets on the resulting ppGMA/DNA was recorded by SPFS. The three targets (i.e., MM0, MM1, MM2, respectively) are labelled at their 5' end with a Cy5 fluorophore (Chapter 3). Figure 6-4 gives the SPFS kinetic measurement for the hybridization process. It can be seen that the hybridization reactions for different mismatch situations, i.e., MM0, MM1, MM2, respectively, could be clearly discriminated by SPFS. After the introduction of a MM2, a small increase in fluorescent intensity was observed, which, however, was almost gone after a short rinse with buffer solution. This indicates that no hybridization occurred for target MM2. The fluorescence observed might be due to the excitation of labelled DNA in the bulk solution by the evanescent tail. In the case of MM1, the injection of MM1 solution gave rise to a gradually increase in fluorescence intensity, which reached the equilibrium after ca. 20 min. Moreover, the buffer rinsing did not result in the complete loss of fluorescence. This result indicates the hybrid formation between MM1 target and the surface attached probe. For MM0, one could observe a faster fluorescence increase compared to that for MM1, suggesting that MM0 target had a faster hybridization kinetic than that for MM1 DNA. Further rinsing the surface with excess buffer solution resulted in a very slow loss in the fluorescence intensity, indicating that the hybrid of MM0 with the surface immobilized probe is much more stable than that for MM1. From the SPFS data in Figure 6-4, one can also obtain the corresponding kinetic constants, K_{on} and K_{off}, respectively, by fitting the data based on a simple Langmuir model. The affinity constants, $K_A=K_{on}/K_{off}$, can be obtained as well. Table 6-2 gives the results. It is apparent that the K_A for MM0 is higher than the case for MM1. This result is also in good agreement with the previous work.

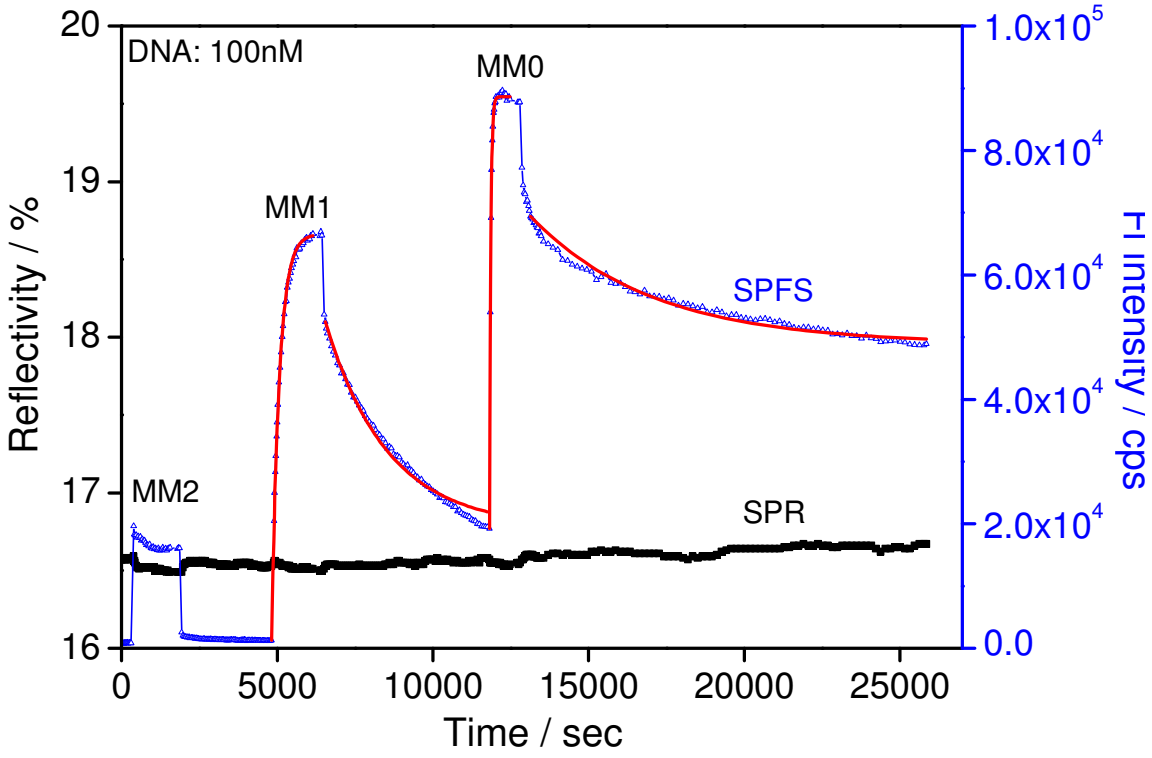

Figure 6-4: SPFS kinetic measurements for hybridization (association) and dissociation processes between the probe DNA and three different target DNA: MM0; MM1; MM2, respectively. The red curves are theoretical calculations based on a simple Langmuir model. The rate constants are given in Table 6-2.

Table 6-2. Summary of the kinetic constants for the hybridization process of MM1 and MM0 on the ppGMA/DNA.

	K_{on} / $M^{-1}s^{-1}$	K_{off} / s^{-1}	K_A / M^{-1}
MM0	2.5 x 10^5	2.6 x 10^{-4}	9.6 x 10^8
MM1	3.6 x 10^4	5.0 x 10^{-4}	7.2 x 10^7

The regeneration of a sensor surface was achieved by treatment of the surfaces using sodium dodecyl sulfate solution at a concentration of 0.01%. As shown in Figure 6-5, the injection of SDS solution resulted in a fluorescence intensity decrease to background value, indicating that all of the hybridized DNA target were removed from the surface and thus a regeneration of the surfaces. Subsequent hybridization and regeneration steps indicated that

the present sensor was re-useable for several cycles. It is apparent that 0.01% SDS solution did not cause any significant damage to the sensor (See SPR result).

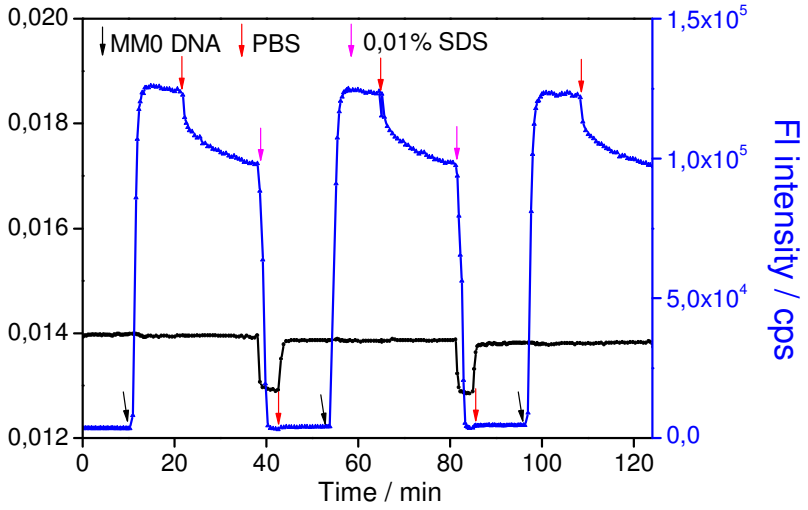

Figure 6-5: SPR and SPFS kinetics showing 3 subsequent hybridization/regeneration reactions on the DNA sensor using 0.01% SDS to dissociate the DNA hybrid.

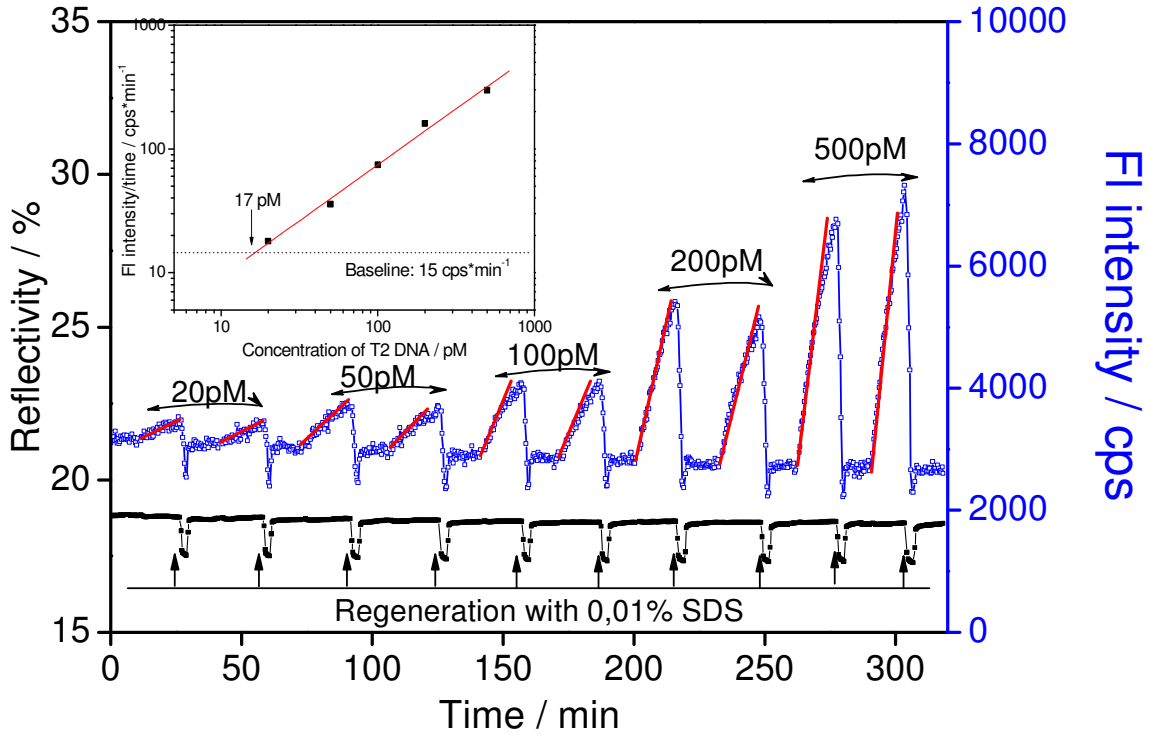

Figure 6-6: SPFS kinetic measurements of the hybridization of MM0 target with concentration ranging from 20 to 500 pmol. The red lines represent the slopes. The inset shows the calibration curve.

In order to identify the limit of detection (LOD) of the present sensor, a series of MM0 DNA solution ranging from 20 pM to 500 pM were tested sequentially, as shown in Figure 6-6. After a certain period for hybridization, a SDS solution of 0.01% was injected for 3 mins in order to regenerate the surface. At such low concentrations, the initial hybridization process is controlled by the diffusion of DNA target from the bulk to the surface, showing a linear signal increase over time, as discussed in Chapter 5. A calibration curve is thus obtained by plotting the slopes versus the DNA concentration. The LOD is reached if the calibration curve intersects with the baseline. The baseline is defined as three times the standard deviation of measurements of the time-dependent fluorescence intensity at c_0 =0, which is about 15 cps·min^{-1} in the present experiments. From the inset of Figure 6-6, it can be seen that the LOD of the sensor is 17 pM.

6.4 Conclusions

Plasma polymerization technique is an alternative approach to generate epoxide surfaces. Covalent attachment of amine-modified DNA was achieved simply by dropping the DNA solution to the epoxide surface in a mild basic environment without any activation step. The resulting DNA sensor was successfully employed to discriminate the DNA targets with single-base mismatch.

References

1. Heise, C.; Bier, F. F. *Top. Curr. Chem.* **2006,** 261, 1-25.
2. Pirrung, M. C. *Angew. Chem. Int. Ed* **2002,** 41, (8), 1277-1289.
3. Zammatteo, N.; Jeanmart, L.; Hamels, S.; Courtois, S.; Louette, P.; Hevesi, L.; Remacle, J. *Anal. Biochem.* **2000,** 280, (1), 143-150.
4. Schena, M.; Shalon, D.; Heller, R.; Chai, A.; Brown, P. O.; Davis, R. W. *Proc. Natl. Acad. Sci. USA* **1996,** 93, (20), 10614-10619.
5. Choithani, J.; Kumar, P.; Gupta, K. C. *Anal. Biochem.* **2006,** 357, (2), 240-248.
6. Wang, Y. Y.; Prokein, T.; Hinz, M.; Seliger, H.; Goedel, W. A. *Anal. Biochem.* **2005,** 344, (2), 216-223.
7. Shen, G.; Anand, M. F. G.; Levicky, R. *Nucleic Acids Res.* **2004,** 32, (20), 5973-5980.

8. Lamture, J. B.; Beattie, K. L.; Burke, B. E.; Eggers, M. D.; Ehrlich, D. J.; Fowler, R.; Hollis, M. A.; Kosicki, B. B.; Reich, R. K.; Smith, S. R.; Varma, R. S.; Hogan, M. E. *Nucleic Acids Res.* **1994,** 22, (11), 2121-2125.
9. Macanovic, A.; Marquette, C.; Polychronakos, C.; Lawrence, M. F. *Nucleic Acids Res.* **2004,** 32, (2), e20.
10. Bocking, T.; Killan, K. A.; Gaus, K.; Gooding, J. J. *Langmuir* **2006,** 22, (8), 3494-3496.
11. Tarducci, C.; Kinmond, E. J.; Badyal, J. P. S.; Brewer, S. A.; Willis, C. *Chem. Mater.* **2000,** 12, 1884-1889.
12. Zou, X. P.; Kang, E. T.; Neoh, K. G.; Zhang, Y.; Tan, K. L.; Cui, C. Q.; Lim, T. B. *Polym. Adv. Technol* **2001,** 12, 583-595.

Chapter 7

Stabilization of Allylamine Plasma Films*

7.1 Introduction

Plasma polymerization of allylamine has attracted considerable interest over the past two decades because of the numerous applications of aminated surfaces in biotechnology. It has been reported that plasma polymerized allylamine (ppAA) films may be applied as substrates for cell culture,[1, 2] and immobilization of biomolecules such as polysaccharides,[3] DNA,[4, 5] and so on.

Recently, it was noticed by many researchers that plasma polymerized allylamine films are not stable in aqueous environments and has been shown the dissociation of low molecular weight materials from the deposited coating.[4-8] In biomedical application, these dissolved small molecules may initiate immune responses or other side effects, and hence lead to failure during the use of biomedical devices. The loss of material also results in a reduction of the plasma polymer thickness.[6-8] In some cases, the thickness of the ppAA films plays an important role in practical applications. For example, Zhang et al.[5] investigated the DNA adsorption on ppAA films and found that the amount of DNA adsorption is thickness dependent. Therefore, it is fundamentally important to stabilize the plasma polymerized film, as well as to determine the extent of materials loss in order to control film thickness.

In this work, ethanol extraction was employed to remove all soluble, non-cross linked material from freshly deposited ppAA films.[8] The thickness change of the ppAA films upon ethanol extraction was determined by SPR and OWS measurements. In order to evaluate the influence of the plasma conditions on the stability of deposited films, ppAA films were prepared at different input power and monomer vapor pressure. The chemistry of ppAA films before and after extraction, as well as the surface morphology, were characterized by FT-IR and AFM, respectively.

* Part of the work in this chapter has been published in *Langmuir*. **2006**, 22, 5548-5551.

7.2 Experimental section

7.2.1 Deposition of ppAA films

Plasma polymerization was carried out in a home-built plasma reactor (see Chapter 3). The flow rate of allylamine vapor is controlled by a Kobold floating ball flowmeter. The plasma power employed in this work ranged from 5 and 150 W. The monomer vapor pressure varied from 0.055 to 0.22 mbar. The deposition time was adjusted to obtain the desired thickness.

7.2.2 Ethanol extraction of ppAA films

In order to remove the soluble part from the ppAA films, the samples were submersed into pure ethanol and shaken for different lengths of time. After extraction, the films were washed with excess ethanol to remove small molecules adsorbed on the surface, and then dried at T = 50^{o}C for 2 h.

7.2.3 SPR and OWS measurements

SPR and OWS measurements were carried out with a home-built setup based on the Kretschmann configuration and has been described in Chapter 3. The SPR and OWS spectra were recorded against air immediately after plasma polymerization for freshly deposited ppAA films and after ethanol extraction. The SPR curve can be fitted using the Fresnel equations obtaining the optical thickness ($n*d$) of the dielectric medium. If the refractive index of the thin film is available, one can determine the geometrical thickness of the film. In contrast to SPR, OWS can distinguish between the refractive index n and the thickness d of the film provided that at least two optical waveguide modes can be excited.

7.3 Results and discussion

7.3.1 Film analysis

FT-IR was employed to identify ppAA film composition before and after ethanol extraction. Figure 7-1 shows typical FT-IR spectra for ppAA films deposited at a CW plasma mode with increasing input powers. The band at 3360 cm^{-1} indicates the presence of primary and secondary amines inside all the ppAA films. With increasing power from 5 to 100 W, the bands for CH_3 and CH_2 at 2960-2850 cm^{-1} increased. The similar trend could also be observed for the bands at 2240-2185 cm-1, which are ascribed to the absorption of C

≡ C or C ≡ N structures. These results could be ascribed to the higher fragmentation of monomer structure, which generally occurred under high plasma power conditions. XPS analysis also carried out to quantify the elemental composition of the ppAA films deposited at different powers. As shown in Table 7-1, the N/C ratio of 5W ppAA is higher than that of 100W ppAA.

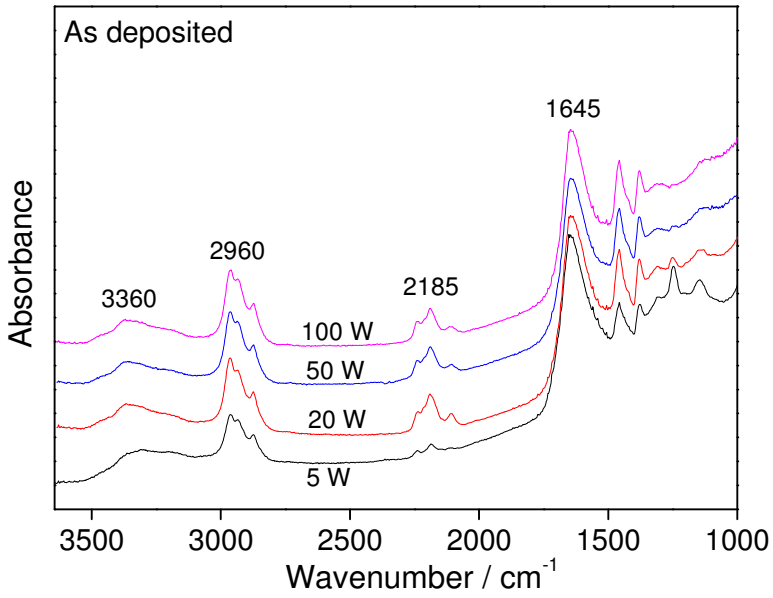

Figure 7-1: FT-IR spectra of the ppAA films deposited at different plasma power. Plasma conditions: CW, 0.1 mbar.

Table 7-1: Surface composition from XPS measurements for the ppAA films deposited at different input powers. Plasma conditions: CW, 0.1 mbar.

Plasma power (Watts)	%C	%N	%O	N/C
5	77.2	20.0	2.8	0.26
100	79.6	17.9	2.5	0.22

Extraction treatment on plasma polymers can remove some of unbound materials. However, FT-IR analysis showed that there are no significant changes in the chemical structure of the ppAA films before and after overnight ethanol extraction, as shown in Figure

7-2. The overall decrease of the band intensity is due to the decrease of the film's thickness. This is also confirmed by XPS data (not given here), which showed no measurable change in the composition of ppAA's surface. The roughness (Rq) of the extracted ppAA was below 1 nm (Figure 6-3). Compared to the fresh ppAA, the roughness of the extracted ppAA was a little higher, which may be due to the loss of some low molecular weight materials.

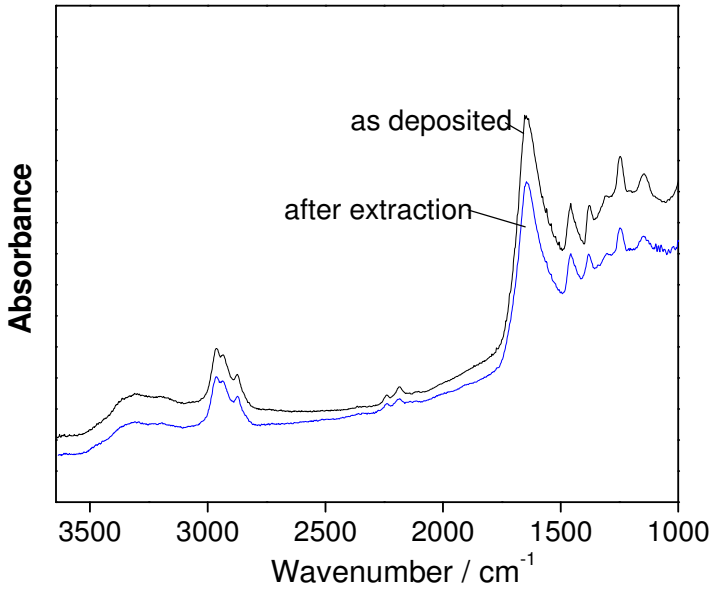

Figure 7-2: Comparison of the FT-IR spectra of ppAA films before and after ethanol extraction. Deposition conditions: 5 W, CW, 0.1 mbar.

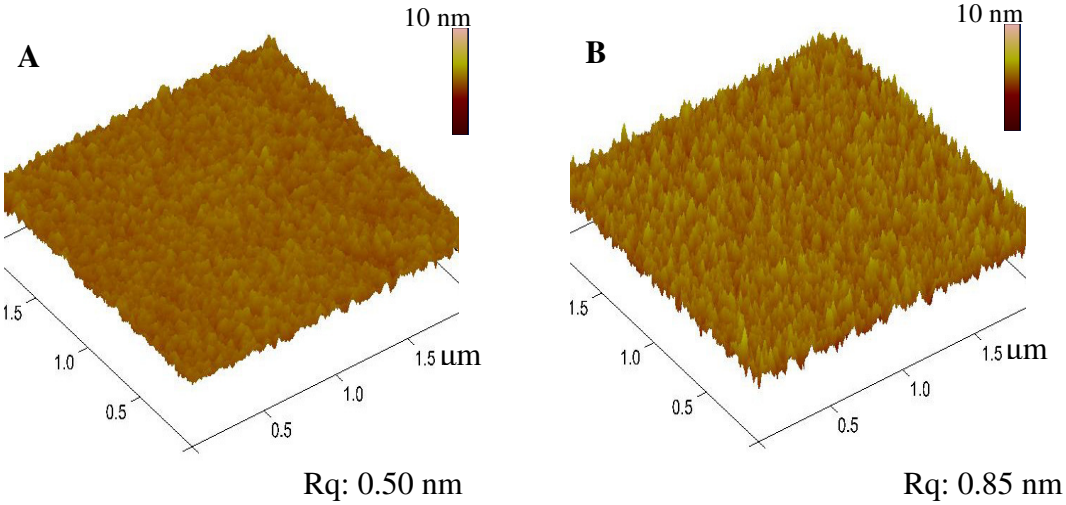

Rq: 0.50 nm Rq: 0.85 nm

Figure 7-3: AFM image of the ppAA films (A) before and (B) after ethanol extraction. Deposition conditions: 5 W, CW, 0.079 mbar.

7.3.2 Film thickness upon ethanol extraction

The thicknesses of both fresh and extracted ppAA were measured using SPR or OWS. For each ppAA film, four positions were measured. The standard derivation of the measured thickness is less than 2%. There is no film delamination from Au substrate observed in the present study. SPR and OWS data show the loss of material from the ppAA films leading to a reduction in the film's thickness. Figure 7-4 shows two OWS spectra of a ppAA film (deposited at 100 W, CW for 7 mins) before and after ethanol extraction. Because there are more than two optical waveguide modes in each spectrum, both the refractive index *n* and thickness *d* of the film can be determined from the simulation. For the fresh ppAA, the thickness was found to be d = 601 nm and refractive index was n = 1.594, while for the extracted ppAA, d and n were 470 nm and 1.585, respectively. It is evident that the ppAA film, after ethanol extraction, shows a large decrease in thickness because of the loss of material. The decrease in refractive index n could correspond to a decrease in film density because some soluble part was extracted upon ethanol treatment. In order to study films of d<150 nm, in the subsequent work, the refractive index of all ppAA films is assumed to be constant regardless of film thickness and plasma conditions. The error from this assumption is estimated to be lower than 2% if the derivation of *n* is lower than 0.010. Consequently, the thickness of thin film with thickness lower than 150 nm can be obtained by SPR measurement.

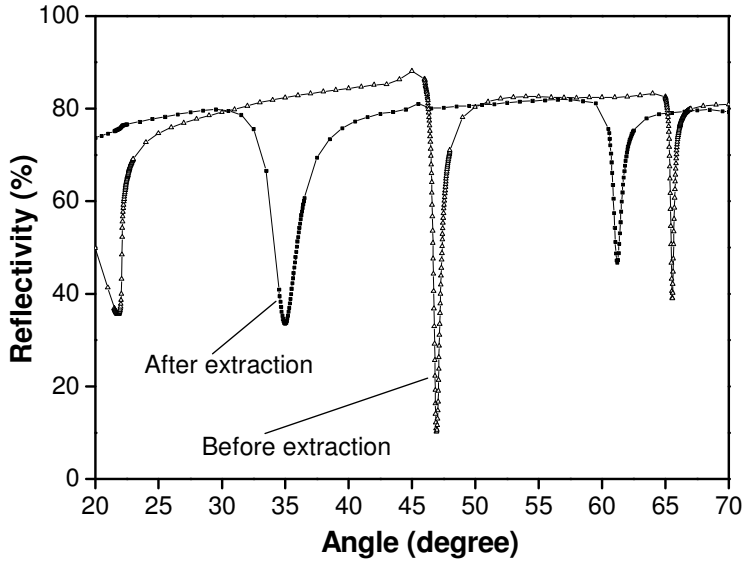

Figure 7-4: Typical s-polarized OWS spectra of ppAA films (d = 601 nm) before and after ethanol extraction.

Firstly, the extraction time sufficient to remove the unbound materials was determined by treating ppAA films in ethanol for different lengths of time. Figure 7-5 shows the thickness evolution of a d=601 nm ppAA film as a function of time. Clearly, 8 h ethanol extraction results in a distinct decrease in film thickness because of the loss of some low molecular weight material from the freshly deposited ppAA. After an additional 7 h of extraction, only small additional changes in thickness were observed. After another 15 h of extraction, no more changes were observed. The decrease is comparable to the measurement error. Therefore, ethanol extraction of 15 hours is sufficient to stabilize the 100W ppAA film at the present conditions.

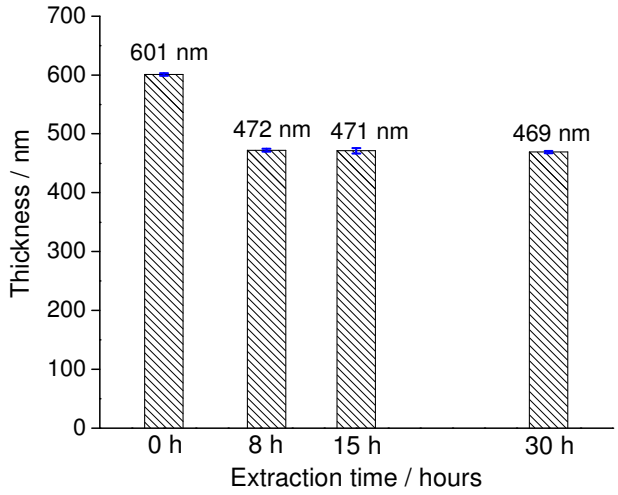

Figure 7-5: Thickness evolution of a 601 nm ppAA film upon ethanol extraction with increasing extraction time.

The percentage of remaining film was used as an indication for the stability of ppAA films.

$$Percentage\ of\ remaining\ film = \frac{d_{extracted}}{d_{fresh}} \times 100\%$$

Here d_{fresh} and $d_{extracted}$ are the thickness of fresh and extracted ppAA, respectively. Figure 7-6 shows the percentage of remaining film for the ppAA deposited at 100W, CW, but with different deposition time. It can be seen that for the 100 W film the relative thickness of the remaining materials increased with increasing thickness. For example, 27.7% was remained for a freshly deposited film of d = 47 nm, but 78.0% remained for a d = 601 nm film. The net thickness decrease for the above films was 34.2 and 132.0 nm,

respectively. This indicates that the ethanol extraction treatment appears to affect the whole ppAA film rather than the outermost layer only. These data clearly show that the extent of ethanol extraction onto ppAA films is related to the thickness of ppAA films. It is well known that UV irradiation initiates the cross linking inside polymer networks. The UV in the plasma may initiate the cross linking reaction inside the deposited film during plasma polymerization process. The thicker film will be exposed to UV for a longer time, and hence may have a higher cross-linking density within the film, which may lead to the better stability observed in comparison to the thinner films deposited at the same conditions.

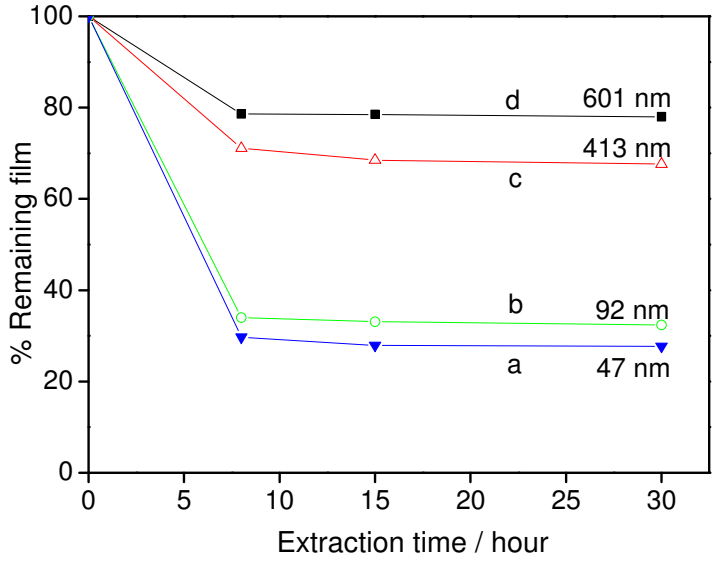

Figure 7-6: The percentage of remaining film after ethanol extraction treatment to the ppAA films with different thicknesses. Plasma conditions: 100 W, CW.

Plasma power also influences the reaction mechanisms during plasma polymerization, thus effecting the surface chemistry and cross-linking density of the deposited films. The effect of plasma deposition power on the extraction behaviors of the ppAA films was also investigated. For this purpose, ppAA films of approximately the same thickness were deposited. From Figure 7-7, it can be seen that as the plasma power was increased from 50 W to 100 W and 143.5 W, the percentage of remaining film increased from 30.4% to 42.4% and 57.9%, respectively. This indicates that high power ppAA film loses less materials after extraction than low power plasma film. The high input power results in a high fragmentation of the monomer molecules in use, and gives rise to high cross-linking density within the deposited plasma polymer. The higher the degree of cross-linking is, the more stable the film

is. When in contact with solvent, it was observed that there would be less loss of materials from the highly cross-linked plasma polymer.

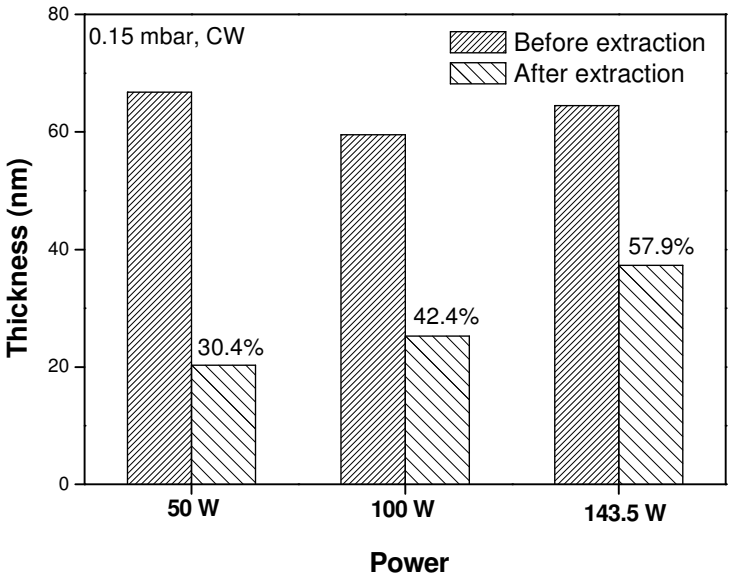

Figure 7-7: The thickness of ppAA films after ethanol extraction as a function of plasma power.

The monomer pressure employed also affects the stability of the ppAA films upon ethanol extraction. After ethanol extraction for 15 h, the films deposited at low monomer vapor pressure showed higher values for the remaining thickness (69.8%) compared to 19.4% for the film deposited at a high monomer vapor pressure (Figure 7-8). This indicates that the ppAA film deposited at high pressure is less stable than that deposited at low monomer vapor pressure. This result may come from two effects. On the one hand, the pressure affects the deposition time. The time for ppAA film deposition at 0.055 mbar was 132 sec, which is longer than 60 sec for the film deposited at 0.22 mbar. This will result in longer UV exposure time for low pressure ppAA, which may lead to higher cross-linking density. On the other hand, at low pressure, the electrons, ions, and radicals have long mean free paths and bombard the surface with high momentum, which may cause surface cross-linking reactions.[9] As a result, the ppAA deposited at low monomer pressure may have a higher cross-linking density than the film deposited at high monomer pressure.

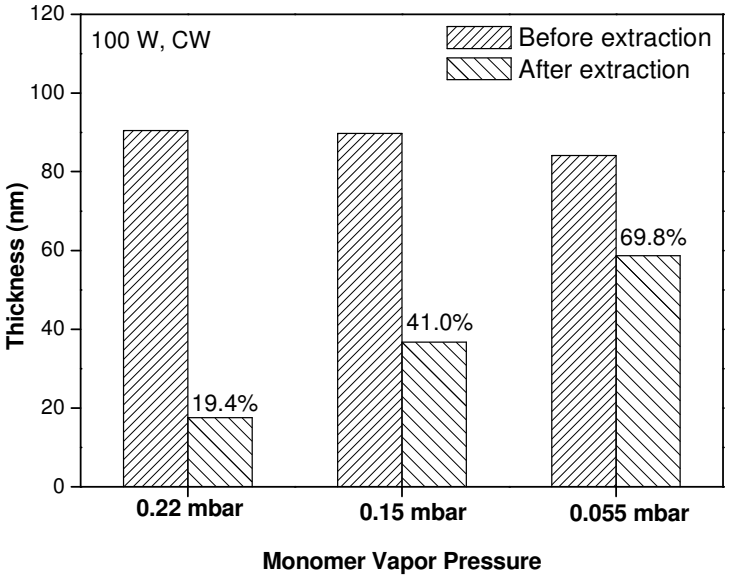

Figure 7-8: The thickness of ppAA films after ethanol extraction as a function of monomer vapor pressure.

The decrease in ppAA thickness can be ascribed to the loss of low molecular weight materials. It is generally believed that high cross-linking degree inhibits the loss of materials from the plasma deposited films. Therefore, there should be a correlation between the decrease of ppAA thickness and the degree of cross linking inside the films. The present data indicate that plasma conditions, such as plasma power and monomer pressure, are of great importance for the formation of cross linking in ppAA films, and thus affecting the stability of films. UV irradiation in the plasma may also be an important factor for the formation of cross linking. That is, the molecules in the deposited film may undergo considerable structural change, e.g. cross-linking of the molecules due to the presence of UV in plasma. Since there is no method up to date to quantify the degree of cross linking inside the plasma deposited films, the exact mechanism of formation of cross linking in the plasma film is not clear.

7.3.3 Swelling behaviour in aqueous solution

Removal of unbound materials by ethanol extraction clearly improved the stability of a 100W ppAA film in PBS buffer solution (Figure 7-9). For the freshly deposited ppAA, a rapid decrease in SPR reflectivity could be observed for the first 100 min. After that a slow process taken over and the film became stable after about 12 hours. This result indicates the

100W ppAA film contain some soluble materials, which could be washed away by PBS buffer solution. After extraction treatment, however, the 100W ppAA film became stable in PBS buffer because the unbound materials have been removed by ethanol extraction.

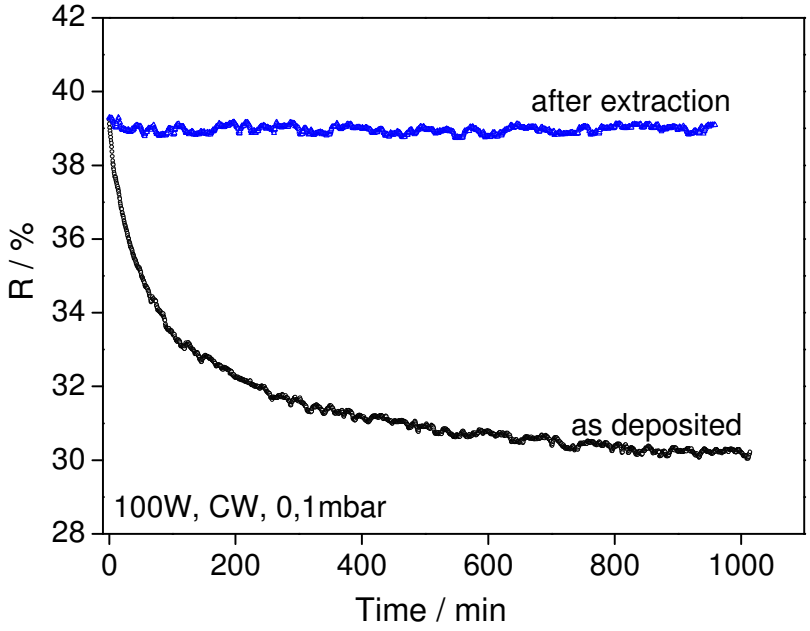

Figure 7-9: SPR kinetic measurement showing the swelling behaviour of a 100W ppAA film before and after extraction, respectively.

For a 5W ppAA film (Figure 7-10), the effect of ethanol extraction onto its swelling behaviour is not so significant. A gradual decrease in SPR reflectivity could be observed when a 5W ppAA was brought into contact to PBS buffer solution. After about 3 hours, the film became stable. It appears that the 5W ppAA film undergos structural change, e.g., rearrangement of polymer chains or reorientation of some functional groups, in buffer solution. In contrast, a 100W ppAA film is believed to have a higher cross-linking density and thus have no structural change in PBS buffer solution.

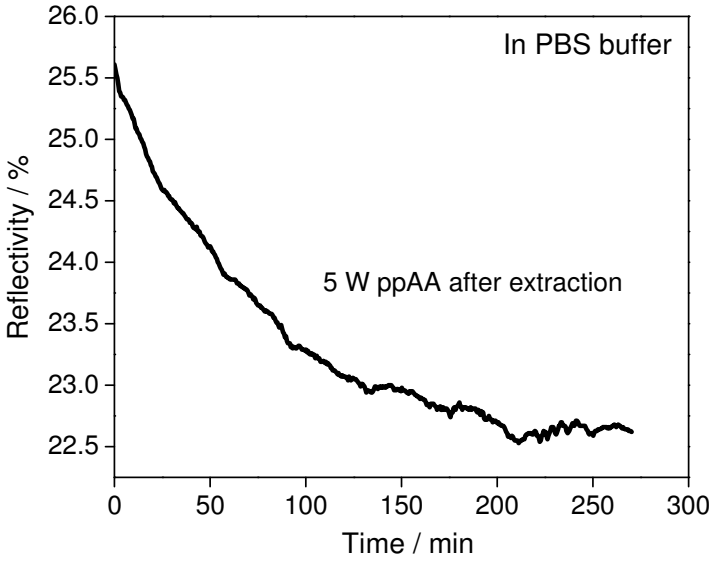

Figure 7-10: Swelling behaviour of a 5W ppAA film after ethanol extraction.

7.4 Conclusions

The soluble part of the ppAA films increases with decreased thickness, as well as the decrease in power and the increase in monomer vapor pressure. This result could be related to different reaction mechanisms occurring during the deposition process. Even after extraction, the chemistry of the films was found to be the same and enough material remains covalently bonded for subsequent reactions. While the stability of a 100W ppAA film in PBS buffer solution could be improved after the removal of unbound materials by ethanol extraction treatment, the case of 5 W ppAA is more complicated because the polymer chains in low power ppAA films might undergo rearrangement when immersed into a liquid environment.

References

1. Harsch, A.; Calderon, J.; Timmons, R. B.; Gross, G. W. *J. Neurosci. Meth.* **2000,** 98, 135-144.
2. Griesser, H. J.; Chatelier, R. C.; Gengenbach, T. R.; Johnson, G.; Steele, J. G. *J. Biomater. Sci. Polym. Ed.* **1994,** 5, (6), 531-554.

3. Dai, L. M.; StJohn, H. A. W.; Bi, J. J.; Zientek, P.; Chatelier, R. C.; Griesser, H. J. *Surf. Interface Anal.* **2000,** 29, (1), 46-55.
4. Chen, Q.; Förch, R.; Knoll, W. *Chem. Mater.* **2004,** 16, 614-620.
5. Zhang, Z.; Chen, Q.; Knoll, W.; Foerch, R.; Holcomb, R.; Roitman, D. *Macromolecules* **2003,** 36, 7689-7694.
6. Zhang, Z.; Chen, Q.; Knoll, W.; Foerch, R. *Surf. Coat. Technol* **2003,** 174-175, 588-590.
7. Tatoulian, M.; Bretagnol, F. R.; Arefi-Khonsari, F.; Amouroux, J.; Bouloussa, O.; Rondelez, F.; Paul, A. J.; Mitchell, R. *Plasma Process. Polym.* **2005,** 2, (1), 38-44.
8. van Os, M. T.; Menges, B.; Foerch, R.; Vancso, G. J.; Knoll, W. *Chem. Mater.* **1999,** 11, 3252-3257.
9. Butoi, C. I.; Mackie, N. M.; Gamble, L. J.; Castner, D. G.; Barnd, J.; Miller, A. M.; Fisher, E. R. *Chem. Mater.* **2000,** 12, (7), 2014-2024.

Chapter 8

Homogeneous DNA Detection*

8.1 Introduction

Rapid detection of the presence/absence of a specific DNA sequence is crucial for the identification of genetically modified organism (GMO) in foods, for the diagnosis of infections, as well as for environmental monitoring. Most available methods rely on the immobilization of DNA probes onto sensor surfaces and the subsequent hybridization of the surface attached probes with the target DNA from solution. Recently, several researchers had demonstrated that it was possible to use conjugated polymers[1-7] or DNA-functionalized nanoparticles[8-14] for homogeneous DNA detection, thus avoid the difficulties associated with DNA probe immobilization. However, those strategies involve several process steps, which make them undesirable for practical DNA detection. Herein I show the possibility of using labelled peptide nucleic acids (PNA) as probes for homogeneous DNA detection.

Peptide nucleic acids (PNA) are DNA analogs in which an uncharged pseudopeptide chain replaces the negatively charged sugar-phosphate backbone of natural DNA (Figure 8-1), resulting in an achiral and neutral mimic.[15-17] PNA is capable of sequence-specific binding to DNA or RNA sequences obeying the Watson-Crick hydrogen bonding rules. When used as the probe strand in a DNA sensor, it was reported that PNA has many advantages over DNA probes, such as higher stability,[17,18] higher selectivity,[19, 20] and low requirements for a particular buffer solution.[17, 21, 22]

In this work a DNA detection method was developed, which takes advantages of the surface sensitivity of SPFS, as well as, the different electrostatic properties of PNA and DNA. Scheme 8-1 illustrates the concept of the present DNA detection method. The labelled PNA is neutral and hence it does not adsorb onto the positively charged surface (Scheme 8-1A). Additionally, as mentioned above, the fluorophores in the bulk solution cannot be seen by SPFS. As a consequence, no fluorescent signal can be detected by SPFS. On the other hand, as shown in Scheme 8-1B, the specific hybridization of target DNA to the labelled PNA results in a negatively charged hybrid, which will adsorb onto the positively charged surface (plasma polymerised allylamine films in this case) by electrostatic interaction. The

* Part of the work in this chapter has been accepted for publication in *Angew. Chem. Int. Ed.*

dye associated with PNA will thus be excited and can be detected using SPFS. In this way, the presence of a particular target DNA can be detected without the necessity to label DNA. Here the labeled PNA serves not only as the DNA catcher recognizing a particular target DNA, but also as a fluorescent indicator.

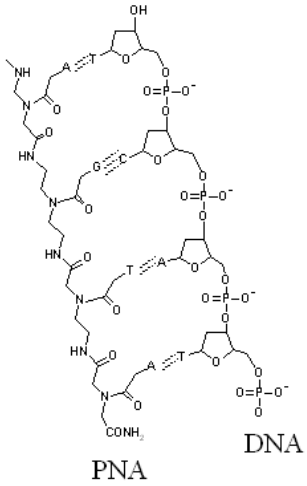

Figure 8-1: Comparison of the chemical structures between PNA and DNA. A, T, G and C represent the nucleobases adenine, thymine, guanine and cytosine, respectively.

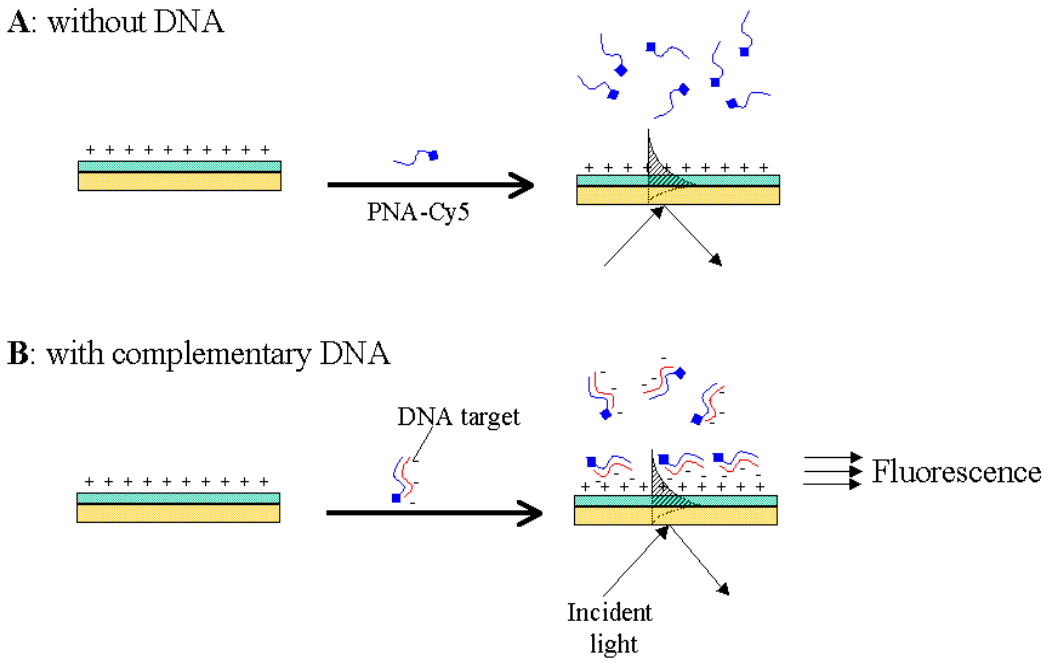

Scheme 8-1: The concept of DNA detection using SPFS and fluorescent PNA as DNA probes.

8.2 Experimental section

8.2.1 Materials

Fluorescently labelled PNA (P1: ACA TGC AGT GTT GAT-Cy5) was purchased from Applied Biosystems, Foster City, CA. The ssDNA used in this work, including the complementary target DNA (T1: 3'-ATC AAC ACT GCA TGT-5'), the one-mismatch target DNA (T2: 3'-ATC AAC ACT ACA TGT-5'), and the competitor DNA (3'-ATC AAC TGA ACA TGT-5'), were purchased from MWG Biotech, Ebersberg, Germany. PBS buffer (0.01 M phosphate buffer, 0.0027 M potassium chloride and 0.137 M sodium chloride, pH 7.4, at 25 °C) (Sigma-Aldrich) was used to prepare PNA and DNA solutions. PNA/DNA hybridization was carried out by adding 100 nmol of P1 into a solution of 100 nmol of T1 and T2, respectively. The mixture was shaken at room temperature for 0.5 h, allowing for the completion of PNA/DNA hybridization.

8.2.2 Preparation of ppAA films

Deposition of ppAA films was carried out in a home-built plasma reactor under continuous wave conditions. The plasma input power employed was 5 or 100 W, and the monomer vapor pressure was 0.1 mbar. In order to achieve an optimized fluorescence signal in SPFS and not to lose too much intensity due to energy transfer to the metallic substrate, the chromophores have to be sufficiently separated from the substrate surface. In the present work the thickness of the ppAA film had to be 40 nm to achieve an optimum signal. The soluble part of the PPAA films was removed by ethanol extraction for 15 hours. After extraction, the films were washed with excess ethanol to remove small molecules adsorbed on the surface, and then dried at T = 50^{o}C for 2 h.

8.2.3 SPFS measurements

SPFS measurements were carried out with a home-built set-up as described in Chapter 3. The ppAA coated slides were attached to a flow cell. A reference experiment was carried out by injecting 1 nmol fluorescent PNA into the flow cell of SPFS. Then the mixture of PNA and DNA targets were sequentially introduced into the flow cell. The fluorescent signal was record in real time. NaOH solution of 50 mM was added to regenerate the sensor surface.

8.3 Results and discussion

8.3.1 Comparison of PNA and DNA adsorption on a ppAA film

Due to the difference in the electrostatic features between PNA and DNA, they will show a different affinity towards a positively charged surface. Figure 8-2 shows the SPFS spectra after either PNA or DNA adsorbing on a ppAA surface. It is apparent that the amount of DNA strands adsorbed onto the ppAA surfaces is much higher than that of PNA. The small fluorescent signal observed when injecting PNA may be due to non-specific interaction.

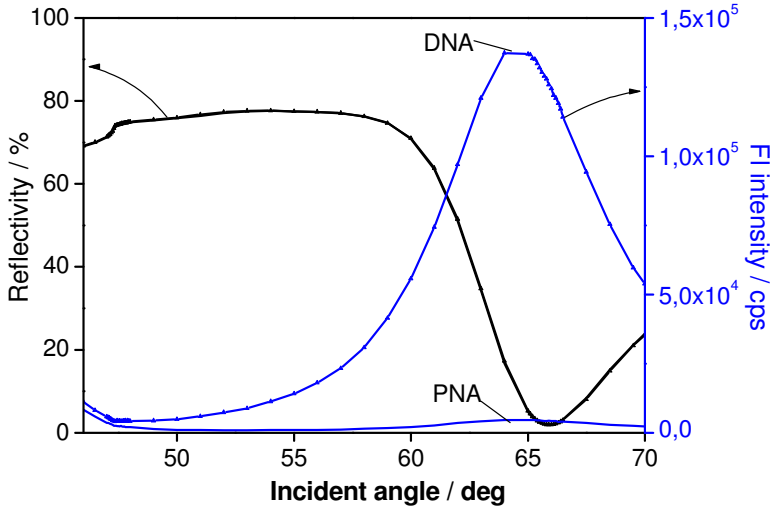

Figure 8-2: SPFS spectra after Cy5-labelled PNA (i.e., P1) and DNA adsorbing on the ppAA surface. PNA and DNA have the same sequences (i.e., ACA TGC AGT GTT GAT-Cy5). The concentration of PNA and DNA solution: 1 nM.

8.3.2 Detection of different DNA targets

In a typical experiment for detecting different DNA sequences, the fluorescently labelled PNA (i.e., P1) was firstly added into different target DNA solutions, i.e., T1 (fully complementary) and T2 (one base pair mismatch), respectively. The PNA/DNA mixture was shaken for 0.5 h, allowing for the hybridization of PNA and DNA, and then was introduced into the flow cell of the SPFS. Figure 8-3A shows the real-time SPFS detection of the fluorescent signal upon injection of the two different solutions. The P1 solution of 1 nmol was used here as a reference. After the introduction of P1, a small increase of the fluorescence intensity was observed. In the case of single-mismatch DNA (i.e., T2/P1), the fluorescece signal showed a small increase, almost comparable to that for the pure P1 injection, most likely because the hybridisation between T2 and P1 was unsuccessful leading

to the same response as P1 only. However, for fully complementary DNA target (i.e., T1/P1), a strong increase of the SPFS signal can be observed. This clearly shows that the T1/P1 hybrid, now a negatively charged entity, is able to bind to the surface. Figure 8-3B shows the SPFS spectra after injection of various sample solutions. The hybrid of PNA and the fully complementary DNA target (i.e., T1/P1) results in a strong fluorescent signal. In contrast, the hybrid of PNA and a DNA strand with one single mismatch (T2/P1) shows a very weak fluorescent signal, which is only slightly higher than the reference PNA solution. It is apparent that this DNA detection method can discriminate effectively between different DNA sequences with one base pair mismatch.

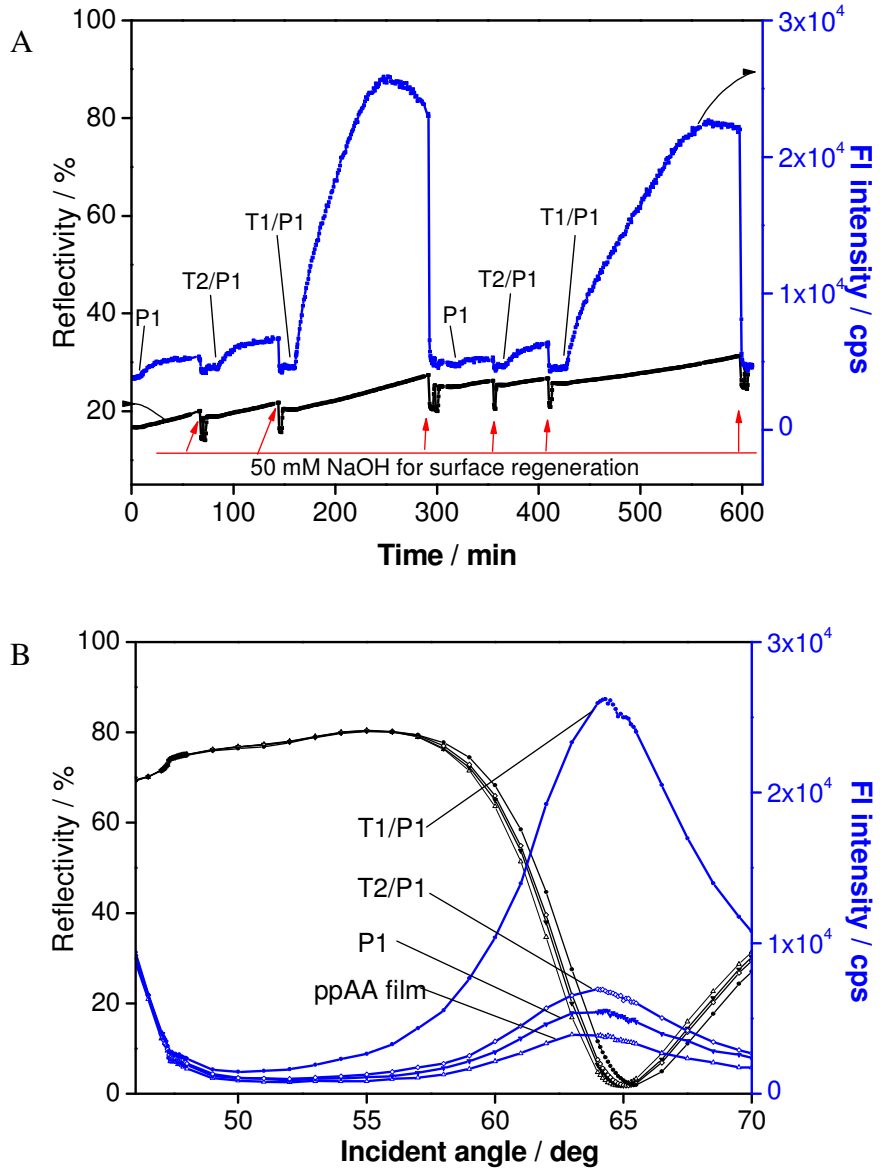

Figure 8-3: A). SPFS kinetic measurements during injecting 1 nmol of P1, T1/P1 and T2/P1, respectively. The surface was regenerated with 50 mM NaOH solution for 2 mins, followed by PBS buffer rinse. B). SPFS spectra after adsorption of various species. The SPFS spectrum of the ppAA surface in PBS buffer is given as a reference.

As shown in Figure 8-3A, the fluorescent signal can return to the baseline after rinsing the sensor surface with 50 mM NaOH, indicating that all of the hybridized PNA strands were removed from the ppAA surface. The SPFS measurements for each sample were repeated twice. It is found that the reproducibility is good. This also indicates that the ppAA surfaces are re-useable after regeneration.

8.3.3 DNA detection using different ppAA surfaces.

From FT-IR and XPS results in Chapter 7, a 5W ppAA film has more amine functional groups compared to a 100W ppAA. This suggests that a 5W ppAA film have higher adsorption capacity with respect to the negatively charged species. Consequently, more T1/P1 hybrid was expected to be observed on a 5W ppAA rather than the case for a 100W ppAA. From Figure 8-4, however, the fluorescence intensity for both case are almost comparable. This appears to indicate that the number of adsorbed T1/P1 is independent on the number of positively charged species on ppAA surfaces. Noted that the T1/P1 concentration employed in this experiment is only 1 nmol·L^{-1}. At such low concentration, it is likely that the adsorption process is controlled by the diffusion step. Considering the longer swelling process of a 5W ppAA film in PBS buffer (see Chapter 6), the 100W ppAA films were employed as the positively charged surface in this study.

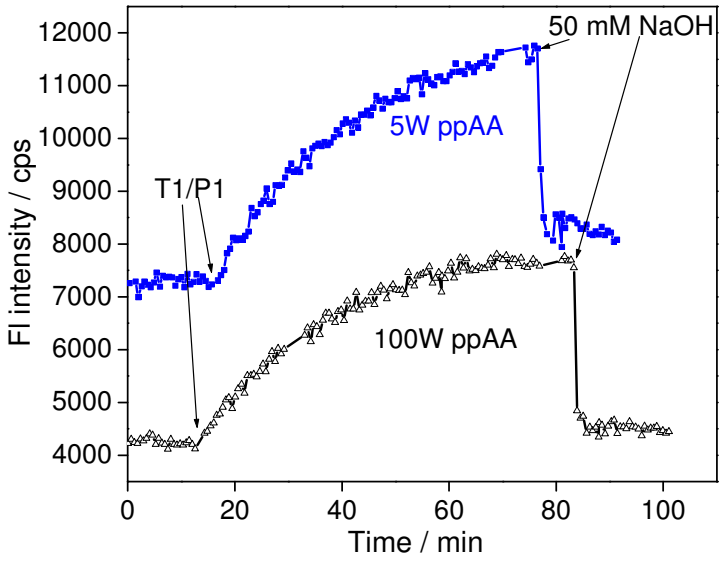

Figure 8-4: Comparison of T1/P1 adsorption on 5W and 100W ppAA films, respectively.

8.3.4 Limit of detection

In order to identify the limit of detection (LOD) of the present method, a series of T1/P1 solution ranging from 100 pM to 1 nM were tested sequentially, as shown in Fig. 3. As reference, a P1 solution of 500 pM was also measured. Compared to the SPFS background, no more fluorescent signal could be observed, indicating that non-specific adsorption of PNA is negligible at such low concentrations. On the other hand, T1/P1 solution with a concentration of 200 pM is sufficient to generate a clear increase in SPFS fluorescence (see the insert in Fig. 3). That means, the lowest concentration that could be detected using the present method is 200 pM. Noted that it appears that under the employed concentration the initial hybridization process might be controlled by the diffusion of DNA target from the bulk to the surface, showing a linear signal increase over time, as depicted by the dashed lines in Figure 3.

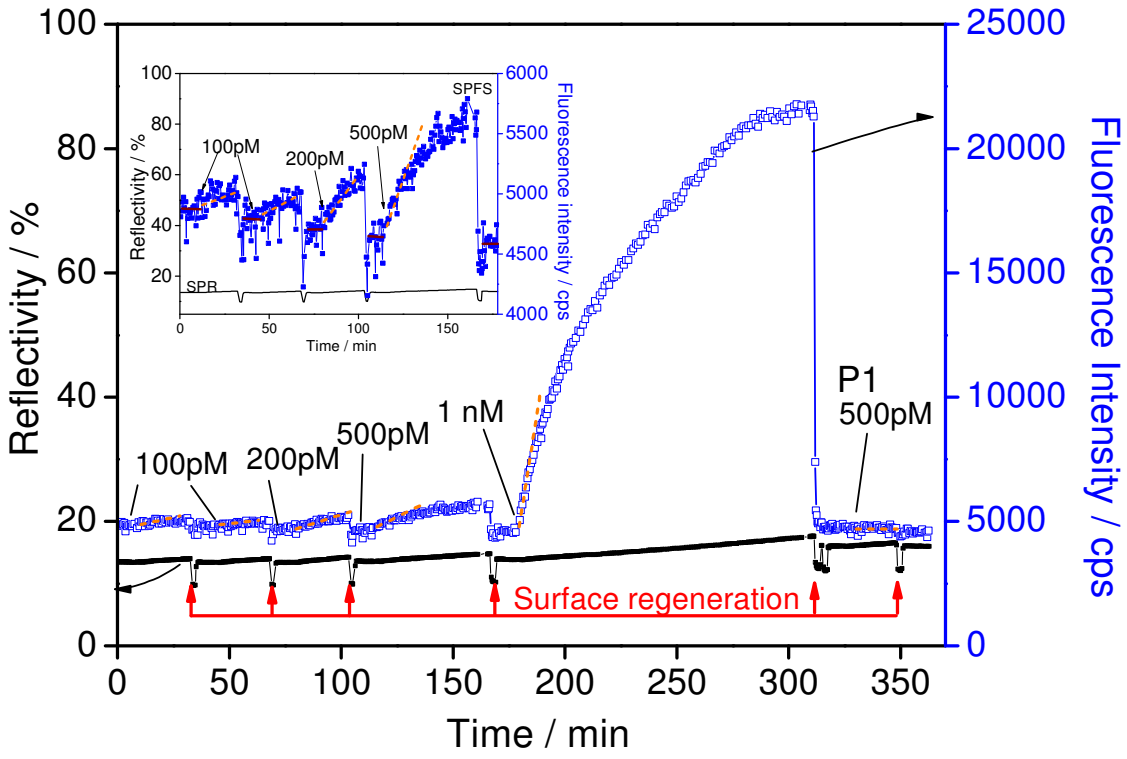

Figure 8-5: SPFS kinetic measurements upon injecting T1/P1 solution with various concentrations. A PNA solution of 500 pM was used here as a reference. The insert shows the magnification. The solid lines and dashed lines represent the baseline and the slope (i.e., the fluorescence increase over time), respectively, and are added to guide the eye. A T1/P1 solution of 200pM leads to a clear increase in SPFS fluorescence, while in PBS buffer the SPFS fluorescence remains almost constant.

Considering that electrostatic interactions are non-specific, other negatively charged species in the sample solution would definitely interfere with the adsorption of a specific PNA/DNA duplex on the ppAA surfaces. In extreme cases, other negatively charged species would occupy all of the positive sites on the ppAA surfaces, resulting in no adsorption of the PNA/DNA complex of interest. In order to address this issue, a T1/P1 sample solution of 1 nmol was mixed with a negatively charged competitor (i.e. single strand DNA with a complete mismatch). The resulting fluorescent intensity of mixture solution using SPFS is shown in Figure 8-6. If the concentration of competitor DNA was increased from 1 to 10 nmol, there was almost no decrease of the SPFS signal. However, upon further increasing the concentration of competitor DNA to 100 nmol, the fluorescent intensity decreased. Furthermore, if the competitor DNA reached 1000 nmol, almost no fluorescence was observed anymore, indicating that the positive sites of the ppAA surface has been occupied by competitor DNA. After a regeneration step, a PNA solution of 1 nmol was injected into the flow cell again. Interestingly, the resulting fluorescent intensity was almost the same as that after the first injection of PNA. It is apparent that the adsorbed DNA can be removed by the regeneration solution. That means, the ppAA surface is still active for DNA detection.

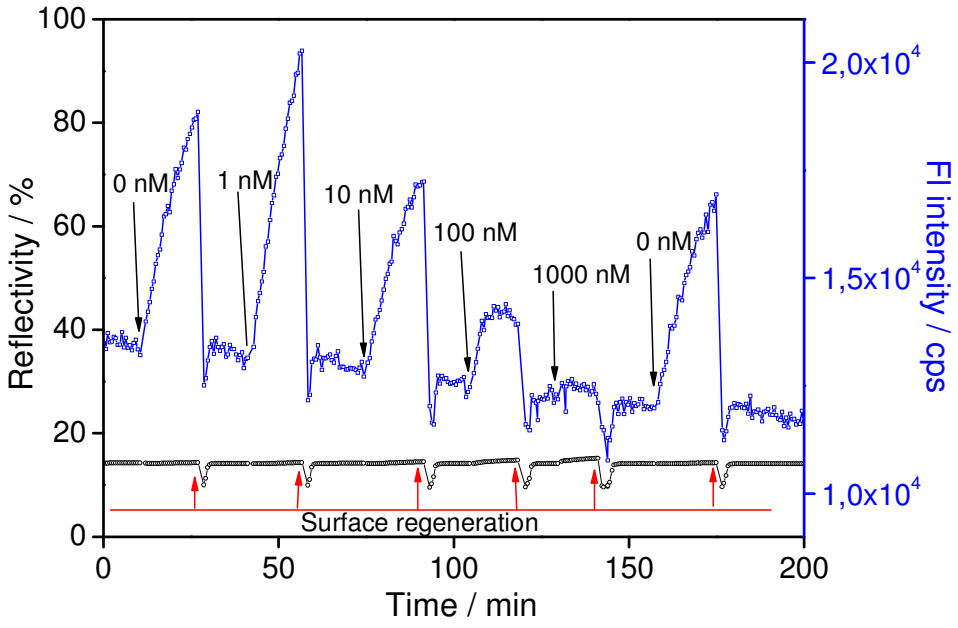

Figure 8-6: SPFS results upon injection of a mixture of 1 nmol of T1/P1 and competitor DNA with increasing concentrations from 1 nmol to 1000 nmol.

8.4 Conclusions

In this work I demonstrate a new homogeneous method for DNA detection, which takes advantages of the surface sensitivity of SPFS, as well as, the different electrostatic properties of PNA and DNA. Several advantages are offered by this method: 1). It avoids the step of immobilization of DNA probes on sensor surfaces, and thus reduces the complexity and the cost for sensor preparation. 2). Since commercially available PNA are used not only as DNA probes, but also as a fluorescent indicator, no labeling to the target DNA is required. 3). DNA/PNA hybridization occurs in solution, and thus is faster than that occurring on the sensor surface.[23] Consequently, the present method promises a rapid identification of a specific gene. 4). The method will make use of all the advantages associated with using PNA as DNA probe, including the high affinity, specificity and easy requirements for the buffer solution.

Since the LOD of the method is 200 pM, PCR amplification of target DNA is still needed, however, PCR amplification of DNA target has become a routine process for DNA analysis. I believe that this method would be particularly suitable for detection of a specific gene in GMO, viral, and pathogen DNA.

References

1. Ho, H. A.; Boissinot, M.; Bergeron, M. G.; Corbeil, G.; Dore, K.; Boudreau, D.; Leclerc, M. *Angew. Chem. Int. Ed.* **2002,** 41, (9), 1548-1551.
2. Gaylord, B. S.; Heeger, A. J.; Bazan, G. C. *Proc. Natl. Acad. Sci. USA* **2002,** 99, (17), 10954-10957.
3. Gaylord, B. S.; Heeger, A. J.; Bazan, G. C. *J. Am. Chem. Soc.* **2003,** 125, (4), 896-900.
4. Liu, B.; Gaylord, B. S.; Wang, S.; Bazan, G. C. *J. Am. Chem. Soc.* **2003,** 125, (22), 6705-6714.
5. Dore, K.; Dubus, S.; Ho, H. A.; Levesque, I.; Brunette, M.; Corbeil, G.; Boissinot, M.; Boivin, G.; Bergeron, M. G.; Boudreau, D.; Leclerc, M. *J. Am. Chem. Soc.* **2004,** 126, (13), 4240-4244.
6. Ho, H. A.; Dore, K.; Boissinot, M.; Bergeron, M. G.; Tanguay, R. M.; Boudreau, D.; Leclerc, M. *J. Am. Chem. Soc.* **2005,** 127, (36), 12673-12676.
7. Liu, B.; Bazan, G. C. *Chem. Mater.* **2004,** 16, (23), 4467-4476.

8. Elghanian, R.; Storhoff, J. J.; Mucic, R. C.; Letsinger, R. L.; Mirkin, C. A. *Science* **1997,** 277, (5329), 1078-1081.
9. Storhoff, J. J.; Lazarides, A. A.; Mucic, R. C.; Mirkin, C. A.; Letsinger, R. L.; Schatz, G. C. *J. Am. Chem. Soc.* **2000,** 122, (19), 4640-4650.
10. Taton, T. A.; Mirkin, C. A.; Letsinger, R. L. *Science* **2000,** 289, (5485), 1757-1760.
11. Storhoff, J. J.; Lucas, A. D.; Garimella, V.; Bao, Y. P.; Muller, U. R. *Nat. Biotechnol.* **2004,** 22, (7), 883-887.
12. Liu, S. H.; Zhang, Z. H.; Han, M. Y. *Anal. Chem.* **2005,** 77, (8), 2595-2600.
13. Stoeva, S. I.; Lee, J. S.; Thaxton, C. S.; Mirkin, C. A. *Angew. Chem. Int. Ed.* **2006,** 45, (20), 3303-3306.
14. Du, B. A.; Li, Z. P.; Liu, C. H. *Angew. Chem. Int. Ed.* **2006,** 45, (47), 8022-8025.
15. Nielsen, P. E.; Egholm, M.; Berg, R. H.; Buchardt, O. *Science* **1991,** 254, (5037), 1497-1500.
16. Egholm, M.; Buchardt, O.; Nielsen, P. E.; Berg, R. H. *J. Am. Chem. Soc.* **1992,** 114, (5), 1895-1897.
17. Egholm, M.; Buchardt, O.; Christensen, L.; Behrens, C.; Freier, S. M.; Driver, D. A.; Berg, R. H.; Kim, S. K.; Norden, B.; Nielsen, P. E. *Nature* **1993,** 365, (6446), 566-568.
18. Jensen, K. K.; Orum, H.; Nielsen, P. E.; Norden, B. *Biochemistry* **1997,** 36, (16), 5072-5077.
19. Ratilainen, T.; Holmen, A.; Tuite, E.; Haaima, G.; Christensen, L.; Nielsen, P. E.; Norden, B. *Biochemistry* **1998,** 37, (35), 12331-12342.
20. Ratilainen, T.; Holmen, A.; Tuite, E.; Nielsen, P. E.; Norden, B. *Biochemistry* **2000,** 39, (26), 7781-7791.
21. Tomac, S.; Sarkar, M.; Ratilainen, T.; Wittung, P.; Nielsen, P. E.; Norden, B.; Graslund, A. *J. Am. Chem. Soc.* **1996,** 118, (24), 5544-5552.
22. Yao, D. F.; Kim, J.; Yu, F.; Nielsen, P. E.; Sinner, E. K.; Knoll, W. *Biophys. J.* **2005,** 88, (4), 2745-2751.
23. Levicky, R.; Horgan, A. *Trends Biotechnol.* **2005,** 23, (3), 143-149.

Chapter 9

Thermosensitive Surfaces by Plasma Polymerization

9.1 Introduction

Polymers with thermosensitivity have attracted a great deal of interests for decades because of their potential applications, such as the control of protein adsorption,[1] cell attachment,[2-4] and for bioseparation.[5, 6] At low temperatures this kind of polymer is soluble in aqueous media and the polymer chains exhibit a random coil configuration, surrounded by water molecules. However, if the temperature is increased above the lower critical solution temperature (LCST), the polymer precipitates out of solution by dehydration and increased hydrophobic interactions occuring between the polymer chains. The mechanism of polymer thermosensitivity is generally ascribed to the temperature dependence of hydration, and hydrophobic interaction.[7, 8] Several N-substituted poly(acrylamides) exhibit this phase transition behavior, as they consist of both hydrophilic amide groups and hydrophobic substituent groups. Particularly, poly(N-isopropylacrylamide) (PNIPAAm) has been extensively investigated because of its low LCST (31-32 ^{o}C), which is between room temperature (~20 ^{o}C) and the human body temperature (37 ^{o}C). PNIPAAm grafted onto a substrate surface shows a phase transition behavior leading to a temperature controlled surface wettability. Below the LCST, the surface is hyphophilic and resists protein adsorption. As temperature is increased to above the LCST, the grafted PNIPAAm chains collapse and the surface becomes hydrophobic.[9-11]

Immobilization of thermosensitive polymers onto a surface has been proposed using a variety of methods, such as atom transfer free radical polymerisation,[11] plasma grafting,[12, 13] photo-induced polymerisation[14] and covalent binding of polymer chains.[15-17] Several groups have shown that plasma polymerisation of NIPAAm is an alternative approach to obtain thermo responsive coating.[18-22] Compared to other methods, plasma polymerisation is attractive because it is a solvent free, one-step technique to produce conformal, ultrathin coating onto various substrates with good adhesion.

It has been reported that poly(N,N-diethylacrylamide) (PDEA) obtained using conventional polymerisation methods also shows a low LCST of 32-35 ^{o}C for phase transition or deswelling.[23, 24] In this work, N,N-diethylacrylamide (DEA) was employed as the precursor in plasma polymerisation processes to deposit ultra thin films exhibiting

thermosensitivity. One particular advantage of DEA is its higher vapor pressure in comparison to that of NIPAAm. Therefore, it does not require heating of either the monomer container or the plasma chamber, which is generally needed in NIPAAm plasma polymerization. Plasma polymerisation at low input power has proved to be a simple approach to obtain a high retention of monomer functionality. The chemical composition of plasma polymerised N,N-diethylacrylamide (ppDEA) was characterized by XPS and FT-IR. The LCST of the deposited ppDEA film was determined by water contact angle measurements.

9.2 Experimental section

9.2.1 Deposition of ppDEA films

Plasma polymerization at continuous wave mode was carried out in a home-built plasma reactor described in Chapter 3. Ihe input power ranged from 1 and 100 W. In order to improve the adhesion between the substrates and ppDEA films, 50 W ppDEA was firstly deposited onto the substrate for ca. 10 sec, then the plasma power was adjusted to the desired value (Scheme 9-1). The monomer vapor pressure during the plasma polymerization process was about 0.035 mbar. The deposition time was adjusted to obtain the desired thickness. In the present study the typical film thickness ranged from 10 to 50 nm. Some AFM measurements were performed on thicker films. The substrates for FT-IR and XPS measurements were 30 x 25 mm glass slides coated with 80 nm gold. Si wafers were used as the substrates for AFM and contact angle measurements.

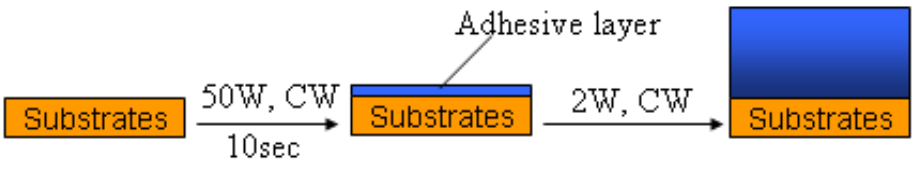

Scheme 9-1: Deposition procedure of thermosensitive ppDEA films with a 50W ppDEA as adhesion promotion layer.

9.2.2 Film analysis

AFM images were recorded using a EnviroScope atomic force microscopy (Veeco) in the tapping mode in humid air (80% relative humidity). The sample for the AFM investigation was scratched with a needle in order to obtain a step. The sample can be heated in situ on the stage of EnviroScope AFM, allowing for measurements at different temperature but at the identical position.

The static water contact angle measurement was carried out on a DSA 10-MK2 (Krüss), equipped with a thermostat chamber (TC3010, Krüss). A vessel containing MillQ-water was put into the chamber in order to obtain higher humidity.[6, 10] Measurements were taken every 2-5°C from 20 to 60°C. The sample was equilibrated at each temperature for 20 minutes. Five sample positions were measured at each temperature.

9.3 Results and discussions

9.3.1 FT-IR results

Figure 9-1 shows the FT-IR spectra of the DEA monomer and ppDEA films deposited at various plasma powers ranging from 1 to 100 W. The C=C stretching band at 1609 cm^{-1} cannot be observed in the spectra of pp-DEA, which indicates that the DEA monomer polymerised through the double bond. The IR band characteristic for amide (N-C=O) stretching vibrations at 1645 cm^{-1} was observed for ppDEA films deposited at 1-5 W plasma power, showing that the monomer structure could be retained under those conditions. At lower input power a shoulder was observed at 1674 cm^{-1}, the intensity of which increased relative to the amide band (1645 cm^{-1}) with increasing power. At input powers above 40 W, the band at 1645 cm^{-1} became little more than a tail of the peak at 1674 cm^{-1}. This shift to higher wavenumber can be associated with the dissociation of the amide and the possible formation of C=N groups. With higher input power one could also observe two new bands at 2154 cm^{-1} and 3338cm^{-1}. The former is characteristic for C≡C stretching vibrations, while the latter can be associated with $–NH_2$ and =NH groups as well as hydrogen bonding between adjacent functional groups. The diversity in the functional groups observed in the film can be ascribed to the high fragmentation of monomers at higher input power.

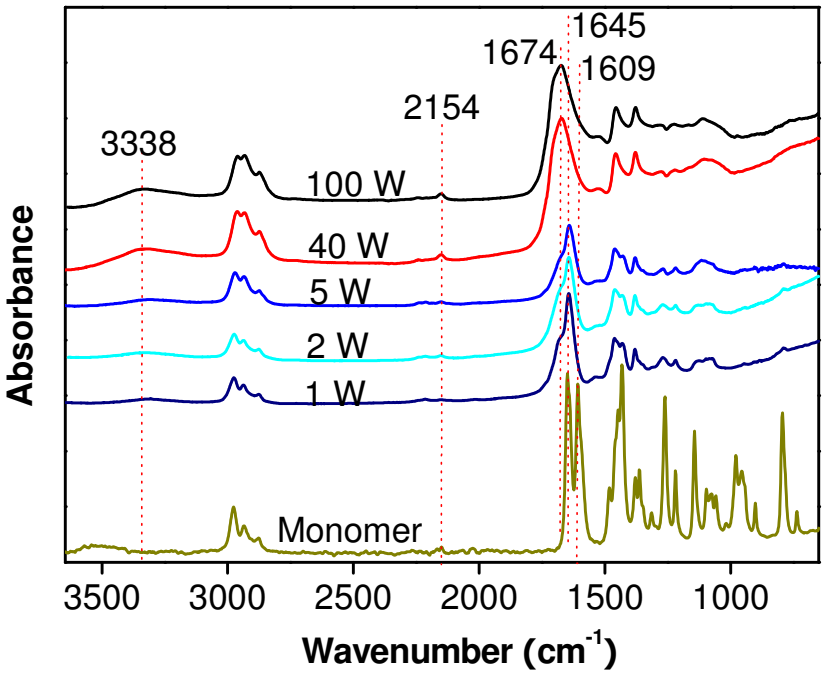

Figure 9-1: FT-IR spectra of DEA monomer and ppDEA films deposited at various plasma powers.

9.3.2 XPS results

XPS analysis of all films showed no signal from the substrate (i.e., Au in this work), indicating a complete coverage of the substrate by the ppDEA films, as shown in Figure 9-2. The C1s XPS spectra of ppDEA films deposited at different input power are given in Figure 9-3. The C1s XPS spectra were fitted according to the following carbon environments: 285.0 eV (C-C and C-H), 286.0 eV (C-N), 286.5 eV (C-O, including C-O-C and C-O-H), 287.8 eV (N-C=O) and 289.1 eV (O-C=O). The binding energies assigned to each of these peaks is in accordance with the accepted value for these functionalities.[18, 25] The O-C=O high energy binding peak may include anhydrides, esters, and carboxylic acid groups, if present. The C1s spectrum of the 40 W films could be fitted with a minimum of 5 peaks according to the above notations. In comparison to those films deposited at lower power, only the 40 W films indicated the presence of carboxylic acid groups at a binding energy of 289.1eV. This result is consistent with FT-IR measurements. The C 1s spectrum of the film deposited at 1W required a minimum of 3 peaks to deconvolute the spectrum. These have been ascribed to C-C, C-N and N-C=O bonds, suggesting that at an input power of 1 W the ppDEA films show excellent retention of monomer structure.

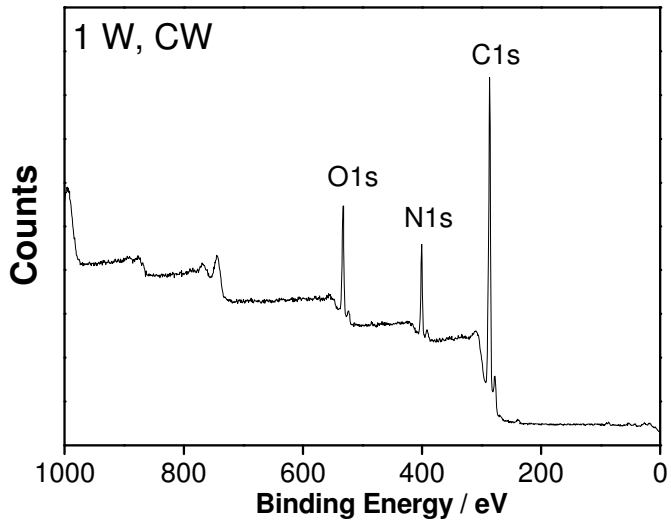

Figure 9-2: XPS wide scan of the ppDEA film deposited at 1 W.

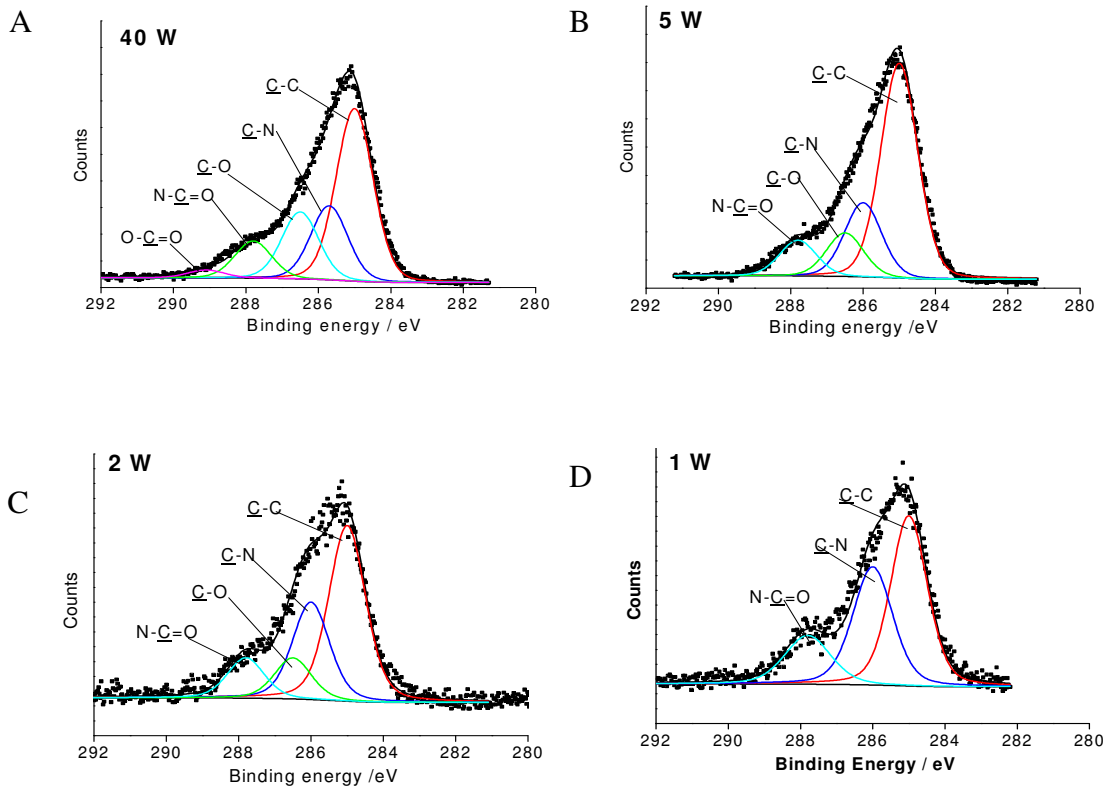

Figure 9-3: XPS C 1s spectra of the ppDEA films deposited at various plasma powers, A). 40W; B). 5 W; C). 2 W; D). 1 W.

9.3.3 Thermosensitivity of ppDEA films

The thermosensitivity of a 2W ppDEA film was measured using an EnviroScope AFM equipped with an environmental chamber. Figure 9-4 shows the AFM images for ppDEA at 25 °C and 50 °C, respectively. The corresponding section analysis allowed for the comparison of film thickness for the identical position. For instance, the thickness of ppDEA at 25 °C was 162 nm, as indicated in Figure 9-4C. If the sample temperature was increased to 50 °C, its thickness at the identical position decreased to 152 nm (Figure 9-4D). The average decrease in ppDEA thickness over several point on the sample was 9±1 nm, which is consistent with reported values for plasma polymerised NIPPAAm films.[20]

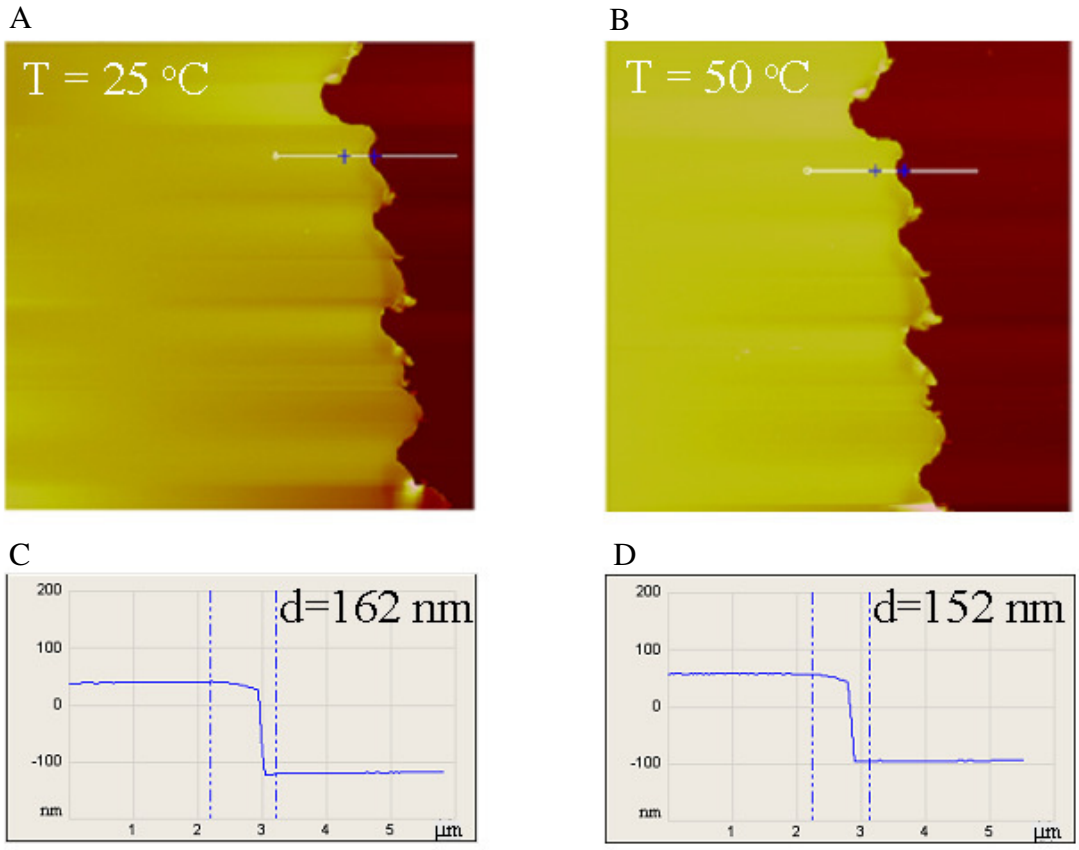

Figure 9-4: AFM images of a ppDEA film at 25 (A) and 50 °C (B). The corresponding section curves at 25 (C) and 50 °C (D) indicate that the thickness of pp-DEA decreased with increasing temperature. The scan area is 15 x 15 µm^2 in each case. Plasma conditions: 2 W, CW.

A convenient method to study the phase transition temperature thermosensitive films are water contact angle measurements.[6, 9-11] The sample was equilibrated at each temperature for 20 minutes before the measurements were taken. At temperatures between room

temperature and 34°C the contact angle of the 2 W ppDEA was about 52±2°, as shown in Figure 9-5. At temperatures between 34 °C and 37 °C, one could observe a rapid increase in contact angle to 66±2°. This increased hydrophobicity remained constant within the error for all temperatures above this. This indicates that the surface of ppDEA at high temperature was more hydrophobic than that at lower temperature with a LCST in the range of 34-37 °C. Similar experiments with the ppDEA film deposited at 5 W input power showed that its surface wettability remained unchanged at temperatures ranging from 25 to 63 °C (Figure 9-6).

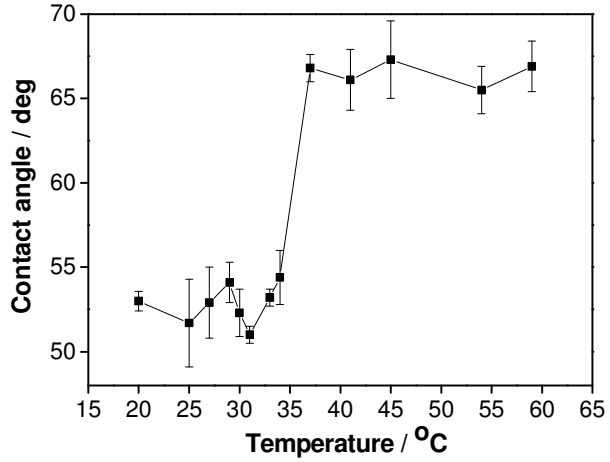

Figure 9-5: Water contact angle measurement on a ppDEA film as a function of temperature. The thickness of the film is 23.1 nm. Plasma conditions: 2 W, CW.

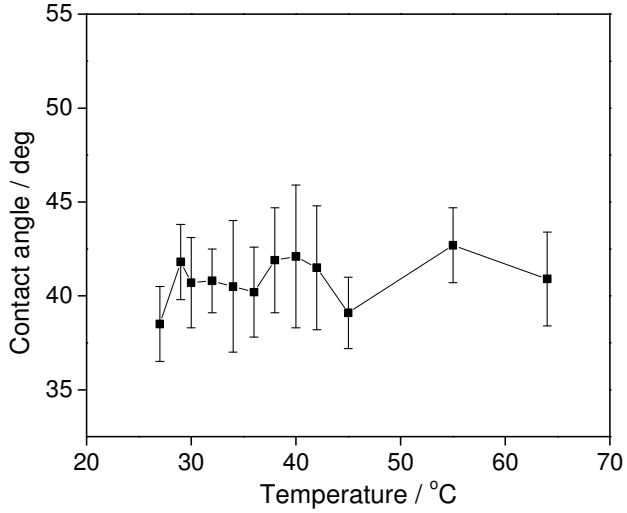

Figure 9-6: Water contact angle measurement on a ppDEA film as a function of temperature. Plasma conditions: 5 W, CW.

Thus, the retention of the DEA structure after plasma polymerization is a prerequisite for obtaining thermosensitivity. Unfortunately, while the low power pp-DEA shows promising thermosensitive properties, its stability in aqueous solution was not satisfactory. The ppDEA deposited at an input power of 1-2W could easily be washed off the gold and Si substrates. To overcome this problem, DEA was initially deposited at 50 W for 10 sec in order to improve the adhesion to the substrate. This was followed by the deposition at low input power to synthesise the thermosensitive layer. While this multilayer-approach improved the stability of the 2 W ppDEA, the ppDEA deposited at 1W on the adhesion-promoting layer was still unstable in aqueous solution. A possible procedure to improve the stability could be the copolymerisation with a crosslinking precusor, such as ethylene glycol dimethacrylate.[26, 27]

9.4 Conclusions

N,N-diethylacrylamide was employed in this work as the monomer for plasma polymerization aiming at obtaining a thermosensitive coating. Compared to the N-isopropylacrylamide monomer used in the literatures, the use of N,N-diethylacrylamide avoids the heating of both the monomer and the plasma reactor. Low power, continuous wave plasma conditions enabled the synthesis of plasma polymer coatings with a high retention of the monomer structure. Contact angle measurements of such films show a typical LCST between 34-37 °C for low input power deposits.

References

1. Nath, N.; Chilkoti, A. *Adv. Mater.* **2002,** 14, (17), 1243-1247.
2. Schmaljohann, D.; Oswald, J.; Jorgensen, B.; Nitschke, M.; Beyerlein, D.; Werner, C. *Biomacromolecules* **2003,** 4, (6), 1733-1739.
3. Akiyama, Y.; Kikuchi, A.; Yamato, M.; Okano, T. *Langmuir* **2004,** 20, (13), 5506-5511.
4. Yamada, N.; Okano, T.; Sakai, H.; Karikusa, F.; Sawasaki, Y.; Sakurai, Y. *Makro. Chem. Rapid Comm.* **1990,** 11, (11), 571-576.
5. Kan, C. W.; Doherty, E. A. S.; Buchholtz, B. A.; Barron, A. E. *Electrophoresis* **2004,** 25, (7-8), 1007-1015.

6. Rao, G. V. R.; Krug, M. E.; Balamurugan, S.; Xu, H. F.; Xu, Q.; Lopez, G. P. *Chem. Mater.* **2002,** 14, (12), 5075-5080.
7. Schild, H. G. *Progress Polym. Sci.* **1992,** 17, (2), 163-249.
8. Maeda, Y.; Higuchi, T.; Ikeda, I. *Langmuir* **2000,** 16, (19), 7503-7509.
9. Takei, Y. G.; Aoki, T.; Sanui, K.; Ogata, N.; Sakurai, Y.; Okano, T. *Macromolecules* **1994,** 27, (21), 6163-6166.
10. Zhang, J.; Pelton, R.; Deng, Y. L. *Langmuir* **1995,** 11, (6), 2301-2302.
11. Balamurugan, S.; Mendez, S.; Balamurugan, S. S.; O'Brien, M. J.; Lopez, G. P. *Langmuir* **2003,** 19, (7), 2545-2549.
12. Schmaljohann, D.; Beyerlein, D.; Nitschke, M.; Werner, C. *Langmuir* **2004,** 20, (23), 10107-10114.
13. Liang, L.; Shi, M. K.; Viswanathan, V. V.; Peurrung, L. M.; Young, J. S. *J. Membrane Sci.* **2000,** 177, (1-2), 97-108.
14. Liang, L.; Rieke, P. C.; Fryxell, G. E.; Liu, J.; Engehard, M. H.; Alford, K. L. *J. Phys. Chem. B* **2000,** 104, (49), 11667-11673.
15. Wang, Z. H.; Kuckling, D.; Johannsmann, D. *Soft Materials* **2003,** 1, (3), 353-364.
16. Kuckling, D.; Harmon, M. E.; Frank, C. W. *Macromolecules* **2002,** 35, (16), 6377-6383.
17. Harmon, M. E.; Kuckling, D.; Pareek, P.; Frank, C. W. *Langmuir* **2003,** 19, (26), 10947-10956.
18. Pan, Y. V.; Wesley, R. A.; Luginbuhl, R.; Denton, D. D.; Ratner, B. D. *Biomacromolecules* **2001,** 2, (1), 32-36.
19. Cheng, X. H.; Wang, Y. B.; Hanein, Y.; Bohringer, K. F.; Ratner, B. D. *J. Biomed. Mater. Res. A* **2004,** 70A, (2), 159-168.
20. Cheng, X. H.; Canavan, H. E.; Stein, M. J.; Hull, J. R.; Kweskin, S. J.; Wagner, M. S.; Somorjai, G. A.; Castner, D. G.; Ratner, B. D. *Langmuir* **2005,** 21, (17), 7833-7841.
21. Teare, D. O. H.; Barwick, D. C.; Schofield, W. C. E.; Garrod, R. P.; Beeby, A.; Badyal, J. P. S. *J. Phys. Chem. B* **2005,** 109, (47), 22407-22412.
22. Tamirisa, P. A.; Hess, D. W. *Macromolecules* **2006,** 39, (20), 7092-7097.
23. Eggert, M.; Freitag, R. *J. Polym. Sci. A: Polym. Chem.* **1994,** 32, (5), 803-813.
24. Liu, H. Y.; Zhu, X. X. *Polymer* **1999,** 40, (25), 6985-6990.
25. Beamson, G.; Briggs, D., *High Resolution XPS of Organic Polymers: The Scienta ESCA300 Database*. John Wiley & Sons: New York, 1992.

26. Tarducci, C.; Schofield, W. C. E.; Badyal, J. P. S.; Brewer, S. A.; Willis, C. *Macromolecules* **2002,** 35, (23), 8724-8727.

27. Chan, K.; Gleason, K. K. *Langmuir* **2005,** 21, (19), 8930-8939.

Chapter 10

Summary & Outlook

The main part of the present study is to develop SPFS-based DNA sensors using different plasma polymerized functional films. A variety of functional thin films, such as nonfouling or thermosensitive coating, as well as, the coatings bearing amine or epoxide groups, were prepared using plasma polymerization and were characterized by various techniques, such as FT-IR, XPS, AFM, SPR, OWS, etc. Some of the plasma thin films were then used for the development of SPFS-based DNA sensors.

In Chapter 4, nonfouling ppEO2 coatings were prepared by plasma polymerization of EO2 monomer with an emphasis on the relationship between the film thickness and their protein-resistance property. The minimum thickness to resist protein adsorption was found to be about 3 and 5.5 nm for BSA and fibrinogen, respectively. Additionally, a higher amount of ether groups in ppEO2 films was found to favor their non-fouling properties. Those nonfouling coatings were then used to make a multilayer protein-resistant DNA sensor (Chapter 5). An ultra-thin layer of ppEO2 was employed to immobilize the streptavidin protein. The ppEO2 is so thin that the embedded streptavidin are able to bind the biotinylated ssDNA probes. The resulted DNA sensors show good anti-fouling properties towards either BSA or fibrinogen. Moreover, this sensor was successfully employed to discriminate different DNA sequences from protein-containing sample solutions. I believe that the present sensor is very promising for the detection of a DNA sequence from a complex solution, as well as, for investigating the interaction between DNA strands and proteins.

Besides using streptavidin-biotin assembly to immobilize DNA probes, another functional surface, i.e., epoxide functional surface, was also obtained using plasma polymerization technique. While the epoxide groups obtained in the low DC ppGMA films could react with amine-modified DNA probes, the resulting films were also found to resist the non-specific adsorption of DNA strands. A DNA sensor based on SPFS and ppGMA films was thus made, and was successfully used to distinguish DNA sequences with one base pair mismatch. Additionally, the ppGMA surfaces are hydrophobic, and have almost no UV/Vis adsorption, suggesting that the ppGMA thin films are potentially promising to be used as substrates for DNA microarray.

Plasma polymerized allylamine (ppAA) films have been used widely as biomaterials. The stability of plasma polymer in contact with aqueous media is essential for many biomedical applications. In Chapter 7, ethanol extraction treatment was employed as a simple approach to remove the unbound materials from ppAA films, thus increasing its stability. It was found that much of the freshly deposited ppAA films is lost upon ethanol treatment, resulting in an decrease in ppAA thickness. Despite the relatively high loss in films thickness, the FT-IR and XPR analysis showed that the density of amine groups in the extracted ppAA are comparable to that of fresh films. The ppAA films in PBS buffer were used to provide a positively charged surface in Chapter 8.

While most DNA detection systems rely on the immobilization of DNA probes onto sensor surfaces, a new homogeneous DNA detection method was demonstrated in Chapter 8. The labeled PNA serves not only as the DNA catcher recognizing a particular target DNA, but also as a fluorescent indicator. This method takes advantages of the surface sensitivity of SPFS, as well as, the different electrostatic properties of PNA and DNA, thus avoid both the immobilization of DNA probes and the labelling of DNA targets. This method can distinguish DNA sequences with one base pair mismatch at a sensitivity of 200 pmol.

In Chapter 9, a temperature sensitive surface was prepared by plasma polymerization of N,N-diethylacrylamide (DEA). Compared to the NIPAAm monomer used in the literatures, one particular advantage of DEA is its higher vapor pressure, thus avoid heating either the monomer container or the plasma chamber, which is generally needed in NIPAAm plasma polymerization. The thermo-sensitivity of ppDEA films was confirmed by AFM and water contact angle measurements.